Authors answer to tc-2018-192 comments

February 14, 2019

Dear Editor,

You will find below our answers to the comments from the referees. We answered all of them and modified the manuscript to accommodate their requests. The text of the manuscript have considerably changed and an appendix have been added. Please note that the title of the manuscript have been changed to de-emphasize the high-resolution of our study following the comments from both reviewers. Note also that the order of the authors have been changed.

Yours sincerely,

On behalf of all the authors,
Damien Ringeisen

Note:

- The referees comments are shown in black.
- **The authors answers are shown in blue.**
- **The modifications brought to the manuscript are shown in bold typeface and colored in gray.**

Answer to tc-2018-192-RC1 – Harry Heorton

R1#1, Modelling Sea Ice fracture at very high resolution with VP rheologies This paper documents idealised very high resolution (25 m) numerical simulations of deformation in sea ice using the viscous plastic VP rheology. The sea ice is predominantly put under uniaxial compression from the top and bottom boundaries and the resulting deformation features are documented. Simulations are performed with longer model run times, decreased spatial resolution, modified boundary conditions, biaxial compression, imposed flaws within the sea ice and alternate rheologies by changing the yield curve shape. The results are well documented, though further detail is required on the model setup. Particular emphasis is put on the resulting deformation or linear kinematic feature intersection angle, as a means to provide a link between simulated and observed deformation features, and thus provides insight into how to select an appropriate sea ice rheology for simulation within climate models or for future studies. This method presents an exciting way to link observations and simulations of sea ice deformation, but there are certain aspects of the study that, in my opinion, need addressing.

We thank the reviewer for a thorough review and for highlighting grammatical mistakes in the original manuscript

R1#2, Firstly is selection of model resolution, and consideration of whether to simulate a single floe or a continuum of many floes. The selected 25 m resolution makes this a simulation of a single floe, and the paper describes the study as such, but there is little discussion of whether the selected VP rheology is a valid representation of a single floe. The VP rheology was developed to simulate a continuum of floes over ocean length scales, and it is not immediately obvious to me, that the VP rheology is a valid representation of the deformation of a single floe just by reducing the model resolution to that of single floe, and setting the ice concentration to unity as performed in this study. I am unaware of previous simulations of solid body deformation from other fields, and it may be the case that VP like rheologies are well studied, but this needs to be discussed in this paper. On the other hand this paper may be be a proof of concept that the VP rheology can be used to simulate the deformation of a single floe, and if it is, then it needs to be worded as such.

Typical floe size in the Arctic Ocean are of the order of 10 km, so that the continuum assumption can only be valid for model spatial resolution of 100km (Overland et al., 1995). Despite this, the use of VP rheologies with spatial resolution lower than 100km is now common practice even in lower resolution Global Climate Models. This raises the valid concern expressed by the reviewer. We argue that if the modes of failure in a single ice floe are the same as those of an aggregate of floes, then the continuum assumption can be used at spatial resolution higher than the 100km barrier. This is the implicit assumption currently made in the community with the use of higher spatial resolutions even in lower resolution Global Climate Models. We note that the mode of fracture in continuum models is independent of the scale of the problem. For instance, the results presented in the paper would not change if the domain and spatial resolution were increased by a factor of 500 (i.e. dx = 125km).

We added on page 2 of the revised manuscript :*"It can be argued that if the mode of deformation of a single floe is similar to that of an aggregate of floes, a given rheology developed for a continuum can still be applicable at spatial resolutions of the order of the floe size (Overland et al., 1998), but the validity of a given flow rule across scales is not clear."*

R1#3, A further implication of simulating a single floe, rather than a continuum floes, is the observations that the paper discusses when validating the results. The RADARSAT and RGPS data is given as a means to validate the yield curve selected. But the RGPS data is given on continuum length scales, so to validate a selected yield curve the comparison will need to be made with simulations over continuum length scales, not on the floe length scales presented in this paper. To validate the simulations of this paper observations of individual floe shape, aspect ratio and floe-to-floe crack intersection angle from aerial images of floes will be best suited. Secondly the presented results are often from the order of 1-10 seconds into the simulations. This is in contrast to idealised deformation experiments of Hutchings et al. (2004) and Heorton et al. (2018) where the results are given at 1 - 24 hours of simulation, and explored over multiple days. Within these studies the initial conditions and early stress/deformation states are explored and documented. Also in both of these cases, the initial state of the ice over was seeded with noise (in strength, or thickness and forcing) to allow for features to develop and stop an unrealistic uniform sea ice cover. Were such considerations performed in this study? Are the initial conditions uniform? What are the implications of using results from 1-10 seconds of model run? I would like to see documentation of the time series of stress/strain state in order to validate the idealised experiments and the initial conditions. I personally found the longer documented run of 45 minutes interesting, with individual floe-like shapes appearing that can be compared to images of floes.

- We did not use observations of angles of fracture from RADARSAT and/or RPGS dataset to validate the model results. Instead, we use a comparison study by Hutter et al. (2018b) between observed (RGPS) and simulated Linear Kinematic Features as a motivation for the present work. As mentioned above, the results presented are independent of spatial resolution, and the conclusions are applicable to continuum scale observations. This shown in Section 3.2.1 and on Figure 5.

- The goal of the study is document the fracture angle as a function of mechanical strength parameters, boundary conditions, and to compare the rheology-dependent model of deformation from those induced by inhomogeneities in the initial thickness field (Fig. 9) as in Heorton et al. (2018), and Hutchings et al. (2005). The fracture angle provides, for the first time, a meaningful diagnostic (since it is related to deformation and motion of sea ice) that allows a discrimination between different rheologies (yield curve and flow rule). Note that prior attempts using sea ice drift and PDF of sea ice deformation did not allow for this discrimination (Kreyscher et al., 1997; Bouchat and Tremblay, 2017; Hutter et al., 2018a). For this reason, we only integrate the model for a few seconds - until the fracture is apparent in the thickness or deformation field. Results from longer simulations were also performed to demonstrate that VP rheologies can simulate secondary fracture lines similar to observations with lead opening and ridging (Fig 7).

- The initial conditions are uniform in ice concentration and ice thicknesses. This has been clarified in Section 2.3 of the revised manuscript. Ice strength was not modified.

- As it is now explained in section 3.1 on page 9 of the revised manuscript, the ice floe fails starting from the first time step with stress states on the edge of the yield curve.

R1#4, Also there is little discussion of the implications and 'robustness' of the presented model results. The authors described the results as 'robust' on multiple occasions but make little effort to inform the reader why they are robust. Figure 5 is presented as a domain/resolution study but only mentioned once in passing as an indication of the models robustness. I'm assuming that the model domain/resolution/run time has been investigated but there is no documentation or discussion of the models limitations. A section describing this is required in order to allow the other results to be published.

As stated above, we are not interested in subsequent deformation after ice fracture. For this reason, we do not present results on the sensitivity to time of integration. We changed the organisation of the results section of the manuscript by regrouping all sensitivity experiments in one section (3.2), including a short description on the sensitivity of the results to spatial resolution and domain size on page 11, Section 3.2.1, of the revised manuscript.

R1#5, Thirdly it is not obvious how the deformation or linear kinematic feature intersection angle were calculated. I would like to see this information given in an appendix, such a method is a very useful contribution to studies of sea-ice rheology and one that I would like to use in the future. A citation to another study where this method was performed and is described is another option. The given appendix showing the theory behind internal friction and Mohr-Coloumb failure criterion, whilst interesting to see, does not appear to be original theory for this paper and is not required and the dependencies can be stated and cited.

- The angle of fracture is measured using a free image processing software (GNU Image Manipulation Program, GIMP). The small number images to treat did not call for a special program to measure angles as done in Linow and Dierking (2017), Mohammadi-Aragh et al. (2018) and Hutter et al. (2018b) was not necessary because the number images to be processed was small. **To clarify this issue, we added the following text on page 7 of the revised manuscript: *"The angle of fracture is measured with the angle measuring tool of the GNU Image Manipulation Program (GIMP, https://www.gimp.org/). A special automatic algorithm to measure angles is described in Linow and Dierking (2017); Hutter et al. (2018b).".***

- We decided to keep the Mohr-Coulomb theory in Appendix A for the sake of completeness. We have added the following reference in Appendix A for readers who want to see a related description of the theory (Hibler and Schulson (2000) Pritchard (1988).

Specific comments:

R1#6, Page 1 Line 6-8 What are the dependencies of typical granular materials? The sand castle analogy is not useful.

We decided to remove the sand castle analogy from the abstract but to keep it in the discussion/conclusion because it is something that anyone within or outside the community is familiar with; it was also well received at the future of Earth System Modeling workshop at CalTech in November 2018. We rewrote the abstract.

The new abstract is *"Recent high resolution pan-Arctic sea ice simulations show fracture patterns (Linear Kinematic Features or LKFs) that are typical of granular materials, but with wider fracture angles than those observed in high-resolution satellite images. Motivated by this, ice fracture is investigated in a simple uni-axial loading test using two different Viscous-Plastic (VP) rheologies: one with an elliptical yield curve and a normal flow rule, and one with a Coulombic yield curve and a normal flow rule that applies only to the elliptical cap. With the standard VP rheology, it is not possible to simulate fracture angles smaller than* $30°$*. Further, the standard VP-model is not consistent with the behaviour of granular material such as sea ice, because: (1) the fracture angle increases with ice shear strength; (2) the divergence along the fracture lines (or LKFs) is uniquely defined by the shear strength of the material with divergence for high shear strength and convergent with low shear strength; (3) the angle of fracture depends on the confining pressure with more convergence as the confining pressure increases. This behavior of the VP model is connected to the convexity of the yield curve together with use of a normal flow rule. In the Coulombic model, the angle of fracture is smaller (*$\theta = 23°$*) and grossly consistent with observations. The solution, however, is unstable when the compressive stress is too large because of non-differentiable corners between the straight limbs of the Coulombic yield curve and the elliptical cap. The results suggest that, although at first sight the large scale patterns of LKFs simulated with a VP sea ice model appear to be realistic, the elliptical yield curve with a normal flow rule is not consistent with the notion of sea ice as a pressure-sensitive and dilatant granular material."*

R1#7, Page 1, Line 8 what model? this paper or previous?

We meant the mathematical description of the ice, the rheology, i.e. the elliptical hibler Viscous-Plastic rheology implemented in MITgcm.

The abstract was changed (see R1#6 above), this sentence has been deleted.

R1#8, Page 1, Line 10-14 More description of 'typical granular materials' that are not accurately described and all comparisons are difficult to follow. I would avoid these loose comparisons in the abstract and stick to definite results.

We wanted to give the reader a hint of the significance of our results by giving a comparison to granular material properties. But it might lead to confusion. We will limit the comparison to the discussion part of the paper.

We modified the abstract as specified above for comment R1#6

R1#9, Page 1, Line 24 are the two citations model studies or observations of sea ice floes? Observational studies are required for this sentence.

Overland et al. (1998) is an observation study base on buoy data, while Tremblay and Mysak (1997) is a modeling study. We remove this last reference and replace it by another observational study (Rothrock and Thorndike, 1984).

R1#10, Page 2 Line 5 Leads plural, dangerous to use the word memory when describing a computer model, 'emergent anisotropy' is more accurate.

Both have been corrected as suggested.

R1#11, Page 2, Line 8 The equations are difficult to solve due to their non-linearity and complexity not because of sea ice. It is however difficult to represent sea ice with

simple, easily solvable equations due to it's non-continuous features.

We changed this sentence to express our thought more clearly.

The first sentence of the 2nd paragraph of the introduction is changed to : ***"The sea ice dynamics are complicated because of sharp spatial changes in material properties associated with discontinuities (e.g. along sea ice leads or ridges) and heterogeneity (spatially varying ice thickness and concentration). The sea ice momentum equations are difficult to solve numerically because of the non-linear sea ice rheology."***

R1#12, Page 3 Line 24 argues - argued
Corrected as suggested.

R1#13, Page 3 Line 28 rheologies plural
Corrected as suggested.

R1#14, Page 3 Line 32 check citations and parenthesis
Corrected as suggested.

R1#15, Page 3 Line 33 check citations and parenthesis
Corrected as suggested.

R1#16, Page 3 Lines 34-35 'Based on these satellite observations, amongst others (provide some examples), and in-situ. . . '

The sentence was re-written as: ***"Based on satellite observations (e.g. RADARSAT Geophysical Processor System, RPGS, or Advanced Very-High-Resolution Radiometer, AVHRR), and in-situ internal ice stress measurements (e.g. from the Surface Heat Budget of the Arctic Ocean, SHEBA, experiment),[. . .]"***

R1#17, Page 3 line 6 space before 'Girard'
Corrected as suggested.

R1#18, Page 3 line 13 delete parenthesis
Corrected as suggested.

R1#19, Page 3 line 15 'are appear as line of' - 'appear as lines of', deformation singular, 'with the deformation' - 'with shear deformation', divergence - convergence
Corrected as suggested.

R1#20, Page 3 Line 18 leads - leading
Corrected as suggested.

R1#21, Page 3 line 19-20 check citation parenthesis
Corrected as suggested.

R1#22, Page 4 line 1 Wilchinsky et al. also deduced intersection angles between floes that are relevant to this paper.

The reference to Wilchinsky et al. (2010) has been added to the list of citation.

R1#23, Page 5 Figure 1. What is 'Mohr-Coloumb flat' In general I found the figure captions to be lacking in content. Can they all be expanded to directly describe what simulation they are from, and the part of the figure that is of interest? A reference link to where in the paper (section number) it is described and discussed is also required. I found myself flipping back and forward trying to work out what simulation was illustrated in which figure, please include more information to avoid this please.

We re-wrote the figure captions and made them self-sufficient as suggested by the reviewer. *Flat* refers to the linear part of the yield curve. We replaced the word *flat* by *linear limb* which is more accurate.

The captions of all figure have been extended to be self-sufficient. The caption of figure 5 now reads *"Elliptical yield curve (black) with ellipse aspect ratio $e = a/b = 2$. Coulombic yield curve (red) and elliptical capping with internal angle of friction (μ). Both e and μ are measures of the shear strength of the material. The normal flow rule applies only to the elliptical part of the yield curves. For the two straight limbs of the Coulombic yield curve, the flow is normal to the truncated ellipse (dash-dot line) with the same first stress invariant. Note that the axes σ_1, σ_2 and σ_I, σ_{II} do not have the same scale."*

R1#24, page 5 Line 5 to 15. I am assuming that this paragraph describes the physical phenomena that the viscous plastic rheology and associated yield curve are designed to replicate. However this paragraph is worded such that it is an accepted and proved fact that sea-ice is viscous plastic and has behaviour that follows all these rules. Also the paragraph contains no citations. Rewriting this paragraph to emphasise that the viscous plastic rheology is designed to simulate the stress/strain relationship of sea ice over continuum length scales is required. It will also help to address the theoretical implications of using a rheology designed for the continuum approximation of sea-ice to simulate the deformation of a single floe.

This paragraph was reworded taking into account the comment from the reviewer. Please see page 6 of the revised manuscript.

This paragraph now starts with *"The VP rheology was originally developed to simulate ice motion on a basin scale (e.g., Arctic Ocean, Southern Ocean) (Hibler, 1979). In this model, stochastic elastic deformation is parameterized as highly viscous (creep) flow (Hibler, 1977). Ice is set in motion by surface air and basal ocean stresses moderated by internal ice stress."*

Page 6 line 11 check parenthesis

The missing parenthesis have been added

R1#25, Page 6 line 15 Is this 'theoretical angle' the one used to retrieve the LKF intersection angles from simulation results, and also with previous studies? If so can you state it here. The paper has not informed me how this study, and previous studies obtained the intersection angles widely discussed.

Yes it the theoretical angle of fraction derived form the Mohr's circle and the Mohr-Coulomb yield criterion. It is described in several paper, e.g. in Ip et al. (1991); Hibler and Schulson (2000), and , as shown in appendix A and B, it is in agreement with the characteristics lines described in Pritchard (1988)

The 3 references above have been added on page 8 of the revised manuscript in the sentence : *"The theoretical angle of fracture θ can be calculated from the Mohr's circle of stress and yield curve written in the local (reference)*

coordinate system (Ip et al., 1991; Pritchard, 1988; Hibler and Schulson, 2000). Details are described in the appendix. For a Mohr-Coulomb yield criterion, θ follows immediately from the internal angle of friction, that is the available shear strength. An instructive analogue is the slope of a pile of sand on a table. Wet sand can support more shear stress and hence the slope angle can be steeper (smaller).”

R1#26, Page 8 line 6 is the model domain used in all experiments? If there are exceptions please list them.

This model domain is used in all experiments, except for two experiments reported in Section 3.2.1 (Figure 5 and Figure 7).

We inserted : *”The model domain is a rectangle of size 10 km × 25 km,except for Sect. 3.2.1 and Sect. 3.2.2”* on page 8 on revised manuscript

R1#27, Page 8 line 10 - 11 This statement about the robustness of the results is not backed up. Please refer the reader to the results that back up this statement. The proof of the robustness of this model needs to come first before any other results.

See Section 3.2 on page 10 of the revised manuscript for a discussion on the sensitivity of the results to different boundary conditions. In our opinion, the demonstration that VP rheologies can simulate realistic fracture lines that have angles in accord with theory should be presented first. This is the reason why we present these results first, before the sensitivity of the results to the boundary conditions. The boundary conditions in this context can be seen as external forcing on the interior solution.

R1#28, Page 8 Lines 11 - 17 Please state how the model time step works? I am not familiar with how the LSR solver for the VP rheology works. How does the model work in time? I am familiar with models that have a constant time step with solution iterations per time step. The model then continues time stepping for the required simulation period. Does your model work in the same way? Or is there a selected simulation time, and then the documented 1500/1500 iterations performed to cover the simulation time? If so then can you describe why the simulation time was selected as you have done with the spatial resolution. Is the simulation time and temporal resolution/number of iterations the same for all simulations?

The non-linear momentum equation is solved iteratively until a converged solution is obtained. Typically 1500 iterations are required to reach convergence. Then the external forcing is then updated and a new solution calculated. This has been clarified on pages 7-8 of the revised manuscript.

We modified the text describing the numerical solver :*”We solve the non-linear sea-ice momentum equations with a Picard or fixed point iteration with 1500 non-linear or outer-loop (OL) iterations. Within each non-linear iteration, the non-linear coefficients (drag coefficients and viscosities) are updated and a linearized system of equations is solved with a Line Successive (over-)Relaxation (LSR) (Zhang and Hibler, 1997). The linear iteration is stopped when the maximum increment is less than $\epsilon_{LSR} = 10^{-11}\, m\, s^{-1}$, but we also limit the number iterations to 1500. Typically, 1500 non-linear iterations are required to reach a converged solution. This is so because of slow convergence due to the highly non-linear rheology term and the high spatial resolution (Lemieux and Tremblay, 2009).”*

R1#29, Results section A paragraph describing which simulations have been performed will be useful here. This will save having to flip back and forward through the

paper to match results discussion and figures. The simulation 'robustness' results need to come first in order to validate the following results.

A paragraph have been added at the beginning of the Section 3 (Results) on page 9 of the revised manuscript, stating the different part of the result section. A paragraph has been added at the beginning of Section 3.2 on page 10 of the new manuscript to list the sensitivity experiment that have been performed.

The first paragraph of Section 3.2 now reads *"We use simple uni-axial loading experiments to investigate the creation of pair of conjugate faults and their intersection angle. After presenting the results of simulations with the default parameters (Section 3.1), we explore the effects of experimental choices: confining pressure, choice of boundary conditions (i.e. von Neumann versus Dirichlet), domain size and spatial resolution and inhomogeneities (i.e. localized weakness) in the initial thickness and concentration field (Section 3.2). Finally, we study the behaviour of two viscous plastic rheologies with different yield curves and compare these dependencies to what we can infer from smaller and larger scale measurements from laboratory experiment and RGPS observations (Section 3.3)."*

R1#30, Page 8 line 29 Figure - figure (no capital), 'measured intersection angle' how was this angle measured?

We modified the manuscript to comply with the journal standards, i.e. using *Fig. or Figure, Eq. or Equation , Table, and Sect. or Section.*

The word *measured* is now replaced by *simulated*. We measured the angle using the GIMP software. See response to comment R1#5 above for more details.

R1#31, Page 8 line 27 quantify 'right away' and how can a fracture appear but not in the deformation field? what field did it appear in? Can you comment on this time scale compared to observations of floe fracture (Dempsey et al. 2011 Fracture of a ridged multi-year Arctic sea ice floe)

After 1 timestep, the stress states reach the yield curve and deformation occurs. We see this immediately in the strain rates (divergence and deformation). For the results presented in the paper, we have iterated for 10 additional seconds in order for the signal to also be seen in the thickness and concentration field. We do this to more clearly show the fixed link between sea ice shear strength and divergence in the standard VP rheology of Hibler. We removed the sloppy term "right away" from the text. The reference to Dempsey et al. (2012) was also added in the discussion.

The new text on page 9 of the revised manuscript now reads: : *"After 1 timestep (or 0.1 s), the stress states already lie on the yield curve and the fracture is readily seen in the deformation fields (divergence and shear). We iterate for a total of 20 seconds in order for the signal to be apparent in the thickness and concentration fields. We do this to more clearly show the link between position of the stress states on the yield curve and the normal flow rule in the standard VP rheology of Hibler (1979)."*

On page 22 of the revised manuscript (discussion section), we added the following sentence : *"Observed time scales of fracture are on the order of 10 seconds for 60 m floe diameters (Dempsey et al., 2012, Figure 6 top right panel) and from typical elastic wave speeds of 200–2000 $m\,s^{-1}$, large cracks of order 1000 km can form in minutes to hours (Marsan et al., 2012)."*

R1#32, Page 9 line 7 The 'robustness' results need to come first, then the model resolution and time period choice can be validated against them.

Please see response to comment **R1#27** above for a justification.

The angle of intersection between a pair of conjugate fault does not change with domain size and spatial resolution (see Fig. 5).

R1#33, page 9 line 9 extended time period, what was the original time period?

The original time period of the simulation is 20 seconds with a 0.1 second time step. The length of the simulations is not important here as we are showing only results from the first timesteps.

We added a reference to Table 1 in the revised manuscript on page 9 section 3.1. We also changed the sentence on page 7 (please see next comment R1#34 below)

R1#34, Page 9 line 10 total iterations or iterations per time step? what is the time step?

It is the number of sub-cycles used to solve the non-linear momentum equation. This should be clearer in the new version of the manuscript (see response to comment R1#28 above)

The first two sentences now read: *"Continuing the integration to 2700 seconds (45 min), compared to 20 seconds in the reference simulation leads to the creation of smaller diamond-shaped ice floes due to secondary and tertiary fracture lines (Figure 6)."*

R1#35, Page 10 Figure 3 Bottom left pane. Please use a bipolar colour scale for bipolar data. As in a different colour for +/-, white for zero for example. These scales are easily selectable.

The colorbar were changed as suggested.

R1#36, Page 10 Line 8 'similarly as' - 'similar to'

Corrected as suggested.

R1#37, Section 3.3 If this section addresses the robustness then it needs to go first and also discuss the results in figure 5. Please also comment on the limitations of this model.

Please see the new Section 3.2 and the answer to the comment R1#27 above.

The limitations of the VP model are discussed in the introduction on page 2 of the revised manuscript. All sensitivity experiments - including sensitivity to spatial resolution and domain size - are now presented together in a new section 3.2 entitled: *Sensitivity experiments*. The limitations of the this study are discusses in the discussion section on page 22 of the revised manuscript.

We added in the discussion section on page 22 :*"The simulations presented in this study are not realistic and cannot be compared directly to observations of ice floe fracture. For instance, our idealized ice floe is homogeneous while sea ice is known to feature some weaknesses like thermal cracks or melt ponds."*

R1#38, Page 11 Figure 5 First change or rescale the colourscale to highlight

features. The max deformation appears to be around 10^{-4}, so limit the colour to this point, Also please label the colour scale legend with units. Why have you selected only 2 seconds of model run. what happens later in the run? Is this on a similar time scale to observations of floe fracture? Consider plotting a later time point if available or discuss how the model proceeds.

We want to keep the same scale for every plot. Yes, the maximum value is approximately equal to 10^{-4}. We added color bar legends with units. We limited the simulation to 2 seconds because of computational constraints. After 2 sec, the fracture angle is already visible, and it is not necessary to run the simulation any longer time, because this would simply make the signal stronger in the thickness and concentration fields. This was tested using a smaller domain. We clarified this on page 11 of the revised manuscript.

We have re-written the captions of all figures including the reference to the appropriate section as suggested by the reviewer. We justified our choice of total integration of 2 sec for this experiment in the revised manuscript.

The caption was modified : ***"Maximum shear strain rate (second strain invariant) after 10 seconds of integration for the default domain size and*** $\Delta x = 100\,m$ ***(a) and*** $500\,m$ ***(b), and for the default*** Δx ***and a doubled domain size of*** $20\,km \times 50\,km$ ***(c). Note that for case of the double domain (c), the southward velocity at the northern boundary was also doubled to keep the deformation rate constant, and that this simulation is limited to 2 seconds for numerical efficiency."***

R1#39, Page 12 again bipolar colour scale for bipolar field would be appreciated. All of your plotted fields so far have been for deformation, a plot of a stress field, if available, will be nice to see. There are lots of crack intersections in this plot. Is it possible to obtain all of these intersection angles? A distribution of angles could then be presented.

While these simulations are indeed cool to look at (especially when you animate them!), it does not seem useful to us to investigate the angles of all of these leads in detail. Most of them were created after the initial fracture, therefore the direction of stress and magnitude of stress have been modified by ensuing fractures and deformations so that the analysis would be confounded. We can see that the fracture pattern is not absolutely symmetrical. This means that the converged solution is not reached. In principle, this is possible, e.g. with the software of Hutter et al. (2018b). We find the stress field not to be helpful in our case, the deformation field showing the fracture lines is more important for us to explore the effects of the rheology.

The colorbar has been corrected as suggested.

R1#40, Page 13 Line 5 Comment on ice strength/thickness vs fracture angle. Is this a result you have observed? Or is it a theory that you are testing? Is there a citation for this theory?

Our statement is a little misleading and has been rephrased to express that because ice strength in the model is a linear function of the ice thickness, see equation 4 on page 5, or (Coon et al., 1974; Hibler, 1979), and the fracture angle depends on ice strength, it implicitly also depends on the ice thickness.

We included on page 13 of the revised manuscript the sentence :*Note that the ice strength is linearly related to the ice thickness (Eq. 4). Therefore the normal stress at the edge of the floe is completely defined by the thickness of the surrounding ice.*

R1#41, Page 13 Line 17 You start this paragraph with statements about the link between initialised faults and deformation. Is this a theory you are testing? If so give a citation. Is it your interpretation of the results? if so you need to state the results and the reference the figure first.

This is a hypothesis that we can support by our simulations shown in Fig.9. The hypothesis was formulated previously and also tested (Aksenov and Hibler, 2001) and (Hibler and Schulson, 2000). It has not been tested using models whether the angle of fracture is dictated by in-homogeneities in the sea ice cover or the yield curve and flow rule (see appendix B1 and B2 for the elliptical and Coulombic yield curve in the VP rheology).

We rewrote the text of this section on page 14 of the revised manuscript : *"So far, all initial conditions have been homogeneous in thickness and concentration within the ice floe. In practice, sea ice (in a numerical model, but also in reality) is not homogeneous. A local weakness in the initial ice field is likely the starting point of a crack within the ice field (e.g., Herman, 2016, her Figure 5c). Local failures raise the stress level in adjacent grid cells and a crack can propagate. Note that the crack propagation in an "ideal" plastic model such as the VP model is instantaneous and this propagation is not seen between time steps. As a consequence, lines of failure will likely develop between local weaknesses. The location of weaknesses in the ice field together with the ice rheology (yield curve and flow rule) both determine the fracture angles (Hibler and Schulson, 2000; Aksenov and Hibler, 2001).*

To illustrate this behavior, we start new simulations from an initial ice field with two areas of zero ice thickness and zero ice concentration, hence weaker ice (Figure 9a). After $5\,s$ *these simulations yield fracture patterns that are dramatically different from those of the control run simulation (Section 3.1): the fracture lines now start and terminate at the locations of the weak ice areas. Still, changing the shear strength of the ice (by changing* e*) changes the fracture pattern (Figure 9b and c). With* $e = 1$*, the angles are much wider than with* $e = 2$*, which is consistent with the general dependence of fracture angles on* e *(see Sect. 3.3.1). Our simulations cannot lead to conclusive statements about the relative importance of heterogeneity of initial conditions and yield curve parameters for the fracture pattern, but we can state that both affect the simulations in a way that requires treating them separately to avoid confounding effects. Details are deferred to a dedicated study."*

R1#42, Page 14 Figure 8 caption is lacking detail. Is this the figure for the lateral confinement experiments, or ice thickness experiments? Please describe what is shown in every pane.

All captions have been re-written. This is the lateral confinement experiment. Thanks for pointing this out.

The caption of figure 8 have been modified to be : *"Maximum shear strain rates (left) and stress state in stress invariant space (right) after 5 seconds of integration for different confinement pressure:* $h_c = 0.05\,m$ *(a) and* $h_c = 0.3\,m$ *(b). Note, how stress states with divergent strain rates (a) migrate left towards convergent strain rates (b)."*

R1#43, Page 15 Figure 9 please label colour scale legends.

Corrected as suggested.

R1#44, Page 16 Figure 11, again please describe the simulation this figure corresponds to? The colorscale are saturated so consider rescaling.

In the case of the top left panel (now panel a)), the log-scale of the colorbar does not allow me to use a non-saturated colormap. There is lot a simulated ice that deforms really slowly (viscous creep) These areas are not interesting for us, so it is not necessary to display them in the colormap. Additionally, logarithm of values close to zero are close to $-\infty$, so impossible to display on a colormap. We use a logarithmic colormap to have a better contrast of value of deformation, that have a really steep changes. We rewrote the caption, see below.

The caption for this figure now read *"Maximum shear strain (a), ice thickness anomaly (b), divergence (c) and stress state in stress invariant space (d) after 5 sec of integration for a smaller ellipse aspect ration ($e = 0.7$ compared to $e = 2$ in the reference run in Sect. 3.1). Compared to the control run on Fig. 3, the angle of fracture is larger ($\theta = (61 \pm 1)^\circ$), the stress states are in the second half of the ellipse (with strain rates pointing into the convergent direction) and there is convergence along the fracture lines (panel b) in agreement with the schematic in Fig. 4"*

R1#45, Page 17 line 18 A lot of LKFs - how many? Or is it more than compared to another simulation? rephrase or quantify.

We do not expect uniform piece of modelled ice to break in any other way than with 2 fractures. We rephrased this sentence to explain why the creation of more than 2 conjugate faults is problematic

We rephrased and changed the sentence by *Sea ice shear strength is small for small stresses, and ice deforms strongly along the ice edge. Many small LKFs develop, but no large fractures spanning the entire floe, as expected in a uni-axial compressive test with an homogeneous plastic material.*

R1#46, Page 17 line 21 space before theta

Corrected as suggested.

R1#47, Page 18 Figure 12 are these Coulombic curve simulations? again this caption needs more detail.

Corrected as suggested

The captions of all figure have been extended to be self-sufficient and the suitable sections referenced.

We changed to caption to *"Maximum shear strain (top) and stress state in stress invariant space (bottom) for different internal angles of friction. (a) $\mu = 0.7$ or $\phi = 44^\circ$, (b) $\mu = 0.85$ or $\phi = 58^\circ$ and (c) $\mu = 0.95$ or $\phi = 72^\circ$ after $5\,s$ of integration. The angles of fracture are $\theta = 23^\circ$, $(28 \pm 2)^\circ$ and 41°. Fig. 10 illustrates how θ depends on μ for a Coulombic yield curve."*

R1#48, Page 18 line 4 'realistic manner' how are they realistic? what simulations are you comparing to what observations? A figure reference and a citation are both needed for this statement.

We mean "look realistic" when compared with observations from RGPS and reported in Hutter et al. (2018b) or lab experiments reported in Schulson (2004). We wanted to

express the way the model produces small floes that appear realistic, but may be not so. Still, we can compare to small lab experiment from Schulson and Duval (2009) and see several similarities, although at different scales.

We changed the sentence to: ***The fracturing of the ice floe creates smaller floes in a realistic manner, for example, compared to to Landsat-7 images (Schulson, 2004, Figure 2)***

R1#49, Page 19 line 12 please refer to the section or figure or both that show the resolution and scale non-dependance.

The section and figure is now referred to on page 20 of the revised manuscript.

R1#50, Page 19 line 15 'appear' - 'appears'

Corrected, as suggested

R1#51, Page 19 line 26 please give a citation for the statement on granular material.

The citation Balendran and Nemat-Nasser (1993) was added

R1#52, Page 20 line 22 Citation required for 'Arctic-wide simulation'

We added a citation to Hutter et al. (2018b)

R1#53, Page 20 line 28 why is it unsurprising? Do mean that your results fit with previous theory and results? If so can you say this and cite them?

This is not surprising because it is the role of the yield and the flow rule to determine the deformation of the solid. **We modified the sentence to clarify our opinion: *"Unsurprisingly, the yield curve plays an important role in fracturing sea ice in a numerical model as it governs the deformation of the ice as a function of the applied stress."***

R1#54, Page 20 line 33 'The ice open and create leads' - The simulated sea ice opens and creates leads

Corrected as suggested

Answer to tc-2018-192-RC2 – Jenny Hutchings

R2#1, I am really pleased to see a paper that is making suggestions for idealised experiments we can use to differentiate between rheological models for sea ice. This in itself is worth publishing. The main result of the paper is that the elliptical rheology is inappropriate for representing observed cracking orientation in the ice pack, which is interesting and helps motivate changing sea ice rheological models used in climate and weather prediction.

We thank the reviewer for the numerous interesting comments about our work. We tried below to answer and address all of them in this new manuscript.

R2#2, I do have some concerns that the interpretation of observational data needs sharpening, and the results must not be overly interpreted given limitations of the use of RGPS data. Identifying intersection angles for lead pairs actually requires more work (and dedicated field data collection) than this paper warrants. You are motivated by the fact that a simulation shows larger intersection angles than RGPS, and I agree that this is something to address. I just do not think you can use RGPS to determine what the intersection angle should be, just that it needs to be smaller. Note, there are others in the community funded to do this work of identifying fracture patterns associated with particular modes of failure. For example I have an NSF and NASA project that is looking at identification of modes of failure from satellite imagery. There are also upcoming field experiments that could provide case studies to constrain the actual behaviour of sea ice, which should provide further guidance for use of your idealised cases to constrain rheological model design. I would be happy to talk to you in person about using this analysis and data to support future model validation efforts. I would also caution you to be more careful in your description of the differences between VP and granular models. Some clarification missing from the manuscript is provided in my comments. I also have suggestions for why the VP model creates LKFs, which I feel is important for understanding the validity of LKFs in the viscous plastic sea ice model representing nature.

We agree with you that determining the intersection angle of conjugate faults from the RGPS LKF data-set has a few limitations (only large cracks, temporal resolution of 3 days,...). Given the large variety of forcing conditions, the RGPS LKF data-set includes LKFs originating from multiple modes of failure, but also shows conjugate fault pairs. We, here, name two advantages of using the RGPS LKF data-set to evaluate intersection angles in Pan-Arctic sea-ice simulation: (1) the data-set covers 65% of the Arctic Ocean and spans over twelve years, which is a much higher coverage compared to hand-picked studies in satellite imagery (Erlingsson, 1988; Walter and Overland, 1993). (2) The data-set enables a consistent comparison with model output as it is based on sea-ice deformation. As the intersection angles are consistent with other studies (e.g. Walter and Overland, 1993) we are confident that this approach can be used to determine whether a model is over- or underestimating the intersection angle. We, here, want to stress that we only use the misfit of intersection angles in the RGPS LKF data-set and in a Pan-Arctic sea ice simulation to motivate our work to further study the dependency of the rheology and yield curve on the intersection angle. In our manuscript, the RGPS LKF data-set is not used to evaluate our idealized experiments. We rewrote the corresponding abstract accordingly to make this point clear.

Specific comments:

R2#3, Check spelling throughout the manuscript. Also check for missing brackets throughout. Grammar can be improved in places, and sometimes words are repeated. Make sure you have someone very carefully proof read the manuscript. I did not correct all the typos I saw because I am short on time and wanted to focus my attention on the central messages in your paper.

We have carefully proofread the manuscript. We apologize for the many technical problems.

R2#4, In the introduction be specific that you are considering conjugate fault pairs that form under specific confining stresses, the orientation of which is controlled by the yield curve shape and flow rule. In particular reference Pritchard in the introduction. It is only when I got to the conclusion that I saw you were aware of this work and it was motivating your study. It is wise to point out that not all applied stress will result in intersecting fault pairs (for example tension and pure compression do not).

We included a citation of Pritchard (1988), and clarified that pure compression and tensile cracks do not form pair of intersecting fault. Thanks for pointing this out.

We added this text in the introduction : *"Pritchard (1988) investigated the yield curve's mathematical characteristics and derived angles between the principal stress directions and characteristics directions that depend on the tangent to the yield curve. These results show that stress states exist in plastic materials where no LKFs form and were later used to build a yield curve (Wang, 2007)."*. We also changed the first sentence of the last paragraph of the introduction by : *In this paper, we simulate the creation of a pair of conjugate faults in an ice floe with two different VP rheologies in an idealized experiment at an unprecedented resolution of 25 m. We explore the influence of various parameters of the rheologies and the model geometry (Scale, resolution, confinement, boundary conditions, and heterogeneous initial conditions).*

R2#5, Page 2 line 4. The appropriate references for efficient solution is Hutchings et al. 2004 or Jean-Francois Lemieux et al. 2010, I would not call LSOR or Hibler's method, which I used in the 2005 paper, as efficient. This introduces the efficient solution method that correctly couples P and U, for a convergent plastic solution. This solution method was not used in Hutchings et al. 2005. Hutchings et al. 2005 is the correct reference for qualitatively reproducing LKFs in the viscous plastic model.

Thank you, we corrected the citations.

R2#6, Page 2 line 15: MEB? typo? I think you need to introduce the acronym for the Maxwell-Elastic-Brittle model here.

Corrected as suggested. We replaced "*Viscous*" by "*Maxwell (viscous)*"

R2#7, Page 2, line 24: argues → argued.

Corrected as suggested.

R2#8, Page 2, line 31: Flato and Hibler 1992 is not a mohr colomb relationship. The cavitating fluid behaves very differently and the first SIMIP (see work by Kreyscher and Harder) indicated this was not a suitable stress-strain relationship for sea ice. Also check that Ip et al. 1991 is not using a different flow rule to Tremblay's. I am wondering if you are missing text here, as these two references were left hanging

The mohr-coulomb yield curve was presented in the appendix of the Flato and Hibler (1992) paper as a possible extension to the cavitating fluid sea ice model. The way we referenced it in the paper was mis-leading.

We replaced the last sentences of this paragraph by : *" Alternative VP rheologies were never widely used in the community. These include a Coulombic yield curve with a normal flow rule (Hibler and Schulson, 2000), a parabolic lens and a tear-drop (Pritchard, 1975), a diamond-shape yield curve with normal flow rules (Zhang and Rothrock, 2005), a Mohr-Coulomb yield curve with a double-sliding deformation law (Tremblay and Mysak, 1997) or a curved diamond (Wang, 2007)."*

Page 2, some important points that I do not think are clear in your introduction:

R2#9, The Elastic-Plastic model developed during AIDJEX was based on assumptions of a material with embedded cracks in all directions that are sub-grid scale. This is closer to a ductile material than granular material.

Assuming that cracks are present in the pack ice in all direction was used to justify the isotropic assumption in the Coon et al. (1974) - later corrected in Coon et al. (2007) where the authors argued that an anisotropic assumption should be used instead. The coarse resolution of sea ice models did nothing to motivate taking into account the granular nature of sea ice in early works on sea ice models.

We have clarified this point in the revised introduction on page 2 of the revised manuscript as *"Originally, Coon et al. (1974) assumed sea ice to have cracks in all directions, justifying isotropic ice properties and isotropic rheologies."*

R2#10, The Viscous-Plastic model is only considered valid on coarse resolution (Hibler 1977). It is possible to consider this model with the ice always being in a state of plastic failure, until you get to high resolutions that allow representation of ice areas between fractures, when the viscous creep, while numerically small, is unphysical. At small scales an elastic model is appropriate for low stress states. The viscous behaviour inside the yield curve is often treated as regularisation required for numerical solution.

It is true that VP rheologies are valid only at coarse resolution, but a lot of recent works feature the use of high-resolution simulation with VP models that already break this assumption (e.g. Wang et al., 2006; Hutter et al., 2018a) We also think that Viscous behavior is a regularisation of small deformations for the numerics. However it looks to us like a detail that may not need to included in the introduction. We propose to add this in the description of the VP rheology in section 2.2

We added in page 2 of the revised manuscript: *"At any scale, the assumption of viscous creep for small deformations is not physical and an elastic model would be appropriate for low stress states. The long viscous time scale, compared to the synoptic time scale of LKFs, of order 30 years (Hibler, 1979), however, allows viscous deformation to be viewed as a small numerical regularization with little implications for the dissipation of mechanical energy from the wind or ocean current (Bouchat and Tremblay, 2014), and the ice model can be considered as an ideal plastic material."*
We also added on page 6 of the revised manuscript the sentence *"Internal ice stress below these thresholds leads to highly viscous (creep) flow that parameterizes the bulk effect of many small reversible elastic deformation events. The timescale of viscous deformation is so high ($\simeq$ 30 years) that viscous deformation can be seen as regularisation for better numerical convergence*

in the case of small deformation..”

R2#11, Personally I think it is still not clear that the failure mode of a single floe is the same as an aggregate of floes. This has not been shown observationally or with models, and statements of scale invariance based on observed qualitative correspondence between failure modes in the lab (cm scale) and ice pack (10-100km scale) do not extend to the floe scale.

By conception, sea ice models used today are scale independent and are being used at resolution approaching the floe scale. We added a sentence to specify that the fracture process at the floe scale as not been shown to have the same failure mode as at arctic and lab scales.

We added a sentence on page 3 of the revised manuscript: ***”The scale invariance of the fracture processes at the floe scale has not yet been shown, especially due to the lack of observations at both high spatial and temporal resolution.”***
We also added on page 2 of the revised manuscript: ***”It can be argued that if the mode of deformation of a single floe is similar to that of an aggregate of floes, a given rheology developed for a continuum can still be applicable at spatial resolutions of the order of the floe size (Overland et al., 1998), but the validity of a given flow rule across scales is not clear.”***

R2#12, Page 3 Discussion regarding orientation of intersecting LKFs from RGPS: I performed a similar analysis back in the early 2000’s and never published the result, which was a wide spread in intersection angle. The reason I did not publish this is because I realised that the RGPS product could potentially be capturing fracture zones that form at different times, and therefore in the product appear to be a conjugate pair because they intersect, but they are not because they were not formed under the same confining stress. This is really obvious if you spend some time on the ice pack in winter and observe leads forming and working. RGPS is not the right satellite product to use to identify conjugate fault pairs in sea ice. Hence I disagree that you can state ”The wide range of intersection angles is presumably due to previous deformation history and associated hetrogeneity in the ice cover that dictates the strength locally”.

Thanks for pointing this out here and also in a recent conversation with co-author Tremblay. It is correct that RGPS data represent a mean over 3 days and for this reason we cannot be certain that intersecting fractures were formed simultaneously. In revising the paper, we have downplayed the RGPS as a dataset used for validation/motivation as per your suggestion and that of the other reviewer.

R2#13, page 3, line 32: Just want to clear up one very important point about my 2005 paper. It is steep stress gradients in the model sea ice stress field that allow LKFs to form. I suspect this opening is related to an instability in the model identified by Nico Gray (Gray and Kilworth 1995). We seeded stress gradients though a random number being added to P* (which defines compressive strength). At the time I wrote this paper I was obsessed with plastic convergence of the VP solution, so made sure there were no spurious stress values due to the numerical error. The pan-Arctic model of Heil’s included in this paper, and other VP models, are able to show LFKs because of the noise introduced by not converging fully to the yield curve. If you play around with a VP model you can create divergence related instabilities along gradients in forcing (e.g. non-smoothly interpolated wind fields), or even have the model blow up and crash due to one localised discontinuity in thickness (e.g. I have seen this when using a nudging method to assimilate data into the CICE model that created open water locally). The reason I bring

this up is that I feel it is very important that people understand how the VP model can create LKFs. The mechanism is quite different from what might actually be happening in a granular or brittle material. I would be very happy to advise on experimental design, repeating and following up on my investigations 15 years ago.

Simulation by Lemieux and Tremblay (2009) show LKFs in a fully converged solution using the JFNK method (Lemieux et al., 2010) using a realistic but smooth thickness and concentration field. In the response to reviewer document for the Lemieux and Tremblay paper (not published), we also showed LKFs in idealized experiments with a constant thickness and concentration field. In the present paper, we also show clear discontinuity in the strain rate fields that becomes apparent in the thickness and concentration field after some integration. We see the VP model as an ideal plastic model as opposed to a viscous plastic model given that the time scale associated with the viscous term (for the default $\eta_{\max}$ an $\zeta_{\max}$) is $\sim$ 35 years and LKFs form over time scale of a few days. So, for all practical purposes, the viscous term does not operate on time scale of interest to LKFs formation. Ideal plastic material in turn can be viewed as an elastic-plastic material with an infinite elastic wave speed (stresses adjusts instantaneously with the forcing in in the "elastic" regime and can form linear kinematic features. For all these reasons, we think that the instability described in Gray and Killworth (1995) is not responsible for the formation of LKFs in a VP model. A formal comparison between elastic-viscous-plastic (MEB) model and a viscous-plastic model is underway by one of the co-authors. This will be studied in more details in that paper. Further discussion with the reviewer on this topic will be very welcome.

R2#14, page 3, line 34: The original study on shape of yield curve and ice arches is in Billy Ip's thesis, that was published later by Hibler in Hibler et al. (2006).

This reference was added to the introduction on page 3 of the revised manuscript. Thanks for pointing this out.

R2#15, page 8, line 14. A reader unfamiliar with numerical solution of the VP model will need some guidance as to what non-linear and linear iterations are. I know you are talking about the sub-cycling to reach plastic equilibrium (or close to it) and converge the velocity solution at each time step. Perhaps use language that is more obvious to a casual reader. Incidentally, did you check convergence properties? Just curious. I think you point out somewhere that the modified coulombic rheology is slower to converge - I found that solutions for yield curves with corners never converged fully. A frustrating reality! If you follow my suggestions to delve into why the model creates LKFs you will need a full description of the interative process and convergence characteristics.

Our theory of yield curve added in appendix B gives an explanation of why a yield curve with corners gives poor convergence. We modified this paragraph to improve clarity about the LSR solver scheme and the presence of sub-cycles (or outer-loops), as also asked by the other referee.

We modified the text describing the numerical solver : ***We solve the non-linear sea-ice momentum equations with a Picard or fixed point iteration with 1500 non-linear or outer-loop (OL) iterations. Within each non-linear iteration, the non-linear coefficients (drag coefficients and viscosities) are updated and a linearized system of equations is solved with a Line Successive (over-)Relaxation (LSR) (Zhang and Hibler, 1997). The linear iteration is stopped when the maximum increment is less than*** $\epsilon_{LSR} = 10^{-11}\, m\, s^{-1}$***, but we also limit the number iterations to 1500. Typically, 1500 non-linear iterations are required to reach a converged solution. This is so because of slow convergence due to the highly non-linear rheology term and the high spatial***

resolution (Lemieux and Tremblay, 2009).

R2#16, page 8, results section: Describe what the applied strains are in the numerical experiments (magnitude, not just direction).

The specified strains are described in equation 17 on page 8 of the original manuscript (or page 8 of the revised paper), and their magnitude is documented in Table 1. We use the same strains for all experiments, excepted for the up-scaled experiment where the magnitude of the strain is up-scaled as well.

R2#17, Page 8 line 26: What are the default parameters? I think you forgot to reference table 1.

We added the reference to Table 1 on page 9.

R2#18, page 9, line 4: Regarding your statement "Fracture occurs when the stress state intersects the yield curve". Plastic failure occurs then. The fact that a "fractures" form is because the ice deforms at a stress discontinuity where the stress accumulates and reaches yield. You are correct in pointing out that the strain-rate has characteristic directions along which divergence will occur, defined by the shape of the yield curve and flow rule. It is this divergence, relative to the confining stress, that defines the directions of the linear deformation features in the model runs.

We agree on this, this paragraph have been modified to clarify this point.

This sentence has been rephrased as ***Fracture occurs after plastic failure when the stress state reaches the yield curve and the ice starts to move in divergence.*** for clarity.

R2#19, Comment on differences between 3.1 and 3.2: The change in nature of cracks when you decrease the number of internal iterations (linear iterations) is probably related to the fact that the ice stress field is more heterogeneous (further from the converged solution) and the LSOR method tends to create noise in the stress field and smoothes with increasing number of iterations (unlike the SIMON method I proposed, Hutchings et al. 2004, that has a smoother convergence to the yield curve). Hence there are more points where LKFs can nucleate when you reduce the number of internal iterations. This is just a suggestion, with out looking at the stress fields in your experiments I can not tell you if this is what is actually happening. Incidentally, another unpublished result that I presented at AGU in 2003: The VP model can create intersecting deformation features across the entire Arctic Ocean is you do not converge to plastic equilibrium and are not careful in smoothing the solution between time steps (which can be done numerically through the choice of advection scheme or Bill's introduction of artificial diffusion in his 1979 paper). I never followed up this work. I suspect that this is a direct consequence of Gray's instability. This instability is damped by the addition of numerical diffusion (or artificial diffusion) in the solution proceedure. We might think the resultant strain-rate fields are more realistic, I just do not believe using the non-convergence and numerical instability is an appropriate way to model the process because we are not controlling the nature of the stress concentrators or stress propagation in the model appropriately. The key point is that the ice pack strength is highly heterogeneous and while we do not know the nature of the stress concentrators in the ice pack, they are likely to be more randomly distributed (which non-convergence to the yield curve might be approximating, but is not controlled for). There is a need to understand the nature and distribution of the stress concentrators in sea ice, so we can appropriately model this. And it would really help future sea ice modellers to point out this issue more clearly in papers that investigate LKFs in the viscous-plastic model.

We are afraid that there is a misunderstanding. The results of section 3.2 (3.2.1 in the revised manuscript) do not critically depend on the number of non-linear iterations. The section 3.2 uses less iterations because we wanted to run the idealized experiment for a longer time, but we do not intend to compare the effect of the number of iterations. If we use the same low number of iterations for the experiments in section 3.1, we obtain almost the same shear pattern although the shear lines are not so well defined. We improved the description in the beginning of 3.2 to try to avoid any misunderstandings. We more than agree with the last statement in this comment.

The description of this experiment is now in Section 3.2.1 of the revised manuscript on page 12 and reads *"Continuing the integration to 2700 seconds (45 min), compared to 20 seconds in the reference simulation leads to the creation of smaller diamond-shaped ice floes due to secondary and tertiary fracture lines (Figure 5). The openings are visible in the thickness and concentration fields with thinner, less concentrated ice in the lead. In this longer experiment, the sea ice also ridges, for instance at the center of the domain where the apex of the diamonds fails in compression. There is also some thicker ice at the northern boundary induced by the specified strain rate at the northern boundary. The fracture pattern and presence of secondary and tertiary fracture lines are in line with results from laboratory experiments Schulson (2004) and with AVHRR and RGPS observations. "* .Figure 6 is on page 14 of the revised manuscript

R2#20, Figure 7: Nice illustration of the role of boundary conditions on the stress solution.

We thank the reviewer.

R2#21, Section 3.5: Good illustration. I would suggest you critically look at the stress fields in your previous experiments to identify what the stress concentrators are there. Did you forget to reference figure 9 in this section. Finally, Bill Hibler has shown similar results where embedded fractures of different orientations would join together to form larger scale fracture patterns. Not sure he published that, but I think he did. Look at the papers he wrote with Aksenov and his first anisotropic paper with embedded leads in grid cells. Unfortunately I am on an airplane right now and don't have access to his papers.

A reference to figure 9 is present on line 17 of the original manuscript. We added the reference to Aksenov and Hibler (2001) In the revised manuscript on page 15. Thanks for pointing this out. We do not have stress concentrators in the previous experiments, except for Figure 7b where the no slip southern boundary forces the fracture to take angle solely determined by geometry.

R2#22, page 16 line 1: Here and in other places you confuse the simulation with reality. "This is in contrast with other granular materials". Remove "other", as this is in contrast with granular materials. The VP model is not modelling a granular material. While sea ice may be a granular material, the rheology is designed for different behaviour.

"Corrected as suggested. Thanks for picking this up. We do understand that model and reality are different!.

R2#23, page 16 line 5: "larger that what" → "larger than that"

Corrected as suggested.

R2#24, page 16, line 9: I would like to see the strain-rate field for the longer simulation with e=0.7 where deformation is in convergence. Where in the field is the

ridging occurring? What do the intersection angles look like?

Figure 11 shows the fracture for $e = 0.7$ after 5 seconds. We added a figure showing the ice field with e=0.7 for 2700 seconds (45 minutes) o, similar to Figure 6.

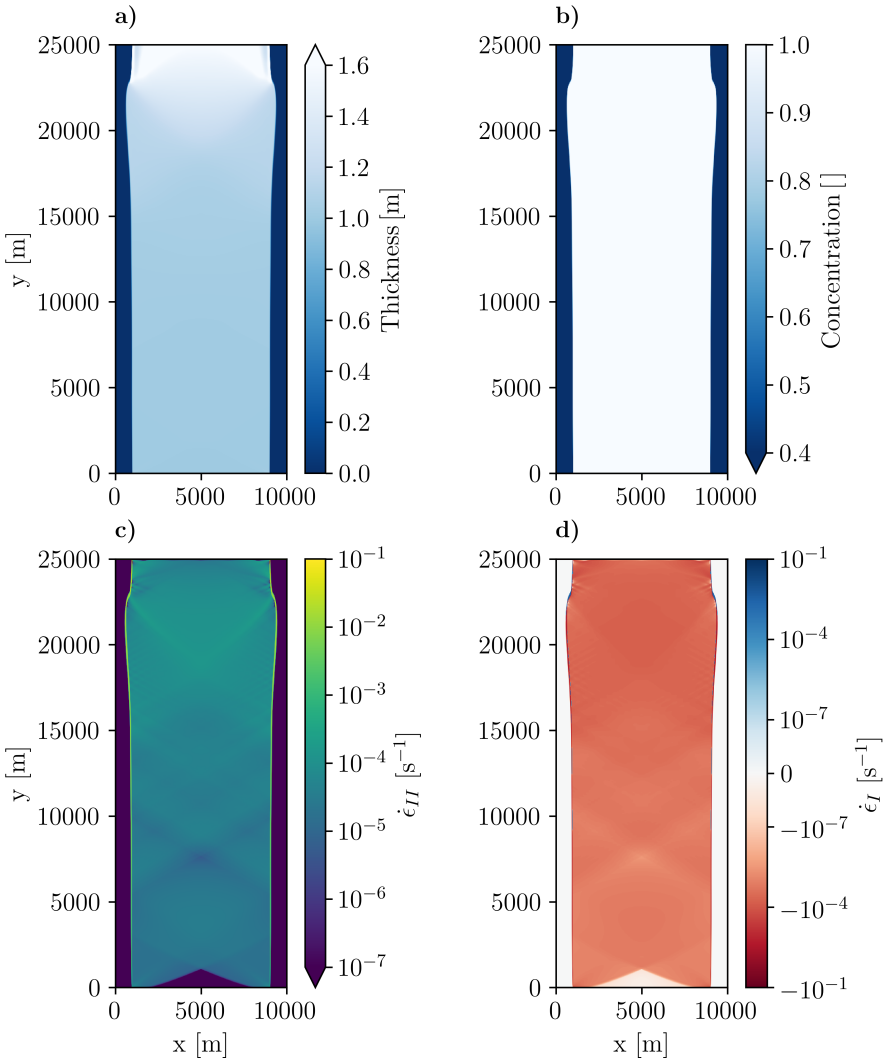

Figure 1: Sea ice thickness (a), concentration (b), maximum shear strain rate (c) and divergence (d) after 45 min of integration (2700 sec) in a uni-axial loading test with an ellipse ratio $e = 0.7$. To make these longer simulations possible, both non-linear and linear iterations are limited to 150 per timestep. Results show that no fracture lines are created, but the ice is pilling close to the northern boundary and the ice got broader without creating open-water.

R2#25, page 17 line 2: "and individual floes form" could be clarified as "4 separate floes form". **Corrected as suggested.**

R2#26, page 17 line 15: Please clarify the statement "the fracture pattern is very sensitive to coefficient of internal friction. This makes measuring the fracture angle very difficult." Surely the sensitivity will help you differentiate fracture angles. Incidentally mu was not defined in section 2 or here. What causes the spread in the stress state? Is this related to the opening/ridging and subsequent ice strength changes? So the spread in stress state is controlled by the strength parameterisation. I feel this is important to point out, because it is another control we have on the spread of intersection angles you

might see under a particular confining stress.

We wanted to express that we observe different behavior depending on the value of μ. We revised the text by rewording this part along a whole paragraph on page 20 of the revised manuscript.

we also added a sentence in section 2.2 defining μ : *"[..] where μ is the slope of the Mohr-Coulomb limbs (Fig. 1), c is the cohesion value (the value of σ_{II} for $\sigma_I = 0$) defined relative to the tensile strength by $c = \mu \cdot T^{\star}$."*

R2#27, page 17 line 25: Clumsy language: "the stress state touches the yield curve on both parts of the yield curve." Very unclear that you mean the stress state falls on the coulombic limb and the ellipse cap. rephrase.

We modified the whole section describing the Coulombic yield curve experiments, on page 18-19 of the revised manuscript. We hope it clearer now.

R2#28, page 19 top paragraph: This is a matter of opinion. I disagree that the ice pack is characterised by diamond shaped floes. Yes, diamond floes form under certain confining stresses, but is this the most prevalent mode of failure in winter? That needs to be proven. This point does not discount your use of your numerical experiments to differentiate between rheologies, but it does question if an anisotropic rheology based on diamond shaped floes is appropriate for all space and time.

We clarified this point in the revised manuscript on page 21 of the revised manuscript.

We modified the text on page 20-21 of the revised manuscript to state : *"The Elastic Anisotropic Plastic (EAP) rheology assumes predominately diamond shaped floes in sea ice (Wilchinsky and Feltham, 2006). A sea ice model with EAP creates sharper fractures than a model with the Elastic Viscous Plastic (EVP, Hunke and Dukowicz, 1997) rheology (Heorton et al., 2018). The authors concluded that the anisotropic model may improve the fracturing process for sea ice, especially by creating areas of oriented weaknesses, and particularly at coarse resolution where the fracture is not resolved by the grid spacing. In the experiments presented here, the VP rheologies lead to sharp and anisotropic fracture lines without any additional assumptions."*

R2#29, Also, did you calculate characteristic directions for the VP model to confirm these are controlling the diamond structures in your simulations? I have a code somewhere (from 15 years ago) that does this. If I can find it I can give it to you.

No we did not. But using the theory we described for the Coulombic yield curve in the original manuscript, we can know predict the fracture angle for the elliptical yield curve. This theory is presented in Appendix B of the revised manuscript.

R2#30, page 19 line 12: This sentence is miss-representative: "Thus, the rheology is shown to be scale independent ... in line with observations". Your numerical experiment is set up to ensure the behaviour is scale independent from the scale of the grid size to the domain size. You would really hope your numerical experiment results do not depend on resolution (good practice to check this) and there is no reason scale should change intersection angles for the reasons you have stated previously. Rephrase this statement so someone does not quote it as evidence supporting Schulson's hypothesis.

We modified the sentence on page 21 of the new manuscript to be *"The fracture angles do not depend on the spatial resolution and domain size as expected in our idealized numerical experiment setup (Sect. 3.2.1, Fig. 5)"*

R2#31, page 19, line 20: Just to clarify, the reason the experiments with thin ice change the fracture angle is because the presence of the thin ice modifies the stress state across the domain. So with an ellipse this will change the intersection angle, with a coulombic rheology it would not. I feel this part of the paragraph needs more clarification.

we modified the sentence on page 21 of the revised manuscript :

"The confining pressure (i.e. thin ice imposed on the side of the domain) changes the distribution of stress within the domain. This results in different deformation patterns (shear and divergence) and different fracture angles because the yield curve is convex and uses a normal flow rule."

R2#32, page 19 line 22: Your interpretation of the RGPS data (if one believes the intersection angles are at conjugate pairs and not leads formed at separate times) would lead one to believe that there is not a constant fracture angle independent of confining stress.

The macroscopic angle of friction in a granular material is not constant and depends on the distribution of the contact normal between floes (Balendran and Nemat-Nasser, 1993). A consequence of a variable macroscopic angle of friction is fracture angle that is not constant. This work is beyond the scope of the present paper.

R2#33, page 20 line 2: Perhaps clarify that the Miller et al. (2005) experiments were using metrics of ice thickness, area and velocity to determine the optimal yield curve shape. It is my memory they did not consider the form of the ice strength parameterisation as an alternative to changing shear strength, or yield curve shape, just the eccentricity of the ellipse.

We think that the metrics do not matter in this context. We would like to keep it simple here, because we are only referring to change of e.

We added on page 21 of the revised manuscript *"Arctic-wide simulations improve metrics of sea ice concentration, thickness and velocity by decreasing the value of e of the standard elliptical yield curve, that is, by adding shear and bi-axial tensile and compressive strength (Miller et al., 2005; Ungermann et al., 2017)."*

R2#34, page 20 line 5: Can you show that your numerical experiments are consistent with Pritchard (1988).

Yes, we can. The fracture angle relative to principal stress corresponds to the angle between the principal stress and characteristics directions given by Pritchard (1988) or Wang (2007). We have added an appendix B with a theory explaining the fracture angle of the yield curve using Mohr's circle. Theory that gives the same relation between the slope of the tangent to the yield curve and the fracture angle.

R2#35, page 20 line 8: questions → questioned

Corrected as suggested.

R2#36, After reading your discussion I wondered if the tear drop yield curve (originally proposed by Pritchard) might be more appropriate that the Hibler modified ellipse / mohr coulomb.

We note that the kink in the MC yield curve of Hibler and Schulson (2000) cannot be eliminated by choosing appropriate values of P* and e. Also, both tear drop and ellipical yield curve use the normal flow rule and have a convex yield curve, which gives the non-physical behavior of the fracture angle as a function of shear strength and confining pressure. It is also known that a normal flow rule with "straight limbs" gives too much dilatation when the stress states are lying on the straight limbs (as stated in Flato and

Hibler, 1992). For this reason we believe that a Mohr-Coulomb or a tear drop with a non-associated (normal) flow rule (e.g. Tremblay and Mysak, 1997) would be more appropriate. This is the subject of future work.

R2#37, Also, Hibler and others recognise that you must have a closed cap on a coulombic rheology to allow ridging. Perhaps the ellipse is not the best choice for this. In engineering it is more common to have a flatter closure to the yield curve.

The flatter closure actually would lead to other problems, if we look at the framework we develop in the new version of the appendix ??, and also with the theory of the characteristics of the yield in Pritchard (1988). A slope of yield curve higher than $|b'| = 1$ does not have solution for fracture.

R2#38, page 20 line 26: sensible → sensitive

Corrected as suggested.

R2#39, page 20 line 26: Another example where it is not so clear you are talking about the VP rheology problem: "The fracture angles is also sensitive to the surrounding sea ice cover, in contradiction to the granular nature of sea ice". Also, the stress field is going to depend on surrounding ice even when the ice is modelled as granular, which I am not sure is what you were meaning to imply is not true for granular materials. I think you need to clarify the language, and I think I disagree with you that this test is suggesting ice is granular - it would be something we could test in an ice tank to find out what the actual behaviour is though. I feel you do not highlight a key result in the paper: That fracture angles below 30o are not possible with the elliptical rheology, and that this is in direct conflict with observational evidence for smaller fracture angles. Even in light of errors of interpretation of the RGPS intersection angles this result still holds.

Thanks for pointing this out. We have made this result (fracture angle below 30deg not possible with ellipse) more prominent on page 22 of the revised manuscript. If we think of the nature of sea ice, it is a granular material composed of floes. At no or small confinement, the ice dynamic is mainly governed by the floes lateral interaction. The difference with "classic" granular material (sand, clay,...) the ice is a 2D material bounded to float on the ocean. So at high confinement the ice can "escape" in 3D and ridge or raft. We agree that sea ice should have different behavior for high and low confinement. This is the conclusion also reached by Wang (2007) if we look at their Figure 5, even if we disagree with the shape of their yield curve.

The first paragraph of the conclusion have been replace by the 4 following :

In our experimental configuration with uni-axial compression, fracture angles below 30° are not possible in a VP-model with an elliptical yield curve. Observations suggest much lower values. We find an empirical relationship between the fracture angle and the ellipse ratio e of the elliptical yield curve that can be fully explained by the convexity of the yield curve (Appendix B). In contrast to expectations, increasing the maximum shear strength in the sea ice model increases the fracture angle. Along a fracture line, there can be both divergence and convergence depending on the shear strength of the ice, linked to the flow rule. The simulated ice opens and creates leads with an ellipse ratio $e > 1$ (shear strength is smaller than compressive strength), and ridges for $e < 1$ (shear strength is larger than compressive strength).

With a modified Coulombic yield curve, the fracture angle can be decreased to values expected from observations, but the non-differentiable corner points of this yield curve lead to numerical (convergence) issues and, for some values

of the coefficient of internal friction μ, to fracture patterns that are difficult to interpret. At these corner points, two different slopes meet and give two non-unique solutions for fracture angles and deformation directions. We recommend to avoid non-differentiable yield curves (with a normal flow rule) in viscous-plastic sea ice models.

More generally, the model produces diamond-shaped fracture patterns. Later the ice floe disintegrates into several smaller floes develop. The fracturing process in the ice floe in our configuration is independent of the experiment resolution and scale, but sensitive to boundary conditions (no-slip or free-slip). The fracture angle in the VP-model is also sensitive to the immediate environment. This is not consistent with the notion of sea ice as a granular material. Unsurprisingly, the yield curve plays an important role in fracturing sea ice in a numerical model as it governs the deformation of the ice as a function of the applied stress.

R2#40, page 21 line 3: Note that at cusps in a yield curve two possible solutions are possible. I feel you can clarify your point about not using non-differentiable yield curves. They are also numerically unstable. The unclear fracture pattern is not something I have issue with. Perhaps this exists in reality when the stress state can spread across opening and closing modes.

Unclear (or chaotic) fracture pattern could happen in reality when there is an high heterogeneity in ice strength, concentration and thickness, but it shall not happen in a uni-axial compression experiment with uniform ice field.

We added the following sentence on page 22 of the manuscript : *"At these corner points, two different slopes meet and give two non-unique solutions for fracture angles and deformation directions."*

R2#41, page 21 line 10: I feel you can be stronger here in stating that the ellipse with normal flow rule can be discounted as unphysical.

We added a sentence in the revised manuscript:

We modified the text on page 22 of the revised manuscript *"In our experimental configuration with uni-axial compression, fracture angles below 30° are not possible in a VP-model with an elliptical yield curve. Observations suggest much lower values. We find an empirical relationship between the fracture angle and the ellipse ratio e of the elliptical yield curve that can be fully explained by the convexity of the yield curve (Appendix B)."*

R2#42, page 21 line 11:
Scale is really unimportant in these experiments. You can perform them on any scale. The more important question is what scale do these types of fracture events actually occur on and can that be resolved in models?

As stated in comment R2#30, we agree on the fact that the scale of such idealized experiment is not important. It appeared important to us to show this fact with simulations. The standard VP model is used by the community at various scales and resolution depending on the goal of each particular studies, i.e. paleoclimate studies and sea ice prediction for ships operations, so the fact that the VP rheologies are scale-independent is important to point out. The observations of spatial power-law scaling in sea-ice deformation down shows that the fracture does not have a preferred scale. The scaling behaviour is seen at lengths ranging from basin scale in satellite observations (Marsan et al., 2004)

down to 50m in ship radar observations (Oikkonen et al., 2017). At high resolution VP-simulations are able to reproduce this spatial scaling behaviour while underestimating the intermittency in temporal scaling (Hutter et al., 2018a). The resolution used in our study is in between the one used in (Hutter et al., 2018a) and the lower limit of scales where we observe power-law scaling.

We replaced the aforementioned sentence by ***"If Arctic-wide sea ice simulations with a resolution of 25 m are not feasible today because of computational cost, we can still imagine small experiments to be useful for process modeling on small scales when local and high-resolution observations (e.g. wind, ice velocities) are available. For example, such process modeling studies could be used to constrain the rheology with data from the upcoming MOSAiC campaign (Dethloff et al., 2016) that will provide a full year of sea ice observations in pack ice."***

R2#43, I see you did not reference work by K. Wang (2007) who used lead intersection angles to try to estimate the shape of a yield curve. He also has a paper were he performed a similar study to you (Wang and Wang 2010), however for the pan-arctic and perhaps with convergence issues that make his findings hard to interprete. While this work suffered from problems of representativeness of the observational data (how can you be sure fractures formed at the same time), as you do, I feel you should consider Wang's papers in light of your findings.

We now included a discussion of the results and findings of these the first references On page 21 of the revised manuscript. We did not wish to include the second one because of the strong convergence issues.

we added the text ***"Based on the results of Pritchard (1988), Wang (2007) used observed fracture patterns to design a*** Curved Diamond ***yield curve. But this yield curve also contains a non-differentiable point, which will be problematic for numerical reasons."***

R2#44, Finally, I believe that the stress state between fractures in your numerical experiments is inside the yield curve (viscous), and the motion close to zero. Is this correct, it was what I found when I was working on this. Just a point to clarify that the accumulation of stress along fractures is due to the yield curve discontinuity, and the associated characteristic directions in the strain field that control the propagation of fracture direction. This accumulation of stress needs to be nucleated at a location with high stress gradient (such as a corner on the boundary or strength/stress difference between grid cells). Once the stress reaches the yield curve, the numerical instability is probably put into play during the inner iterations. You do not see LKFs in VP models that have smooth boundaries and strength fields. The formation of LKFs is grid resolution dependent (as the linear instability identified by Gray is). You have speculated on why LKFs form in the VP model only at higher resolutions in a previous paper and I would suggest the place to look is in the convergence of the solver, and the splitting of velocity solution from the ice strength (pressure). I do not think it is just the fact that divergence (and strength reduction) can be greater at higher resolution. Clarifying this mechanism will help readers understand why VP models show this behaviour. It will also hopefully get people thinking about how to represent stress accumulators in the model, because many people using the VP model and studying fractures are unaware of how the model produces these.

Jenny

The stress states outside of the LKFs are effectively inside the yield curve, at the

exception of the cells on the border of the ice floe, that move into open-water. We think that the creation of fractures in the model VP is explained by the Mohr's circle and failure envelope theory and we create LKFs in our uniform ice strength field. We have added a new appendix discussing this, Appendix B.

References cited in this referee comments

Gray and Kilworth (1995) Stability of the viscous plastic sea ice rheology. J. Phys. Ocean. 25(5), 971-978.

J-F. Lemieux, B. Tremblay, J. Sedlacek, P. Tupper, S. Thomas, D. Huard, J-P. Auclair. 2010. Improving the numerical convergence of viscous-plastic sea ice models with the Jacobian-free Newton-Krylov method. J. Comp. Phys., 2840-2852.

Hutchings J.K., H. Jasak and S. W. Laxon 2004. A strength implicit correction scheme for the viscous-plastic sea ice model. Ocean Modelling.

Hibler W.D. III, J.K. Hutchings, and C. F. Ip, 2006. Sea-ice arching and multiple flow state of Arctic pack ice. Ann. Glaciol. 44.

Hibler W.D. III. 1977. A viscous sea ice law as a stocahastic average of plasticity.

Wang, K. 2007, Observing the yield curve of compacted pack ice, J. Geophys. Res. 112, C05015.

Wang, K. and Wang, C. 2010, Modelling linear kinematic features in pack ice, J. Geophys.Res. 114, C12

References

Aksenov, Y. and Hibler, W. D. (2001). Failure Propagation Effects in an Anisotropic Sea Ice Dynamics Model. In Dempsey, J. P. and Shen, H. H., editors, *IUTAM Symposium on Scaling Laws in Ice Mechanics and Ice Dynamics*, Solid Mechanics and Its Applications, pages 363–372. Springer Netherlands.

Balendran, B. and Nemat-Nasser, S. (1993). Double sliding model for cyclic deformation of granular materials, including dilatancy effects. *Journal of the Mechanics and Physics of Solids*, 41(3):573–612.

Bouchat, A. and Tremblay, B. (2014). Energy dissipation in viscous-plastic sea-ice models. *Journal of Geophysical Research: Oceans*, 119(2):976–994.

Bouchat, A. and Tremblay, B. (2017). Using sea-ice deformation fields to constrain the mechanical strength parameters of geophysical sea ice. *Journal of Geophysical Research: Oceans*, pages n/a–n/a.

Coon, M., Kwok, R., Levy, G., Pruis, M., Schreyer, H., and Sulsky, D. (2007). Arctic Ice Dynamics Joint Experiment (AIDJEX) assumptions revisited and found inadequate. *Journal of Geophysical Research: Oceans*, 112(C11):C11S90.

Coon, M. D., Maykut, A., G., Pritchard, R. S., Rothrock, D. A., and Thorndike, A. S. (1974). Modeling The Pack Ice as an Elastic-Plastic Material. *AIDJEX BULLETIN*, No. 24(Numerical Modeling Report):1–106.

Dempsey, J. P., Xie, Y., Adamson, R. M., and Farmer, D. M. (2012). Fracture of a ridged multi-year Arctic sea ice floe. *Cold Regions Science and Technology*, 76-77:63–68.

Dethloff, K., Rex, M., and Shupe, M. (2016). Multidisciplinary drifting Observatory for the Study of Arctic Climate (MOSAiC). *EGU General Assembly Conference Abstracts*, 18.

Erlingsson, B. (1988). Two-dimensional deformation patterns in sea ice. *Journal of Glaciology*, 34(118):301–308.

Flato, G. M. and Hibler, W. D. (1992). Modeling Pack Ice as a Cavitating Fluid. *Journal of Physical Oceanography*, 22(6):626–651.

Gray, J. M. N. T. and Killworth, P. D. (1995). Stability of the Viscous-Plastic Sea Ice Rheology. *Journal of Physical Oceanography*, 25(5):971–978.

Heorton, H. D. B. S., Feltham, D. L., and Tsamados, M. (2018). Stress and deformation characteristics of sea ice in a high-resolution, anisotropic sea ice model. *Phil. Trans. R. Soc. A*, 376(2129):20170349.

Herman, A. (2016). Discrete-Element bonded-particle Sea Ice model DESIgn, version 1.3a - model description and implementation. *Geoscientific Model Development*, 9.

Hibler, W. D. (1977). A viscous sea ice law as a stochastic average of plasticity. *Journal of Geophysical Research*, 82(27):3932–3938.

Hibler, W. D. (1979). A Dynamic Thermodynamic Sea Ice Model. *Journal of Physical Oceanography*, 9(4):815–846.

Hibler, W. D. and Schulson, E. M. (2000). On modeling the anisotropic failure and flow of flawed sea ice. *Journal of Geophysical Research: Oceans*, 105(C7):17105–17120.

Hunke, E. C. and Dukowicz, J. K. (1997). An Elastic–Viscous–Plastic Model for Sea Ice Dynamics. *Journal of Physical Oceanography*, 27(9):1849–1867.

Hutchings, J. K., Heil, P., and Hibler, W. D. (2005). Modeling Linear Kinematic Features in Sea Ice. *Monthly Weather Review*, 133(12):3481–3497.

Hutter, N., Martin, L., and Dimitris, M. (2018a). Scaling Properties of Arctic Sea Ice Deformation in a High-Resolution Viscous-Plastic Sea Ice Model and in Satellite Observations. *Journal of Geophysical Research: Oceans*, 123(1):672–687.

Hutter, N., Zampieri, L., and Losch, M. (2018b). Leads and ridges in Arctic sea ice from RGPS data and a new tracking algorithm. *The Cryosphere Discussions*, pages 1–27.

Ip, C. F., Hibler, W. D., and Flato, G. M. (1991). On the effect of rheology on seasonal sea-ice simulations. *Annals of Glaciology*, 15:17–25.

Kreyscher, M., Harder, M., and Lemke, P. (1997). First results of the Sea-Ice Model Intercomparison Project (SIMIP). *Annals of Glaciology*, 25:8–11.

Lemieux, J.-F. and Tremblay, B. (2009). Numerical convergence of viscous-plastic sea ice models. *Journal of Geophysical Research: Oceans*, 114(C5).

Lemieux, J.-F., Tremblay, B., Sedláček, J., Tupper, P., Thomas, S., Huard, D., and Auclair, J.-P. (2010). Improving the numerical convergence of viscous-plastic sea ice models with the Jacobian-free Newton–Krylov method. *Journal of Computational Physics*, 229(8):2840–2852.

Linow, S. and Dierking, W. (2017). Object-Based Detection of Linear Kinematic Features in Sea Ice. *Remote Sensing*, 9(5).

Marsan, D., Stern, H., Lindsay, R., and Weiss, J. (2004). Scale Dependence and Localization of the Deformation of Arctic Sea Ice. *Physical Review Letters*, 93(17):178501.

Marsan, D., Weiss, J., Larose, E., and Métaxian, J.-P. (2012). Sea-ice thickness measurement based on the dispersion of ice swell. *The Journal of the Acoustical Society of America*, 131(1):80–91.

Miller, P. A., Laxon, S. W., and Feltham, D. L. (2005). Improving the spatial distribution of modeled Arctic sea ice thickness. *Geophysical Research Letters*, 32(18).

Mohammadi-Aragh, M., Goessling, H. F., Losch, M., Hutter, N., and Jung, T. (2018). Predictability of Arctic sea ice on weather time scales. *Scientific reports*, 8.

Oikkonen, A., Haapala, J., Lensu, M., Karvonen, J., and Itkin, P. (2017). Small-scale sea ice deformation during N-ICE2015: From compact pack ice to marginal ice zone. *Journal of Geophysical Research: Oceans*, 122(6):5105–5120.

Overland, J. E., McNutt, S. L., Salo, S., Groves, J., and Li, S. (1998). Arctic sea ice as a granular plastic. *Journal of geophysical research*, 103(C10):21845–21868.

Overland, J. E., Walter, B. A., Curtin, T. B., and Turet, P. (1995). Hierarchy and sea ice mechanics: A case study from the Beaufort Sea. *Journal of Geophysical Research: Oceans*, 100(C3):4559–4571.

Pritchard, R. S. (1975). An Elastic-Plastic Constitutive Law for Sea Ice. *Journal of Applied Mechanics*, 42(2):379–384.

Pritchard, R. S. (1988). Mathematical characteristics of sea ice dynamics models. *Journal of Geophysical Research: Oceans*, 93(C12):15609–15618.

Rothrock, D. A. and Thorndike, A. S. (1984). Measuring the sea ice floe size distribution. *Journal of Geophysical Research: Oceans*, 89(C4):6477–6486.

Schulson, E. M. (2004). Compressive shear faults within arctic sea ice: Fracture on scales large and small. *Journal of Geophysical Research: Oceans*, 109(C7):C07016.

Schulson, E. M. and Duval, P. (2009). *Creep and fracture of ice*, volume 432. Cambridge University Press Cambridge.

Tremblay, L.-B. and Mysak, L. A. (1997). Modeling Sea Ice as a Granular Material, Including the Dilatancy Effect. *Journal of Physical Oceanography*, 27(11):2342–2360.

Ungermann, M., Tremblay, L. B., Martin, T., and Losch, M. (2017). Impact of the Ice Strength Formulation on the Performance of a Sea Ice Thickness Distribution Model in the Arctic. *Journal of Geophysical Research: Oceans*, pages n/a–n/a.

Walter, B. A. and Overland, J. E. (1993). The response of lead patterns in the Beaufort Sea to storm-scale wind forcing. *Annals of Glaciology*, 17:219–226.

Wang, K. (2007). Observing the yield curve of compacted pack ice. *Journal of Geophysical Research: Oceans*, 112(C5):C05015.

Wang, K., Leppäranta, M., and Kõuts, T. (2006). A study of sea ice dynamic events in a small bay. *Cold Regions Science and Technology*, 45(2):83–94.

Wilchinsky, A. V. and Feltham, D. L. (2006). Anisotropic model for granulated sea ice dynamics. *Journal of the Mechanics and Physics of Solids*, 54(6):1147–1185.

Wilchinsky, A. V., Feltham, D. L., and Hopkins, M. A. (2010). Effect of shear rupture on aggregate scale formation in sea ice. *Journal of Geophysical Research: Oceans*, 115(C10):C10002.

Zhang, J. and Hibler, W. D. (1997). On an efficient numerical method for modeling sea ice dynamics. *Journal of Geophysical Research: Oceans*, 102(C4):8691–8702.

Zhang, J. and Rothrock, D. A. (2005). Effect of sea ice rheology in numerical investigations of climate. *Journal of Geophysical Research: Oceans*, 110(C8):C08014.

~~Modeling Sea Ice fracture at very high resolution~~ Simulating intersection angles between conjugate faults in sea ice with different VP rheologies

Damien Ringeisen [1], Martin Losch [1], L. Bruno Tremblay [2], and Nils Hutter [1]

[1]Alfred-Wegener-Institut, Helmholtz-Zentrum für Polar und Meeresforschung (AWI), Bremerhaven, Germany
[2]Department of Atmospheric and Oceanic Sciences, McGill University, Montréal, Quebec, Canada

Correspondence: Damien Ringeisen (damien.ringeisen@awi.de)

Abstract. Recent high resolution pan-Arctic sea ice simulations show fracture patterns (Linear Kinematic Features ~~-~~ or LKFs) that are typical of granular materials~~but with intersection (fracture) angles wider~~ , but with wider fracture angles than those observed ~~from~~ in high-resolution satellite images~~(with a modal value of $\theta = 20°$). In thisarticle, We investigate the mechanism of formation and parameter dependencies of ice fracture in simple numerical bi-axial test on a 8 x 25 ice floe at an unprecedented resolution of 25 for two different yield curves: an elliptical~~ . Motivated by this, ice fracture is investigated in a simple uni-axial loading test using two different Viscous-Plastic (VP) ~~and a~~ rheologies: one with an elliptical yield curve and a normal flow rule, and one with a Coulombic yield curve ~~both with~~ and a normal flow rule ~~. In~~ that applies only to the elliptical cap. With the standard VP ~~model, the simulated angle of fracture is $\theta = 33.9°$, compared to $20°$ in observations. The dependence of the angle of fracture on the ice shear strength is also contrary to that of typical granular materials with larger angle of fracture for higher shear strength- think of a wet sand castle with steeper walls than a dry sand castle. In this model,~~ rheology, it is not possible to simulate fracture angles smaller than 30°. Further, the standard VP-model is not consistent with the behaviour of granular material such as sea ice, because: (1) the fracture angle increases with ice shear strength; (2) the divergence along the fracture lines (or LKFs) is ~~entirely dictated by the ice shear strength used in the model with~~ uniquely defined by the shear strength of the material with divergence for high shear strength ~~resulting in convergence along LKFs and~~ and convergent with low shear strength~~resulting in divergence along LKFs. This is again contrary to typical granular materials where divergence (or dilation) is linked with the orientation of contacts normals that oppose the flow with divergence present for larger shear resistance and convergence for lower shear resistance. Moreover, the~~ ; (3) the angle of fracture depends on the confining pressure ~~in the uni-axial test~~ with more convergence as the confining pressure increases~~, again contrary to granular material that have an angle of fracture that is independent of the confining pressure. We note that all three behaviors~~ . This behavior of the VP model ~~are linked with the use of an associative (normal)~~ is connected to the convexity of the yield curve together with use of a normal flow rule. In the Coulombic model, the angle of fracture is smaller (~~$\theta = 23.5°$) , but the solution~~$\theta = 23°$) and grossly consistent with observations. The solution, however, is unstable when the compressive ~~stresses are~~ stress is too large because of ~~the discontinuity~~ non-differentiable corners between the straight limbs of the Coulombic yield curve and the elliptical ~~capping. Our results show thatwhile the VP model gives angles of fracture that are visually correct, the bias in the magnitude of the angle of fracture and the physical dependencies of the angle of fracture on mechanical strength parameters~~

and stress fields couple the sea ice mechanical strength parameters, the sea-ice drift, sea-ice deformation (strain-rate) field in an inconsistent way. We consider this evidence to move away from the cap. The results suggest that, although at first sight the large scale patterns of LKFs simulated with a VP sea ice model appear to be realistic, the elliptical yield curve and associative (normal) flow rule , a deformation law that is not applicable to with a normal flow rule is not consistent with the notion of sea ice as a pressure-sensitive and dilatant granular materialsuch as sea ice.

1 Introduction

Sea ice is a granular material; i.e. , that is, a material that is composed of ice floes of different size and shape (Tremblay and Mysak, 1997; Over and shapes (Rothrock and Thorndike, 1984; Overland et al., 1998). In most large-scale modelsused in the community, sea ice is treated as a continuum deforming viscous-plastic continuum. It deforms plastically when the internal stresses reaches critical values stress becomes critical in compression, shearand tensionand deforming , or tension; it deforms as a very viscous (creepingcreep) flow when the internal stresses are relatively small (e. g. Hibler (1979); Zhang and Hibler (1997); Hunke and Dukowicz (199 Using modern numerical solvers, the stress is relatively small (e.g., Hibler, 1979; Zhang and Hibler, 1997; Hunke and Dukowicz, 1997). The corresponding highly non-linear sea-ice momentum equations can be solved to convergence to reproducequalitatively observed with modern numerical solvers to reproduce, in a qualitative way, observed linear patterns of sea ice deformation with within reasonable computing time (Hutchings et al., 2005; Losch et al., 2010; Hutter et al., 2018a). These linear features where large shear and divergence are present are called (Hutchings et al., 2004; Lemieux et al., 2010; Losch et al., 2010; Hutter et al., 2018a). These Linear Kinematic Features (LKFs) (Kwok, 2001). Lead opening are places of large shear and divergence (Kwok, 2001). Leads that open along LKFs are the memory responsible for an emergent anisotropy of such models, affecting the subsequent dynamics, mass balance, and the heat /salt and matter exchanges between the ocean, ice and atmosphere. It is therefore important to investigate whether the mode of sea-ice fracture is represented accurately in continuum sea ice models.

The sea-ice momentum equations are difficult to solve numerically sea ice dynamics are complicated because of sharp spatial changes in material properties associated with discontinuities (e.g. along sea ice leads or ridges) and heterogeneity (different ice types)in the pack ice spatially varying ice thickness and concentration). The sea ice momentum equations are difficult to solve numerically because of the non-linear sea ice rheology. Since the birth of modern first sea ice dynamics in the mid-seventies with the development of the model, the Elastic-Plastic sea ice model based on data collected during the Arctic Ice Dynamics Joint Experiment (Coon et al., 1974, (AIDJEX)), several other (AIDJEX Coon et al., 1974), several approaches to modeling sea ice were developed. In these models, sea ice was treated have been developed. Sea ice has been modeled as an incompressible fluid (Rothrock, 1975), a Viscous-Plastic (VP) material (Hibler, 1979), an Elastic-Viscous-Plastic (EVP) material (Hunke, 2001), a granular material (Tremblay and Mysak, 1997), an Elastic Anisotropic Plastic (EAP) medium (Wilchinsky and Feltham, 2006), an elastic-decohesive medium (Schreyer et al., 2006), an Elasto-Brittle (EB) material (Rampal et al., 2016) and a Visco-Elastic-Brittle (Maxwell(viscous)-Elastic-Brittle (MEB) material (Dansereau et al., 2016). The actual diversity in number of approaches to sea-ice modeling in the communityhowever , however, is much smaller; e. g. .

For example, 30 out of 33 ~~Global Climate Models~~ global climate models in CMIP5 use some form of the standard VP rheology ~~Stroeve et al. (2014)~~(Stroeve et al., 2014).

In spite of its success, the standard VP rheology is not undisputed. Coon et al. (2007) critically reviewed the assumptions behind current modeling practice since the original model of ~~(Coon et al., 1974);~~ Coon et al. (1974), namely the zero-tensile strength (ice is a highly ~~fracture~~ fractured material) and isotropy assumptions of the sea ice cover and the rheological model. Originally, Coon et al. (1974) assumed sea ice to have cracks in all directions, justifying isotropic ice properties and isotropic rheologies. The use of continuum models such as the standard VP model for high-resolution simulations (~~1–10km~~grid spacings of 1–10 km) is also ~~put in question~~ debated since the grid size approaches a typical floe size and clearly violates the continuum assumption. For instance, recent high-resolution simulations using the VP model used spatial resolution of approximately 500 m for a regional domain (Wang et al., 2006) and 1 km for a pan-Arctic domain (Hutter et al., 2018a). ~~While it can be argues~~ It can be argued that if the mode of deformation of a single floe is similar to that of an aggregate of floes, a given rheology developed for a continuum can still be applicable at spatial resolutions of the order of the floe size ~~Overland et al. (1998),~~ (Overland et al., 1998), but the validity of a given flow rule across scales is not clear. At any scale, the assumption of viscous creep for small deformations is not physical and an elastic model would be appropriate for low stress states. The long viscous time scale, compared to the synoptic time scale of LKFs, of order 30 years (Hibler, 1979), however, allows viscous deformation to be viewed as a small numerical regularization with little implications for the dissipation of mechanical energy from the wind or ocean current (Bouchat and Tremblay, 2014), and the ice model can be considered as an ideal plastic material. Tsamados et al. (2013) included anisotropy explicitly in ~~the~~ a VP model and show that it improved the representation of ice thickness and ice drift compared to an EVP model. ~~Other VP sea ice rheology were also developed but were~~ Alternative VP rheologies were never widely used in the community. These include ~~the coulombic~~ a Coulombic yield curve with a normal flow rule ~~of (Hibler and Schulson, 2000), the lens~~ (Hibler and Schulson, 2000), a parabolic lens and a tear-drop ~~, ice-cream cone,~~ (Pritchard, 1975), a diamond-shape yield curve with normal flow rules ~~((Zhang and Rothrock, 2005), the~~ (Zhang and Rothrock, 2005), a Mohr-Coulomb yield ~~with~~ curve with a double-sliding deformation law ~~Tremblay and Mysak (1997); Ip et al. (1991); Flato and Hibler (1992)~~(Tremblay and Mysak, 1997) or a curved diamond (Wang, 2007).

~~Early work by (Marko and Thomson, 1977) identified~~ Previously, fracture lines (LKFs) in the pack ice ~~and explained the presence of the LKFs~~ were explained by brittle fracture (Marko and Thomson, 1977). Similar fracture patterns ~~have also been observed~~were also observed, from the centimeter scale in the lab ~~,~~ to hundreds of kilometers in satellite observations ~~(Schulson, 2004; Weiss et al., 2007). Based on these (and others) satellite observations~~ (Schulson, 2004; Weiss et al., 2007). The scale invariance of the fracture processes at the floe scale has not yet been shown, especially due to the lack of observations at both high spatial and temporal resolution. Based on satellite observations (e.g. RADARSAT Geophysical Processor System, RPGS, or Advanced Very-High-Resolution Radiometer, AVHRR), and in-situ internal ice stress measurements ~~,~~ (e.g. from the Surface Heat Budget of the Arctic Ocean, SHEBA, experiment), Weiss et al. (2007) proposed to model winter sea ice as a material that undergoes brittle failure with subsequent inelastic deformation by sliding along LKFs~~governing inelastic deformations. Girard et al. (2011); Rampal et al. (2016); Dansereau et al. (2016) formalized the idea with the development of~~

an Elastoc-Brittle (EB) and Maxwell-Elasto-Brittle (MEB) model with an . This idea was formalized with an additional parameterization to simulate damage associated with brittle fracture in an Elasto-Brittle (EB) and Maxwell-Elasto-Brittle (MEB) model (Girard et al., 2011; Rampal et al., 2016; Dansereau et al., 2016). We note that subsequent plastic deformations deformation in this model are is considered as elastic deformation (EB) or visco-elastic deformation (MEB) instead of plastic. I.e. That is, in the elastic approaches, the material does not weaken when fracture occurs, but rather the Young's modulus is reduced, leading to larger elastic deformations deformation for the same stresses. Girard et al. (2009) compared the stress. From the scaling behavior of simulated sea-ice deformation fields from the EB and VP models with observations from the RADARSAT Geophysical Processor System (RGPS)and showed of EVP models (with 12 km grid spacing), it was found that the heterogeneity and the intermittency of deformation in the VP model are not consistent with observations. These results however could not be reproduced by other authors in the community. For instance, Spreen et al. (2017); Hutter et al. (2018a); Bouchat and Tre show that VP models are RGPS data (Girard et al., 2009). In contrast, VP-models were shown to be indeed capable of simulating the PDFs of sea ice deformations and some of the scaling characteristics over the whole Arctic in agreement with the same observations, when using appropriate either with sufficient resolution (Spreen et al., 2017; Hutter et al., 2018a) or with tuned shear and compressive strength of the materialparameters (Bouchat and Tremblay, 2017).

Similar fracture angles between intersecting LKFs $30 \pm 10°$) were observed with different instruments (Landsat, Seasat/SAR, areal photographs,AVHRR) at different scales from 1 to 100 (Erlingsson, 1988; Walter and Overland, 1993). In the VP model, LKFs are appear as line of high shear deformations. High-resolution sea-ice models simulate LKF patterns in pack ice, where they appear as lines of high deformation (Hutchings et al., 2005; Hutter et al., 2018a). Previously fractured ice will be weaker and will affect future sea ice deformation fields. The weakening associated with the shear deformation results from divergence and a reduction in ice concentration along the LKFs. This mechanism introduces an anisotropy in high resolution simulations as seen in observations of comparable spatial resolutions. Previously fractured ice will be weaker and will affect future sea ice deformation fields. High-resolution sea-ice models simulate LKF patterns leads to anisotopy in the pack ice (Hutter et al., 2018a). Previous studies that looked at lead that is similar to observations with comparable spatial resolution. Lead characteristics, including intersection angle between LKFs include (Hutchings et al., 2005; Bröhan and Kaleschke, 2014; Lindsay and F Of particular interest, Hutter et al. (2018b) compare LKFs and their intersection angles between RGPS data and a 2angles between LKFs were studied a number of times (Lindsay and Rothrock, 1995; Hutchings et al., 2005; Wilchinsky et al., 2010; Bröhan and Ka These studies show that VP models produce LKFs with various confinements, scales, resolutions, and forcings, although the LKFs creation mechanism is still unclear. From observations with different instruments (Landsat, Seasat/SAR, areal photographs, AVHRR), typical fracture angles between intersecting LKFs of $(15 \pm 15)°$ emerge at scales from 1 km-model simulation similar to the one described in Hutter et al. (2018a). For the RGPS data, they find km to 100 km (Erlingsson, 1988; Walter and Ove Hutter et al. (2018b) present an LKF tracking algorithm and show that fracture angles (half of the intersection angles) between LKFs in RGPS data follow a broad distribution of intersection angles between LKFs that peaks around 20° (in line with previous assessments, The wide range of intersection angles is presumably due to previous deformation history and associated heterogeneity in the ice cover that dictates the ice strength locally. Their results show a simulated distribution of intersection angles that is biased high with a , in line with previous assessments (e.g. Walter and Overland, 1993). Hutter et al. (2018b) also show that that the

distribution of fracture angles in a VP simulation with 2-km grid spacing is biased with a high modal value of 45° and with too few small intersection angles between ~~15~~ 15° and 25°. The ~~fact that a VP model overestimates the angles of intersection between LKFs is one motivation for the present thorough~~ observed bias motivates the present investigation of the ~~fracture angles at small scales and the dependencies of the fracture angle to~~ dependence of fracture angles in different VP rheologies and model settings, that is, scale, resolution, boundary conditions, model geometry, ~~variability in sea in~~ and variability in initial ice thickness field~~and mechanical strength parameters used in the model.~~ .

The simulation of fractures in sea ice models ~~have been the focus of several previous studies using~~ has been studied in idealized model geometries before. Hibler and Schulson (2000) investigated the effect of embedded flaws - that favors certain angles of fractures - in idealized experiments using a Coulombic yield curve. Hutchings et al. (2005) showed that LKFs can be simulated with an isotropic VP model using ~~a~~ an idealized model geometry. The shape of the elliptical yield curve (ratio of shear to compressive strength) in the standard VP model ~~has an impact on the presence or absence of ice arches~~ determines if ice arches can form in an idealized channel experiment ~~(Dumont et al., 2009).~~ (Hibler et al., 2006; Dumont et al., 2009). Pritchard (1988) investigated the yield curve's mathematical characteristics and derived angles between the principal stress directions and characteristics directions that depend on the tangent to the yield curve. These results show that stress states exist in plastic materials where no LKFs form and were later used to build a yield curve (Wang, 2007). To build an anisotropic rheology, Wilchinsky et al. (2010) used a Discrete Element Model (DEM) model in an idealized model domain and showed clear diamond-shaped fracture patterns. Idealized experiment are also used to investigate new rheologies~~(e.g. Dansereau et al., 2016; Sulsky et al., 2~~ ~~or~~ , for example, the Maxwell-Elastic-Brittle (MEB) rheology (Dansereau et al., 2016) or the Material-Point Method (MPM) (Sulsky et al., 2007), or to study the theoretical framework explaining the fracture angles ~~(e.g. Dansereau et al., 2017, with the Mohr-Coulom~~ Recently, Heorton et al. (2018) compared simulated fractures by the EVP and EAP models using an idealized model geometry and wind forcing, and showed that the anisotropic model creates sharper deformation features. To the best of our knowledge, the dependency of the fracture angles in sea ice on the shape of the yield curve using high resolution models has not yet been investigated. This is another motivation of this study.

In this paper, we ~~explore the details of fracture with two VP rheologies using~~ simulate the creation of a pair of conjugate faults in an ice floe with two different VP rheologies in an idealized experiment at an unprecedented resolution of 25 ~~.~~ m. We explore the influence of various parameters of the rheologies and the model geometry (Scale, resolution, confinement, boundary conditions, and heterogeneous initial conditions). The remainder of this paper is structured as follow : Section 2 presents the experimental setup: the VP framework (2.1), the definition of the yield curve (2.2), and the description of the idealized experiment (2.3). Section 3 presents the results: ~~from~~ First the reference simulation is presented (3.1), ~~the effect of boundary conditions (??), the effects of~~ then we explore the sensitivity of the setup in section 3.2 to scale, resolution and longer run-time (3.2.1), modified boundary conditions and lateral confinement (~~??~~3.2.1), and ~~the influence of heterogeneity (??). Furthermore~~to heterogeneity in initial conditions (3.2.1). Finally, we consider the effects of two different yield curves with ~~normal flow rule in subsection~~different flow rules in subsection 3.3: the elliptical (3.3.1) and the ~~coulombic~~ Coulombic yield curve (3.3.2). Discussion and conclusions follow in sections~~4 and~~ 4 and 5.

2 Experimental Setup

2.1 Viscous-Plastic model

We use the Massachusetts Institute of Technology general circulation model ~~(MITgcm, Marshall et al., 1997)~~ (MITgcm, Marshall et al., 1997) its sea ice package that allows for the use of different rheologies (Losch et al., 2010). All thermodynamic processes have been turned off for our experiments. The initial sea ice conditions~~—~~, mean (grid cell averaged) thickness h and fractional sea ice cover A~~—~~, are advected by ice drift velocities with a third order flux limiter advection scheme (Hundsdorfer et al., 1995). Ice drift is computed from the sea ice momentum ~~equation~~ equations

$$\rho h \frac{\partial \boldsymbol{u}}{\partial t} = -\rho h f \boldsymbol{k} \times \boldsymbol{u} + \boldsymbol{\tau}_{air} + \boldsymbol{\tau}_{ocean} - \rho h \nabla \phi(0) + \nabla \cdot \boldsymbol{\sigma}, \tag{1}$$

where ρ is the ice density, h is the grid cell ~~average~~ averaged sea ice thickness, $\boldsymbol{u}$ is the velocity field, f is the Coriolis parameter, $\boldsymbol{k}$ is the vertical unit vector, $\boldsymbol{\tau}_{air}$ is the surface air stress, $\boldsymbol{\tau}_{ocean}$ is the ocean drag, $\nabla\phi(0)$ is the gradient of sea surface height, and σ is the vertically integrated internal ice stress tensor. The form of σ defines the rheology. In the case of the standard VP model described in (Hibler, 1979), the components of σ ~~is~~ are defined as

$$\sigma_{ij} = 2\eta_{ij}\dot{\varepsilon}_{ij} + (\zeta - \eta)\,\dot{\varepsilon}_{kk}\delta_{ij} - \frac{P}{2}\delta_{ij}, \tag{2}$$

where δ_{ij} is the Kronecker delta and summation over equal indices is implied. η and ζ are the shear and bulk viscosities, $\dot{\epsilon}_{ij}$ is the strain rate tensor defined as

$$\dot{\epsilon}_{ij} = \frac{1}{2}\left(\frac{du_i}{dx_j}\frac{\partial u_i}{\partial x_j} + \frac{du_j}{dx_i}\frac{\partial u_j}{\partial x_i}\right), \tag{3}$$

and P is the maximum compressive stress defined as a function of the ice strength parameter $P^\star$, mean sea ice thickness ~~h~~ h, and the sea ice concentration ~~A:~~ A:

$$P = P^{*\star}\, h\, e^{-C^*(1-A)}. \tag{4}$$

~~The values of parameters and constants in the model are given on Table 1.~~, where $C^\star$ is a free parameter.

The stress tensor σ is often expressed in terms of principal stresses σ_1 and σ_2 and stress invariants σ_I and σ_{II}. The principal stresses σ_1 and σ_2 are the principal components or eigenvalues of the stress tensor on an sea ice element. Eigenvalues always exist, because the stress tensor is by definition symmetric. The principal stresses σ_1 and σ_2 can be expressed as a function of σ_{ij} as :

$$\sigma_1 = \frac{1}{2}\left(\sigma_{11} + \sigma_{22} + \sqrt{(\sigma_{11} - \sigma_{22})^2 + 4\sigma_{12}^2}\right), \tag{5}$$

$$\sigma_2 = \frac{1}{2}\left(\sigma_{11} + \sigma_{22} - \sqrt{(\sigma_{11} - \sigma_{22})^2 + 4\sigma_{12}^2}\right), \tag{6}$$

Table 1. Model parameters of the reference simulation

Symbol	Definition	Value	Unit
ϱ	Density of ice	910	$\mathrm{kg\,m^{-3}}$
$P^\star$	Ice strength	27.5	$\mathrm{kN\,m^{-1}}$
C	Strength reduction parameter	20	~
Δ_{min}	Maximum Viscosity	10^{-10}	s^{-1}
Δx, Δy	Grid spacing	25	m
C_w	Water drag coefficient	5.21×10^{-3}	
N_x, N_y	Size of the domain	400×1000	~
L_x, L_y	Size of experiment	10×25	km
l_x, l_y	Ice floe's size	8×25	km
A	Initial ice concentration	100	%
h	Initial ice thickness	1.0	m
N_{lin}	Nbr. linear iteration	1500	~
N_{nlin}	Nbr. non-linear iteration	1500	~
ϵ_{err}	Max. error in LSR	10^{-11}	$\mathrm{m\,s^{-1}}$
dt	Timestep	0.1	s
e	Ellipse ratio (a/b)	2.0	~
v_i	Initial velocity	0	$\mathrm{m\,s^{-1}}$
a_v	Acceleration	$5 \cdot 10^{-4}$	$\mathrm{m\,s^{-2}}$

This change of coordinates can then be represented as a rotation of the coordinates by ψ (Fig. A1). This angle is (Tremblay and Mysak, 1997):

$$\tan(2\psi) = \frac{2\sigma_{12}}{\sigma_{11} - \sigma_{22}}. \tag{7}$$

Any linear combination of the principal stresses are stress invariants. One common sets of stress invariants are the mean normal stress (σ_I) and the maximal shear stress (σ_{II}). They can be written as

$$\sigma_I = \frac{1}{2}(\sigma_1 + \sigma_2) = \frac{1}{2}(\sigma_{11} + \sigma_{22}), \tag{8}$$

$$\sigma_{II} = \frac{1}{2}(\sigma_1 - \sigma_2) = \frac{1}{2}\sqrt{(\sigma_{11} - \sigma_{22})^2 + 4\sigma_{12}^2}. \tag{9}$$

2.2 Yield curve

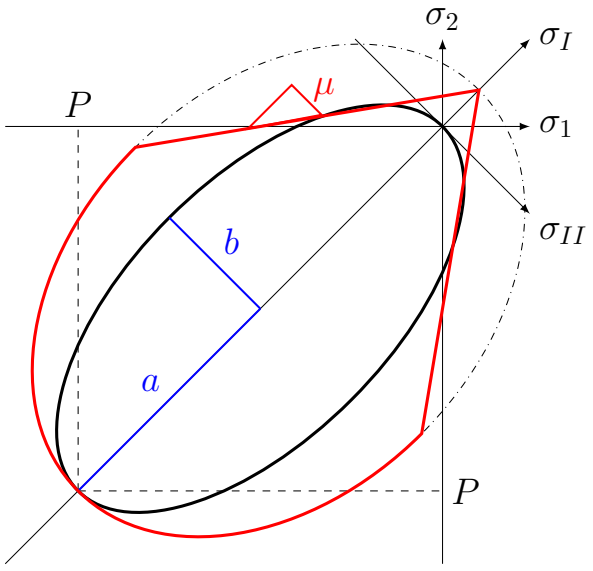

Figure 1. ~~Example of~~ Elliptical yield ~~curves used in VP models shown in : Ellipse with $e = 2$ in~~ curve (black~~, coulombic~~) with ellipse aspect ratio $e = a/b = 2$. Coulombic yield curve ~~in~~ (red) and elliptical capping with internal angle of friction (μ). Both e and μ ~~is~~ are measures of the ~~slope~~ shear strength of the ~~Mohr-Coulomb flat on~~ material. The normal flow rule applies only to the ~~coulombic~~ elliptical part of the yield curves. For the two straight limbs of the Coulombic yield curve~~as defined in equation~~ , the flow is normal to the truncated ellipse (~~A7~~dash-dot line) with the same first stress invariant. Note that the axes σ_1, σ_2 and σ_I, σ_{II} do not have the same scale.

~~When~~ The VP rheology was originally developed to simulate ice motion on a basin scale (e.g., Arctic Ocean, Southern Ocean) (Hibler, 1979). In this model, stochastic elastic deformation is parameterized as highly viscous (creep) flow (Hibler, 1977). Ice is set in motion by surface air and basal ocean stresses moderated by internal ice stress. When the internal sea-ice ~~stresses reach~~ stress reaches a critical value in compression, tension or shear, sea ice fails and relatively large plastic ~~deformations are present. For internal ice stresses that are lower than the same thresholds ,~~ deformation takes place. Internal ice stress below these thresholds leads to highly viscous (~~creeping) flow is present mimicking~~ creep) flow that parameterizes the bulk effect of many small reversible elastic ~~deformations.~~ deformation events. The timescale of viscous deformation is so high ($\simeq 30$ years) that viscous deformation can be seen as regularisation for better numerical convergence in the case of small deformation. Plastic deformations are relatively large and non-reversible. Viscous deformation ~~are negligibly smalland also~~ is negligibly small; in contrast to elastic deformation it is also non-reversible~~contrary to elastic reversible deformation in real sea ice~~. The yield criterion is expressed as a 2D envelope either in principal stress space or stress invariant space with a normal flow rule~~assuming that the principal stress and strain-rate axis~~ . The normal flow rule requires that the direction of stress and ensuing deformation (strain rate) coincide. The stress state on the yield curve together with the normal flow rule therefore determines the relative importance of divergence (positive or negative) and shear strain rate at a point in stress space. The magnitude of the deformation is such that the stress state remains on the yield cure during plastic deformation.

In this study, we use two different yield curves~~, the~~ : an elliptical yield curve (Hibler, 1979) and ~~coulombic~~ a Coulombic yield curve (Hibler and Schulson, 2000)~~both with the~~ . The elliptical yield curve has a normal flow rule, while the Coulombic yield curve has a normal flow rule on the elliptical cap and a flow rule corresponding the truncated ellipse for the same first principal stress (Hibler and Schulson, 2000, Appendix A). For the elliptical yield curve (~~in black in Figure 1~~Fig. 1, black line), η and ζ are given by :

$$\zeta = \frac{P}{2\Delta}, \tag{10}$$

$$\eta = \frac{\zeta}{e^2}, \tag{11}$$

with the abbreviation

$$\Delta = \sqrt{(\dot{\epsilon}_{11}+\dot{\epsilon}_{22})^2 + \frac{1}{e^2}\left((\dot{\epsilon}_{22}-\dot{\epsilon}_{11})^2 + 4\dot{\epsilon}_{12}^2\right)} = \frac{a}{b}\sqrt{\dot{\epsilon}_I^2 + \frac{1}{e^2}\dot{\epsilon}_{II}^2}. \tag{12}$$

~~where~~ In this abbreviation, the strain rate invariants are the divergence $\dot{\epsilon}_I = \dot{\epsilon}_{11} + \dot{\epsilon}_{22}$ and the shear deformation rate $s = \dot{\epsilon}_{II} = \sqrt{(\dot{\epsilon}_{22}-\dot{\epsilon}_{11})^2 + 4\dot{\epsilon}_{12}^2}$, $e = \frac{a}{b}$ is the ellipse aspect ratio with the semi-major half-axes a and b ~~are~~ (shown in blue ~~on figure 1.~~ in Fig. 1). The ellipse aspect ratio e defines the shear strength ~~$S^\star$~~ $S^\star = \frac{P^\star}{2e}$ of the material as a fraction of its compressive strength ~~: $S^\star = \frac{P^\star}{2e}$~~ (Bouchat and Tremblay, 2017). For the Coulombic yield curve ~~,~~ (Fig. 1, red curve), the shear viscosity η ~~above~~ is capped on the two straight limbs~~(see appendix A for a detailed derivation.~~

$$\eta_{MC} = \min\left\{\eta, \frac{1}{s}\left[\mu\left(\frac{P}{2} - \zeta\cdot\dot{\epsilon}_{kk}\right) - c\right]\right\} \tag{13}$$

~~with~~

$$s = \sqrt{(\dot{\epsilon}_{22}-\dot{\epsilon}_{11})^2 + 4\dot{\epsilon}_{12}^2} \tag{14}$$

:

$$\eta_{MC} = \min\left\{\eta, \frac{1}{\dot{\epsilon}_{II}}\left[\mu\left(\frac{P}{2} - \zeta\cdot\dot{\epsilon}_{kk}\right) - c\right]\right\} \tag{15}$$

where μ is the slope of the Mohr-Coulomb limbs (Fig. 1), c is the cohesion value (the value of σ_{II} for $\sigma_I = 0$) defined relative to the tensile strength by $c = \mu \cdot T^\star$.

The theoretical angle of fracture θ can be calculated from the ~~generalized state of stress equations on a rotated frame of referenceat an angle~~ Mohr's circle of stress and yield curve written in the local (reference) coordinate system (Ip et al., 1991; Pritchard, 1988; Details are described in the appendix. For a Mohr-Coulomb yield criterion, θ ~~from a reference coordinate frame of reference. The stress tensor σ can be expressed in different sets of coordinates: in terms of principal stresses σ_1~~ follows immediately from the internal angle of friction, that is the available shear strength. An instructive analogue is the slope of a pile of sand on a table. Wet sand can support more shear stress and ~~σ_2 and stress invariants σ_I and σ_{II}. The principal stresses σ_1 and σ_2 are the~~

~~principal components or eigenvalues of the stress tensor on an sea ice element. Eigenvalues always exist, because the stress tensor is by definition symmetric. The principal stresses σ_1 and σ_2 can be expressed as a function of σ_{ij} as :~~

$$\sigma_1 = \frac{1}{2}\left(\sigma_{11}+\sigma_{22}+\sqrt{(\sigma_{11}-\sigma_{22})^2+4\sigma_{12}^2}\right),$$

$$\sigma_2 = \frac{1}{2}\left(\sigma_{11}+\sigma_{22}-\sqrt{(\sigma_{11}-\sigma_{22})^2+4\sigma_{12}^2}\right),$$

~~This change of coordinates can then be represented as a rotation of the coordinates of value ψ as shown on Figure A1. This angle, from Tremblay and Mysak (1997), is :~~

$$\tan(2\psi) = \frac{2\sigma_{12}}{\sigma_{11}-\sigma_{22}}.$$

~~Any linear combination of the principal stresses would be stress invariants. One commonly used definition called the stress invariants are the mean normal stress (σ_I) and the maximal shear stress (σ_{II}). They are expressed as function of stresses σ_{ij} or principal stresses σ_k as~~

$$\sigma_I = \frac{1}{2}(\sigma_1+\sigma_2) = \frac{1}{2}(\sigma_{11}+\sigma_{22}),$$

$$\sigma_{II} = \frac{1}{2}(\sigma_2-\sigma_1) = -\frac{1}{2}\sqrt{(\sigma_{11}-\sigma_{22})^2+4\sigma_{12}^2}.$$

hence the slope angle can be steeper (smaller).

2.3 Idealized Experiment

~~An idealized uni-axial~~ An idealized compressive test is used to investigate the modes of sea ice fracture (Figure 2). This experiment is standard in engineering (Schulson, 2004; Weiss et al., 2007)~~and also analogous to an experiment described in Dansereau et al. (2016)and Herman (2016)~~. The numerical configuration is inspired by Herman (2016) and similar to the one shown in Dansereau et al. (2016). All experiments presented below use the same set-up unless specified otherwise. The values of parameters and constants are presented in Table 1.

The model domain is a rectangle of size $10\,\mathrm{km} \times 25\,\mathrm{km}$~~.~~, except for Sect. 3.2.1 and Sect. 3.2.1. An ice floe of size $8\,\mathrm{km} \times 25\,\mathrm{km}$, surrounded by $1\,\mathrm{km}$ of open water on the eastern and western sides, is compressed with a linearly (in time) increasing strain rate from the North against a solid ~~Southern~~ southern boundary. The eastern and western strips of open-water ~~areas on the East and West boundary are used so that interesting dynamics are not influence~~ avoid interesting dynamics to be confounded by the choice of ~~boundary conditions~~lateral boundary conditions along the open boundaries to the East and the West. We use a no-slip condition for the southern boundary, constraining ~~the ice laterally~~lateral ice motion. Note that the results presented below are ~~robust of~~ not sensitive to the choice of boundary condition on the ~~east, west and south boundary~~eastern and western boundaries. Because the simulation time and ~~ice velocity~~ the ice velocities are small, the Coriolis force in the momentum equations are neglected. ~~The ocean~~ Ocean and sea ice are initially at rest. The only term left in the momentum equation (Equation (1) that is relevant for our experiment is the stress divergence term, $\nabla \cdot \sigma$. The ice floe

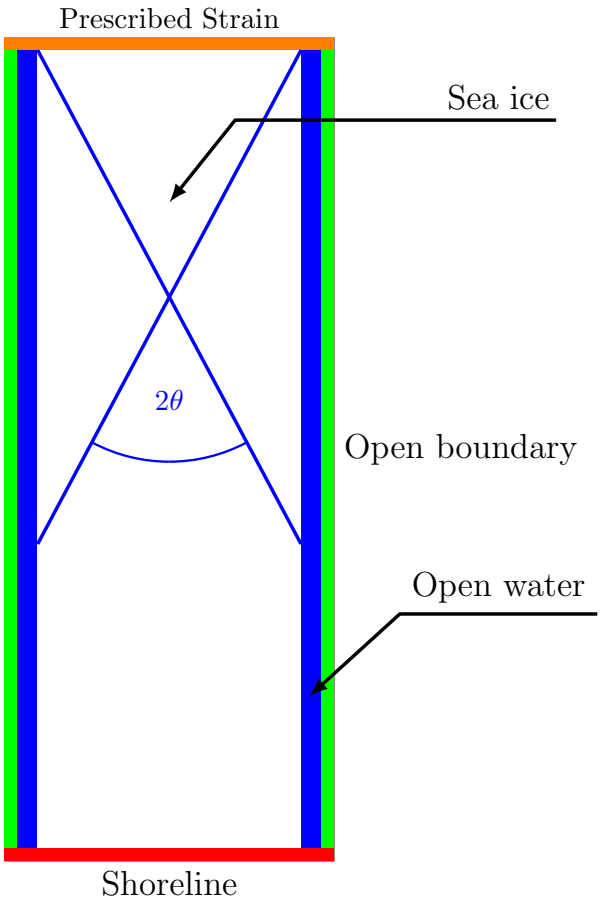

Figure 2. ~~*Schematic of*~~ *Model domain with a solid wall on the* ~~*experiment. The*~~ *southern (red*~~*area represent blocked grid cells*~~*) boundary (Dirichlet boundary conditions with* $\boldsymbol{u} = 0$*), and prescribed southward velocities on the* ~~*green area is open*~~ *northern orange boundary* ~~*that let ice leave*~~ *(*$u = 0$*,* $v = a_y \cdot t + v_i$*, Eq. 17) and open boundaries to the* ~~*domain*~~ *East and the West (green) with* ~~von Neumann~~ *von Neumann boundary conditions.* ~~*The orange area represent the prescribed area where the ice is forced with southward velocity.*~~ θ *is the measured fracture angle with the blue line representing an LKF.*

has a uniform concentration of 100% and a thickness of 1 m. The spatial resolution of the model is 25 m. ~~We use the Line Successive (over)Relaxation (LSR) solver to solve the sea ice~~ The angle of fracture is measured with the angle measuring tool of the GNU Image Manipulation Program (GIMP, https://www.gimp.org/). All angles measured in this study have an error range around 1°. The finite size of the grid spacing widens the deformation line, and the fracture spreads over several pixels because of the obliquity of the fracture. Automatic algorithms for measuring LKF intersection angles are described in Linow and Dierking (2017); Hutter et al. (2018b).

We solve the non-linear sea-ice momentum equations with a Picard or fixed point iteration with 1500 non-linear ~~iterations and 1500 linear iterations within~~ or outer-loop (OL) iterations. Within each non-linear iteration~~(Zhang and Hibler, 1997; Lemieux and Tremblay, ... A high number of iterations is required~~ , the non-linear coefficients (drag coefficients and viscosities) are updated and a linearized system of equations is solved with a Line Successive (over-)Relaxation (LSR) (Zhang and Hibler, 1997). The linear iteration is stopped when the maximum increment is less than $\epsilon_{LSR} = 10^{-11}\,\mathrm{m\,s^{-1}}$, but we also limit the number iterations to 1500. Typically, 1500 non-linear iterations are required to reach a converged solution. This is so because of slow convergence ~~of~~ due to the highly non-linear ~~nature of the~~ rheology term and the high spatial resolution (Lemieux and Tremblay, 2009).

On the open eastern and western boundaries, we use von Neumann boundary conditions for velocity, thickness and concentration and ice can escape the domain ~~unrestricted~~with out any restrictions:

$$\left.\frac{\partial u}{\partial x}\right|_{E,W} = \left.\frac{\partial v}{\partial x}\right|_{E,W} = \left.\frac{\partial A}{\partial x}\right|_{E,W} = \left.\frac{\partial h}{\partial x}\right|_{E,W} = 0, \tag{16}$$

where ~~E and W denote the Eastern and Western respectively. The ice is initially at rest.~~ E and W denote the eastern and western boundaries, respectively. Strain is applied ~~on~~ to the ice at the northern boundary by prescribing a velocity that increases linearly with time :

$$v|_N(t) = a_v \cdot t + v_i\ ;\ u|_N = 0\ ;\ \left.\frac{\partial A}{\partial y}\right|_N = \left.\frac{\partial h}{\partial y}\right|_N = 0, \tag{17}$$

where a_v is the prescribed acceleration, and N ~~denote~~ denotes the northern boundary.

~~Model parameters for the reference simulation Symbol Definition Value Unit ρ Density of ice 910 $P^\star$ Ice strength 27.5 C strength reduction parameter 20 dx, dy Grid Spacing 25 C_w Water drag coefficient 5.21×10^{-3} N_x, N_y Size of the Domain 400×1000 L_x, L_y Size of Experiment 10×25 l_x, l_y Ice floe's size 8×25 A Ice Concentration 100 % h Ice Thickness 1.0 N_{lin} Nbr.Linear Iteration 1500 N_{nlin} Nbr.Non-linear Iteration 1500 ϵ_{err} Max.error in LSR 10^{-11} dt timestep 0.1 e ellipse ratio (a/b)2.0 v_i initial velocity 0 a_v acceleration $5 \cdot 10^{-4}$~~

3 Results

3.1 ~~Uni-axial compressive test~~

We use simple uni-axial loading experiments to investigate the creation of pair of conjugate faults and their intersection angle. After presenting the results of simulations with the default parameters (Section 3.1), we explore the effects of experimental choices: confining pressure, choice of boundary conditions (i.e. von Neumann versus Dirichlet), domain size and spatial resolution and inhomogeneities (i.e. localized weakness) in the initial thickness and concentration field (Section 3.2). Finally, we study the behaviour of two viscous plastic rheologies with different yield curves and compare these dependencies to what we can infer from smaller and larger scale measurements from laboratory experiment and RGPS observations (Section 3.3).

3.1 Uni-axial compressive test - Default parameters

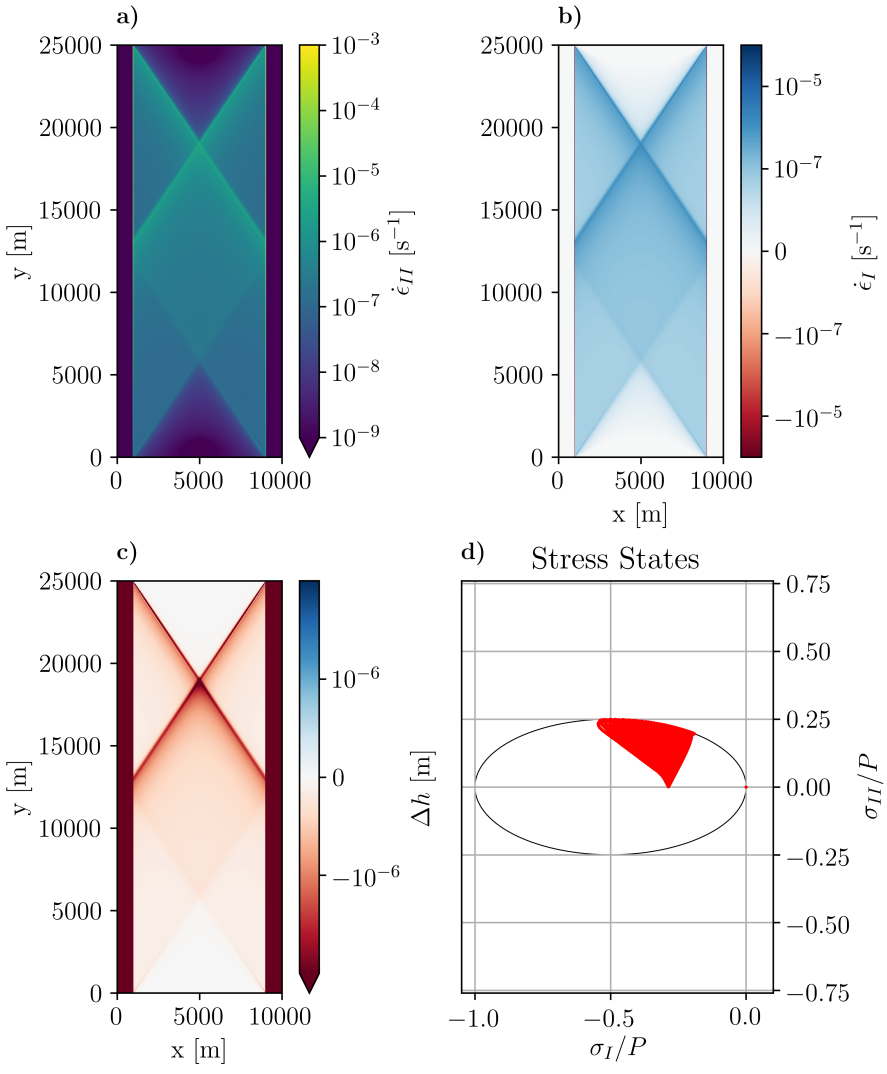

Figure 3. ~~Results of the reference simulation after 10 seconds of simulation. **Top left:** Shear deformation inside the ice floe, showing (a~~diamond shape fracture. ~~**Bottom left:** Divergence deformation inside the ice floe~~) First and (b) second strain invariants, ~~showing the divergence in the fracture line that lead to an opening. **Top right:** Modification of the~~ (c) ice thickness ~~compared to initial state of 1 , the opening with a diamond shape is visible. **Bottom right:** Stress~~ anomaly ($\Delta h = h - 1$) and (d) stress states in ~~red,~~ normalized stress invariant space along with the elliptical yield curve ~~in black~~after 5 seconds of integration. The first and second strain invariants represent the divergence and maximum shear strain rate, respectively. The modeled angle of fracture is $\theta = (34 \pm 1)^\circ$

~~In the reference experiment with default parameters~~ With default parameters (Table 1), a diamond shape fracture appears in the shear strain rate and divergence fields after a few seconds of integration (Figure 3). ~~The fracture appears right away but is visible~~ After 1 timestep (or 0.1 s), the stress states already lie on the yield curve and the fracture is readily seen in the

deformation ~~field only after a few seconds of integration~~fields (divergence and shear). We iterate for a total of 20 seconds in order for the signal to be apparent in the thickness and concentration fields. We do this to more clearly show the link between position of the stress states on the yield curve and the normal flow rule in the standard VP rheology of Hibler (1979). The shear deformation ($\dot{\epsilon}_{II}$) shows where the ice slides in friction and deforms plastically. From ~~Figure~~Fig. 3, the ~~measured~~ simulated intersection angle is ~~$\theta = 33.8 \pm 0.5°$. All angles measured in this study have an error range around 1deg. Because we model an oblique fracture on a grid, the size of the grid spacing spread the deformation line, and the fracture spread on several pixels because of the obliquity of the fracture.~~ $\theta = (34 \pm 1)°$.

~~Results after~~ After a few time steps~~show lower (or equal) ice thickness in the model domain,~~ , the ice thickness decreases particularly along the LKFs (Fig. 3~~, middle panel~~c) where divergence is ~~present~~maximal. Note that the loading axis in our simple 1D experiment is also the second principal axis and consequently the stress states are ~~slowing~~ migrating along the ~~σ_1~~ σ_2 axis as the strain rate at the northern boundary increases. Fracture occurs after plastic failure when the stress state ~~intersects~~ reaches the yield curve ~~; this~~ and the ice starts to move in divergence. This occurs in the ~~first~~ half of the ellipse ~~(for $e < 1$~~closer to the origin (for $e > 1$) where the normal to the flow rule points in the direction of positive divergence (or first strain rate invariant) ~~direction (see Figure~~(see Fig. 4). This explains the simulated divergent flow field and lower ice thickness particularly along LKFs.

~~The results presented above are robust with respect to the spatial resolutionand model domain size (see Figure~~

3.2 Sensitivity experiments

In this section, we test the sensitivity of the standard VP model simulation (Sect. 3.1) to the choice of resolution, scale, and run-time (3.2.1), boundary conditions and confinement pressure (3.2.1), and heterogeneity in the initial sea ice mass field (3.2.1).

3.2.1 Domain size, spatial resolution and length of integration

The angle of intersection between a pair of conjugate faults does not change with domain size and spatial resolution (Fig. 5).

This is expected, because non-dimensionalizing the divergence of the internal ice stress term (the only term that remains in this simple uni-axial test experiment) by setting $u' = u/U$, $x' = x/L$, gives the same equations in non-dimensional form irrespective of the initial ice thickness or spatial resolution. Consequently, the control and sensitivity experiments are scale independent and the behaviour of the standard VP model can be readily compared with results from RGPS, AVHRR, or laboratory experiments.

3.3 ~~Fracture and generation of smaller floes~~

~~Here, the reference simulation is extended for a longer time period (~~Continuing the integration to 2700~~seconds or~~ seconds (45 min), ~~using a smaller number of numerical iterations because of computational constraints (150 iterations instead of 1500 for both linear and non-linear iterations with the LSR solver, see~~ compared to 20 seconds in the reference simulation leads

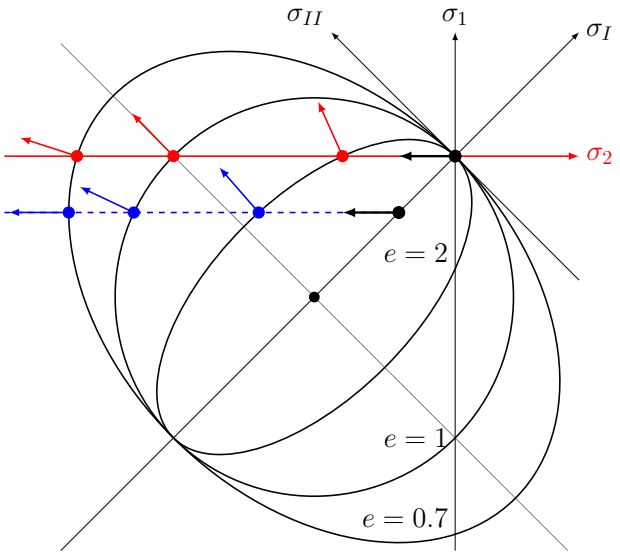

Figure 4. Schematic of stress ~~state migration during uni-axial~~ states and failure in principal stress space. Black arrows show how stresses move from zero at the beginning of loading ~~experiments~~towards the yield curve until failure. Red ~~arrows shows~~ points show the stress ~~state~~ states at ~~fracture~~ failure — the intersection point between the second principal axis~~σ_1~~ 2 (in red) and the elliptical yield curve — for different ellipse ~~ratio: $e = 2$, $e = 1$, and $e = 0.7$~~ratios $e = 2, 1, 0.7$. The red arrows show the direction of deformation with a normal flow rule. The blue points and arrows show the case when the ice floe is confined ~~. The~~ and the loading will lead to extra stress ~~states migrate from a point with a higher compressive stress~~in the direction of σ_1.

to the creation of smaller diamond-shaped ice floes due to secondary and tertiary fracture lines (Figure 6). The ~~ice floe is broken into separated ice floes of smaller diamond-scale. The~~ openings are visible in the thickness and concentration fields with thinner, less concentrated ice in the lead. ~~Contrary to the previous short~~ In this longer experiment, the sea ice ~~ridged at several points and thickness increases, especially in~~ also ridges, for instance at the center of the ~~central diamond, where the tip of the upper triangle is compressed~~domain where the apex of the diamonds fails in compression. There is also some thicker ice at the northern boundary ~~because of the boundary condition~~induced by the specified strain rate at the northern boundary. The fracture ~~into several floes that move independently on open-water at this resolution appears realistic. Several fractures develop in parallel similarly as the comb crack or secondary fault lines , described in Schulson (2004)~~pattern and presence of secondary and tertiary fracture lines are in line with results from laboratory experiments Schulson (2004) and with AVHRR and RGPS observations.

In the following, we always show results after 5 seconds of integration because our main focus is on the initial fracture of the ice, that is, the instant when the ice breaks for the first time under compression.

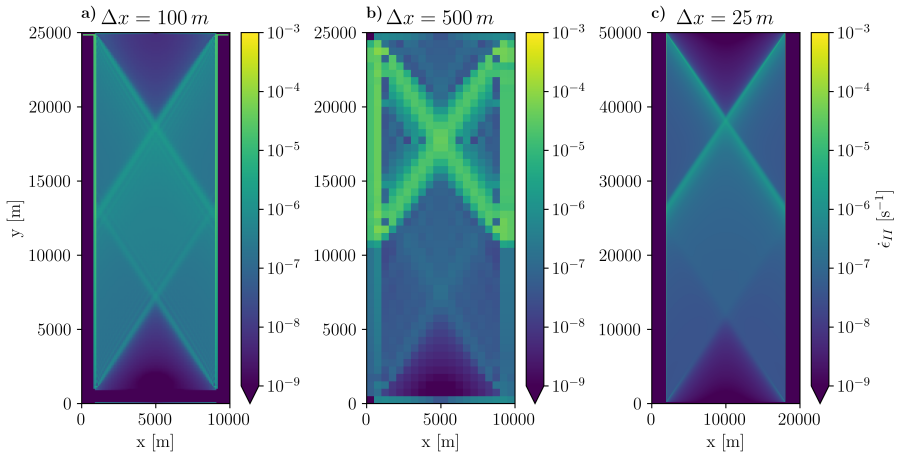

Figure 5. ~~Shear deformation~~ Maximum shear strain rate (~~or $\dot{\epsilon}_{II}$~~second strain invariant) after ~~2 with **(left)** a coarser resolution~~ 10 seconds of ~~100 , **(middle)**~~ integration for the default domain size and $\Delta x = 100\,\mathrm{m}$ (a~~coarser resolution of 500)~~ and ~~**c)** in~~ $500\,\mathrm{m}$ (b), and for the default Δx and a ~~experiment with a domain that has been~~ doubled ~~in both directions to a~~ domain size of $20\,\mathrm{km} \times 50\,\mathrm{km}$ ~~at resolution~~ (c). Note that for case of ~~25~~ the double domain (c), ~~with a doubled prescribed~~ the southward velocity at the northern boundary was also doubled to keep the deformation rate constant, and that this simulation is limited to 2 seconds for numerical efficiency.

3.3 ~~Effects of no-slip boundary condition and geometry~~

3.2.1 Boundary conditions and geometry

The dynamics ~~presented above are happening~~ responsible for the ice fracture and location of the fracture (presented above) take place far away from the ~~east/west boundaries~~ eastern and western boundaries and therefore do not depend on the choice of the corresponding boundary conditions. We now investigate the ~~robustness~~ sensitivity of the results to the choice of ~~southern boundaries~~boundary condition at the southern boundary. To this end, we ~~reduce the~~ force the fracture line to intersect the southern boundary by reducing the domain size to $10\,\mathrm{km} \times 10\,\mathrm{km}$ with an ice floe of $8\,\mathrm{km} \times 10\,\mathrm{km}$ in the interior~~, in such a way that the ice fracture ends on the southern boundary where a no-slip boundary condition is imposed - as opposed to the east/west boundaries as presented above~~. In this case, the fracture develops from corner to corner and the angle is solely determined by the geometry of the ice floe, that is, $\theta = \arctan(l_x/l_y)$ (~~right hand side of~~ Fig. 7~~shows an example~~b). With a free-slip boundary condition ~~on the South~~ at the southern boundary, the fracture angle is similar to the one ~~of the reference simulation (left hand side of Figure 7). I.e.~~ from the control simulation (Fig. 7a). That is, the no-slip condition ~~acts as a stress concentrator on~~ concentrates the stress to the corner of ~~ice floe~~ the ice floe touching the boundary and pre-determines the fracture location. A ~~slip~~ free-slip boundary condition is therefore considered more physical in such idealized experiments ~~.~~ where fractures lines can extend from one boundary to another. This result can have implications for simulation of LKFs in the Arctic that would extend from one boundary to another, for instance in the Beaufort Sea.

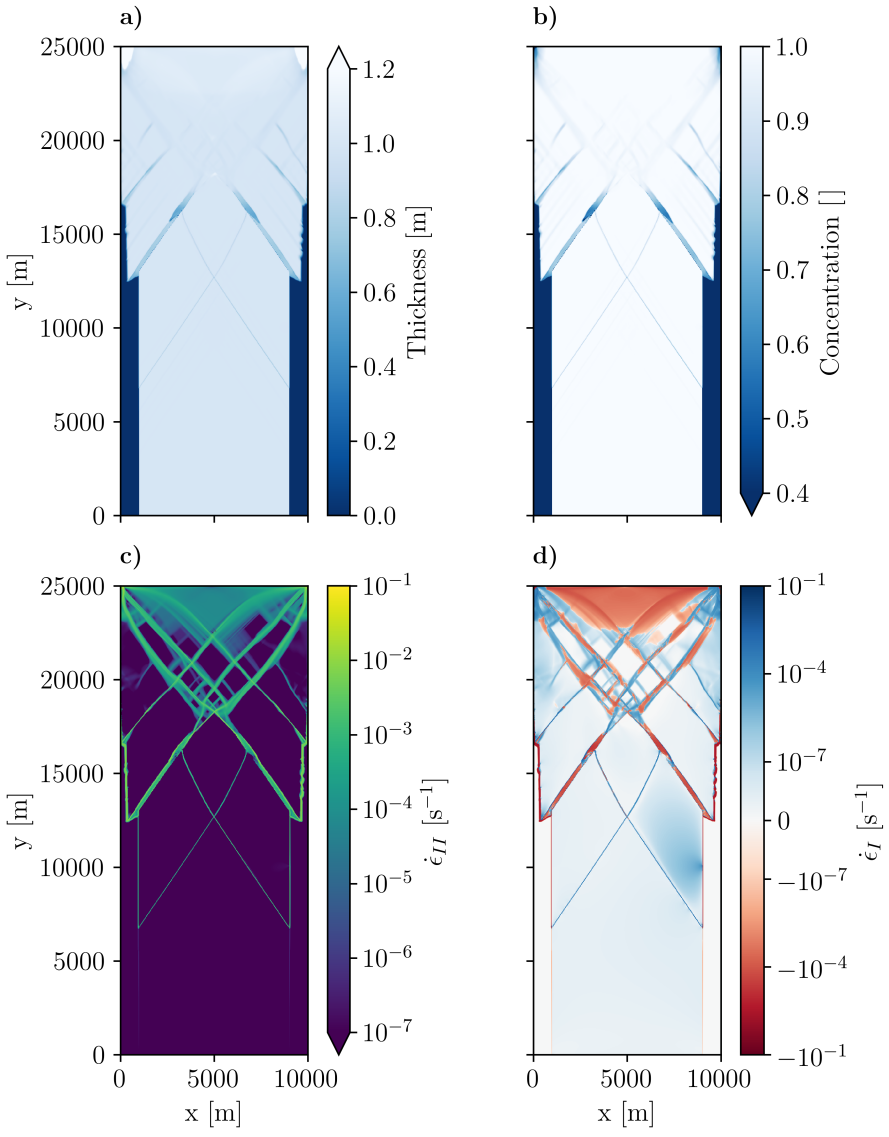

Figure 6. ~~Uni-axial compressive test after 2700~~ Sea ice thickness (a), concentration (b), maximum shear strain rate (c) and divergence (d) after 45 min of integration (2700 sec) in a uni-axial loading test. o make these longer simulations possible, both non-linear and linear iterations are limited to 150 per timestep. Results show the ~~primary and~~ development of secondary fracture lines ~~**(top left)**: sea ice thickness; **(top right)**: sea ice concentration; **(bottom left)**: shear strain rate $\dot{\epsilon}_{II}$; **bottom right**: divergence $\dot{\epsilon}_{I}$~~ in all fields after the first fracture line has formed.

.

No-slip or free-slip boundary conditions have little impact on the fracture angle in the larger ~~reference domain with longer floe~~domain used in the control run simulation, because the LKFs always ~~end on the~~ only touch one boundary and end in open-water ~~boundaries of the floe (~~(results not shown). With the free-slip boundary conditions, the ~~stress and strain~~ stresses

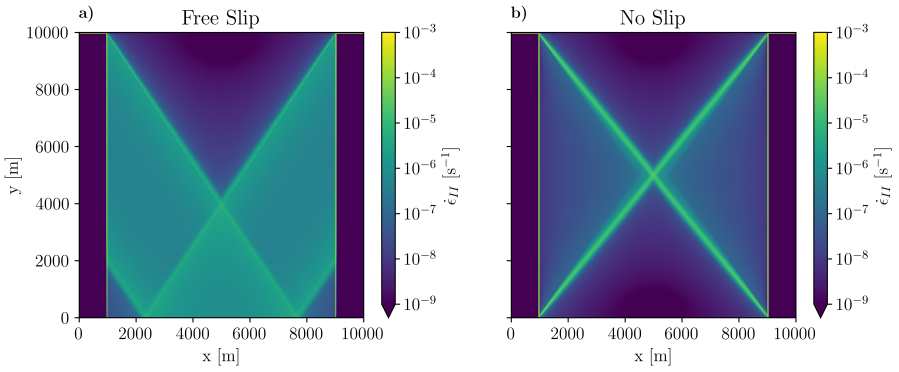

Figure 7. ~~Snap shot of~~ Maximum shear strain rate after ~~15 with a reduced-size ice floe~~ 5 seconds of ~~8 km × 10 km~~integration in a reduced size domain (8 km × 10 km) ~~**(left))**~~ with free-slip (a~~slip~~) and no-slip (b) boundary ~~condition on~~ conditions. Note that the ~~southern boundary, $\theta = 33.8° \pm 0.5$, and **(right)** with a~~ no-slip boundary condition forces the fracture to occur at the corner of the domain, ~~$\theta = 39° \pm 0.5$~~leading to a larger angle of $\theta = 39°$ vs. $34 \pm 1°$ in the control experiment. This suggests that the choice of boundary conditions in current sea ice model needs to be revisited.

and strains are only different south of the diamond fracture pattern because ice can move along the southern boundary and the second fracture cannot form.

3.3 ~~Effects of lateral confinement~~

~~We~~ The angle of fracture in a granular material is independent of confining pressure in uni-axial loading laboratory experiment. We now explore the effect of confining pressure on the eastern and western boundaries on the angle of fracture when using a (convex) elliptical yield curve with a normal flow rule. To do so, we ~~introduce solid walls on the eastern and western boundaries of the domain (similar to the southern boundary) and fill the open water gap between the ice and wall~~ replace the open boundaries to the East and the West with solid walls and the open water gaps with ice of ~~different~~ thicknesses h_c. ~~As the strength of sea ice increases linearly with thickness , the fracture angle changes depending on the~~ Note that the ice strength is linearly related to the ice thickness (Eq. 4). Therefore the normal stress at the edge of the floe is completely defined by the thickness of the surrounding ice.

With an increasing lateral confinement ~~(~~pressure (i.e. an increasing ice thickness h_c next to the main floe), all stress states are moved to higher compressive stresses (blue curve in ~~Figure~~Fig. 4) and the fracture angle increases (Figure ~~8~~). ~~The deformation points are migrating towards~~ In this case, the stress states are again migrating in a direction parallel to the σ_2 axis but with a non-zero σ_1 value. The stress states of the ice along the fracture are therefore located in a region of higher compressive stresses on the yield curve ~~. As the ice is under pressure on the eastern and western boundaries, it cannot move freely eastward and westward so that it then enters the ridging phase more readily~~where the divergence is reduced or even changes sign. With increasing confinement, the stress states of the ice ~~floes~~ floe move to more negative values of σ_1 along a ~~$\sigma_2 = constant$ line~~

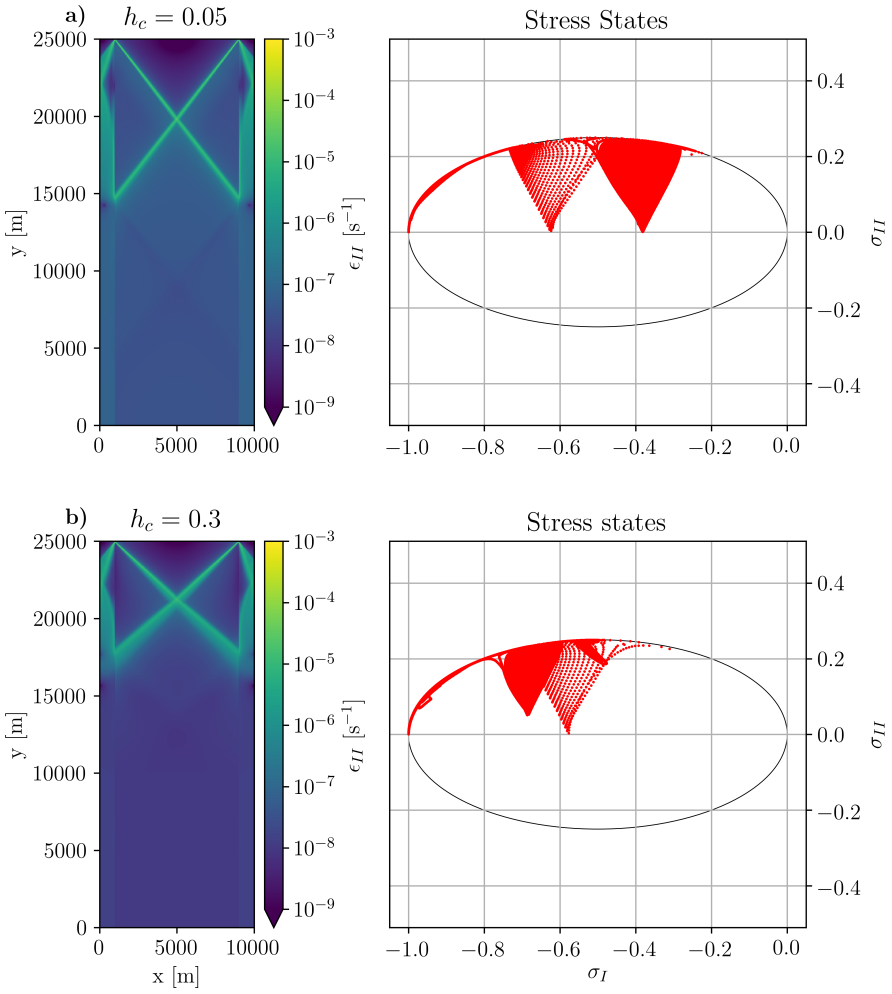

Figure 8. ~~Shear~~ Maximum shear strain rates (left) and stress ~~states for **(Top)** $h_c = 0.05\,\mathrm{m}$ and **(Bottom)** $h_c = 0.3\,\mathrm{m}$~~ state in stress invariant space (right) after 5 seconds of ~~simulation~~integration for different confinement pressure: $h_c = 0.05\,\mathrm{m}$ (a) and $h_c = 0.3\,\mathrm{m}$ (b). Note, how stress states with divergent strain rates (a) migrate left towards convergent strain rates (b).

line of constant σ_2 (blue line in ~~Figure~~Fig. 4) with deformation moving towards more convergent states. Between $h_c = 0.2$ and $h_c = 0.3$, the regime changes from lead opening to ridging, as the fracture angle ~~pass above 45~~increases to values above 45°.

3.3 ~~Effects of the heterogeneity~~

3.2.1 Effects of the heterogeneity

~~Local weaknesses in the initial ice field also has an effect on the fracture angle. When weaknesses are embedded~~ So far, all initial conditions have been homogeneous in thickness and concentration within the ice floe. In practice, sea ice (in a

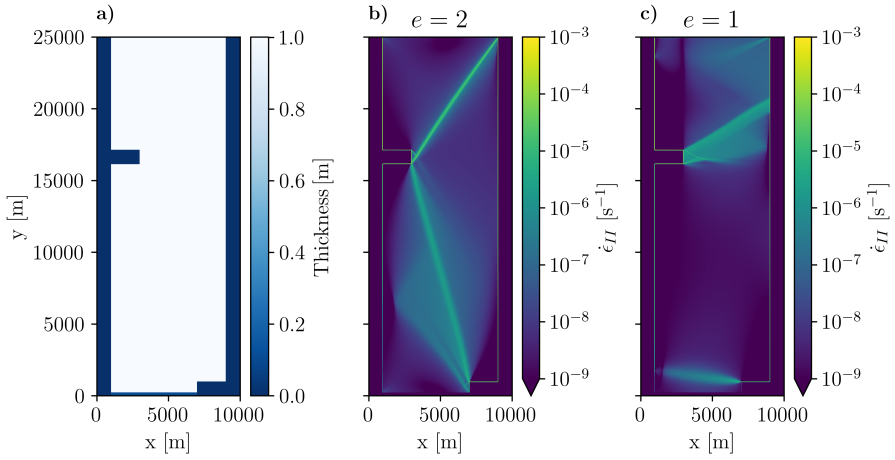

Figure 9. ~~(left)~~ ~~Initial~~ Sea ice thickness with two ~~weak~~ ice-free areas ~~of lower ice thickness. Shear~~ (a), and maximum shear strain ~~rate $\dot{\epsilon}_{II}$~~ rates for two different ellipse aspect ratios (b and c) after 5 seconds ~~with (middle) $e = 2$~~ of integration. The position of the ice weaknesses determines the location and ~~(right) with $e = 1$~~angle of the fracture lines, and also the rheology parameter e has an entirely different effect. The main fractures lines are at angles of 25 $^\circ$ and 34 $^\circ$ for $e = 2.0$, and 57.6 $^\circ$ for $e = 1.0$.

numerical model, but also in reality) is not homogeneous. A local weakness in the initial ice field ~~, failure occurs first at this points. This lead to a stress concentration which raises the stress level and causes failure. This in turn raises~~ is likely the starting point of a crack within the ice field (e.g., Herman, 2016, her Figure 5c). Local failures raise the stress level in ~~the adjacent grid cell and crack propagation proceeds in this manner. In this case, the fracture links stress concentrators together to form a fracture and the angle of fracture is determined also by the distribution of initial ice weaknesses rather than only by the shape of the yield curve or mechanical stress parameters. Figure 9 shows~~ adjacent grid cells and a crack can propagate. Note that the crack propagation in an "ideal" plastic model such as the VP model is instantaneous and this propagation is not seen between time steps. As a consequence, lines of failure will likely develop between local weaknesses. The location of weaknesses in the ice field together with the ice rheology (yield curve and flow rule) both determine the fracture angles (Hibler and Schulson, 2000; Aksenov and Hibler, 2001).

To illustrate this behavior, we start new simulations from an initial ice ~~thickness~~ field with two areas of ~~lower ice thickness~~ zero ice thickness and zero ice concentration, hence weaker ice (~~left hand side), and the results of two simulations after 50 , with $e = 2$ (middle) and $e = 1$ (right hand side). The fracture patterns are very different from~~ Figure 9a). After 5 s these simulations yield fracture patterns that are dramatically different from those of the control run simulation (Section 3.1): the ~~reference case as the~~ fracture lines now start ~~or~~ and terminate at the ~~corners~~ locations of the weak ice areas. Still, changing the ~~yield curve by means of~~ shear strength of the ice (by changing e) changes the fracture pattern (Figure 9b and c). With $e = 1$, the angles are much wider than with $e = 2$, which is consistent with the general dependence of fracture angles on e (see Sec. 3.3.1). Our simulations cannot lead to conclusive statements about the relative importance of heterogeneity of initial conditions and

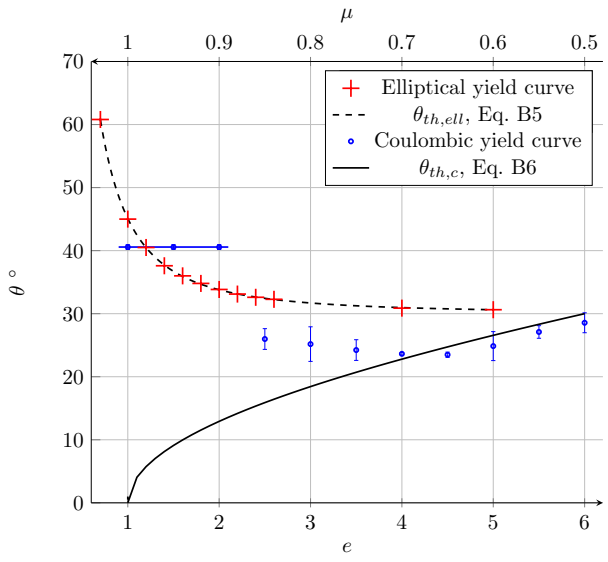

Figure 10. Fracture angles as a function of ellipse aspect ratio e with constant P~~*~~* (red, bottom scale, Section 3.3.1). The ~~red~~ theoretical relationship $\theta_{th,ell} = \frac{1}{2}\arccos -1\left[\frac{1}{2}\left(\frac{1}{e^2}-1\right)\right]$ (dashed black curve, Eq. B4 in the appendix) fits the ~~data~~ modeled angles almost perfectly with ~~$a = 15.1$, $b = -1.96$,~~ $R^2 = 0.9995$ and ~~$e = 29.9$~~ $\sqrt{\text{VAR}} = 0.089$. The ~~R-square value~~ simulated fracture angles for the Coulombic yield curve as a function of the slope of the Mohr-Coulomb limbs (blue, top scale, Section 3.3.2) fit ~~is $R^2 = 0.9997$ and~~ the ~~standard-deviation value is $\sqrt{\sigma} = 0.0639$~~theoretical relationship $\theta_{th,c} = \frac{1}{2}\arccos -1(\mu)$ only for $\mu \leq 0.7$ (black line, Eq.~~Rounding~~ B5 in the ~~value to 2 significant numbers~~appendix). The errors bars mean that they were more than one unique fracture line: For a small μ, ~~we get~~ the ~~parameters~~ice breaks easily along the lateral edges of the floe. For $\mu > 0.7$ ($\phi = 44°$), ~~$a = 15$, $b = -2$,~~ the ambiguity appears because the stress states are both on the linear limbs and ~~$e = 30$~~on the elliptical cap. ~~These rounded values still give an excellent fit with $R^2 = 0.9995$ and $\sqrt{\sigma} = 0.089$. The simulated~~ For $\mu \geq 0.9$ (blue line), the fracture angle is the same as ~~function of e becomes $\theta = \frac{\pi}{6} + \frac{\pi}{12}e^{-2}$ when expressed in radians~~for the ellipse for $e = 1.4$.

yield curve parameters for the fracture pattern, but we can state that both affect the simulations in a way that requires treating them separately to avoid confounding effects. Details are deferred to a dedicated study. ~~The weakness influences the fractures resulting in angles different than expected for these yield curve settings in both cases. Nevertheless, the two fractures are different as the yield curve has an impact on the preferred fracture angle. With $e = 1$, the angles are much wider compared to $e = 2$ (see section 3.3.1 below).~~

3.3 Effects of the yield curve on the fracture angle

3.3.1 Elliptical yield curve

~~The idealized experiment are repeated changing only the ellipse ratio e. Thus~~Keeping $P^\star = 27.5\,\text{kN m}^{-1}$ at its default value, the maximal shear strength ~~$S^\star$ increases or decreases while the maximal compressive strength $P*$ remains constant at 27.5~~ $S^\star = \frac{P^\star}{2e}$

is varied by changing the ellipse ratio e. Scaling the absolute values of $P^\star$ and $S^\star$ while keeping e constant does not change the fracturing pattern as the tangent to the ellipse stays the same (not shown). Changing the ellipse aspect ratio e ~~, however,~~ has a large effect on the fracture angle. The fracture angle decreases monotonically as the shear strength of the material (or e) decreases, from ~~60.9°~~ 61° for $e = 0.7$ to ~~32.3°~~ 32° for $e = 2.6$. ~~An empirical function $\theta = \frac{\pi}{6} + \frac{\pi}{12}e^{-2}$ can fit the data points and is presented on Figure 10. This is in contrast~~ This is clearly inconsistent with the behaviour of ~~other granular materials with an angle of fracture that decreases with increasing shear strength or cohesion.~~ a granular material; in the sand castle analogue this would correspond to a dry sand castle with steeper walls than a moist sand castle. From the simple schematic of Fig. 4 it becomes clear that with increasing e the intersection of the σ_2 axis with the yield curve gradually migrates from the left side of the ellipse to the right where the normal to the yield curve points increasingly towards convergent motion. We present a theoretical explanation for the sensitivity of the fracture angle to the shear strength of the material (e, for the ellipse) in Appendix B by re-writing the elliptical yield curve in local coordinates in the fracture plane (σ, τ) instead of principal or stress invariant coordinates. The fracture angle is then determined from the slope of the tangent to the yield curve in local coordinates and this angle follows from the Mohr's circle (see for instance Popov, 1976).

~~Bouchat and Tremblay (2017) suggest the use of~~ Bouchat and Tremblay (2017) suggest a smaller ellipse aspect ratio (e.g. $e = 0.7$) to obtain a closer match with ~~radarsat-derived~~ RADARSAT-derived distribution of deformation rates in pan-Arctic simulations at 10 km resolution. From ~~Figure~~Fig. 10 and 11, the corresponding fracture angle is ~~$\theta = 60.9°$; i.e. much larger that what~~ $\theta = (61 \pm 1)°$, that is, much larger than that is derived from ~~radarsat~~ RADARSAT images. e also changes the distribution of the stress states on the yield curve. As the stress state migrates along the principal stress ~~σ_1~~ σ_2 until it reaches the yield curve in our uni-axial compressive test, ~~for $e < 1$,~~ the stress state are in the second half of the ellipse for $e < 1$ and the resulting deformation ~~are~~ is in convergence (or ridging). The ice thickness increases due to ridging along the shear lines (Figure 11). In a longer simulation with $e = 0.7$ (not shown) the ice does not open but only ridges, with ~~thickness~~ thicker ice building up within the ice floe. This is in strong contrast to the results with $e = 2.0$ presented in ~~Section ?? above~~ Sect. 3.2.1, where the initial floe breaks up and ~~individual ice~~ separate floes form.

3.3.2 Coulombic yield curve

In this section, we ~~report results from~~ replace the elliptical yield curve with a Coulombic yield curve ~~with normal flow rule Hibler and Schulson (2000)~~(Hibler and Schulson, 2000). This yield curve ~~consist~~ consists of a Mohr-Coulomb failure envelope ~~(two straight lines —~~ two straight limbs in principal or stress invariant space ~~),~~ with a slope μ — capped by an elliptical yield curve for high compressive stresses. ~~For~~ Note that the flow rule applies only to the elliptical cap in this yield curve. For the two straight limbs, the yield curve is normal to the truncated ellipse with the first stress invariant σ_I. For a Mohr-Coulomb yield curve, the fracture angle depends directly on the slope of the Mohr-Coulomb ~~envelope. (AppendixA)~~limb of the yield curve. Appendix A provides a theoretical explanation of how the angle of fracture depends on the internal angle of friction.

The slope of the ~~modified~~ Mohr-Coulomb limbs of the Coulombic yield curve μ is varied between 0.3 and 1.0 (corresponding to an internal angle of friction $\phi = \arcsin(\mu)$ of 17.5° to ~~study~~ 90°) to study how the fracture angle depends on the ~~dependency of the fracture angle to the~~ shear strength of the material. In all experiments with the Coulombic yield curve, ~~We~~ we use a

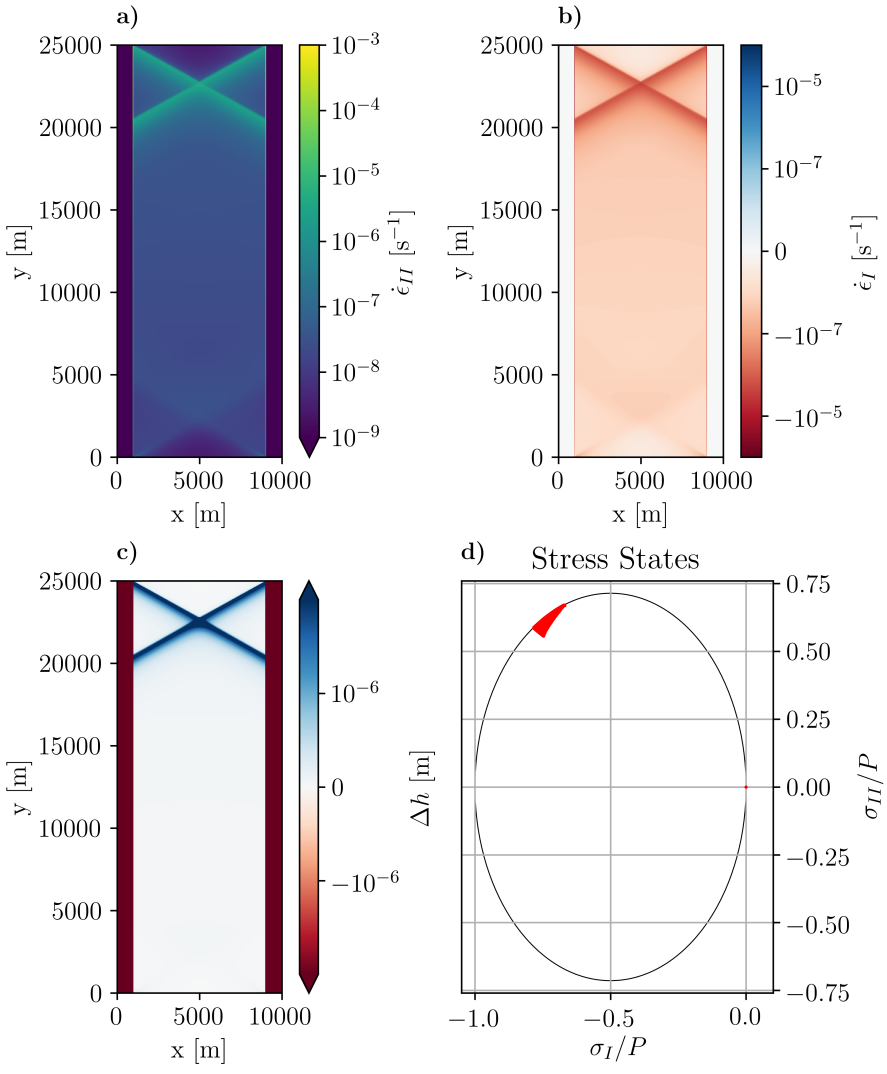

Figure 11. ~~After~~ Maximum shear strain (a), ice thickness anomaly (b), divergence (c) and stress state in stress invariant space (d) after 5 ~~seconds~~ sec of ~~simulation with~~ integration for a smaller ellipse aspect ration ($e = 0.7$. ~~**Top left:** Shear deformation inside~~ compared to $e = 2$ in the ~~ice floe, showing a diamond shape fracture. **Bottom Left:** Divergence deformation~~ reference run in Sect. 3.1). Compared to the ~~floe~~control run on Fig. 3, ~~showing~~ the ~~convergence zone at the~~ angle of fracture ~~location~~is larger ($\theta = (61 \pm 1)^\circ$), ~~leading a ridging event. **Top right:** Modification of~~ the ~~thickness compared to initial state~~ stress states are in the second half of ~~1 ,~~ the ~~ridging~~ ellipse (with ~~a diamond shape~~ strain rates pointing into the convergent direction) and there is ~~visible. **Bottom right:** Stress states~~ convergence along the fracture lines (panel b) in ~~red,~~ agreement with the ~~elliptical yield curve~~ schematic in ~~black~~Fig. 4.

tensile strength of 5% of P* and an ellipse ratio $e = 1.4$, ~~similar to~~ following Hibler and Schulson (2000). The tensile strength is introduced mainly for numerical reasons. With zero tensile strength, the state of stress in a simple uni-axial compressive test

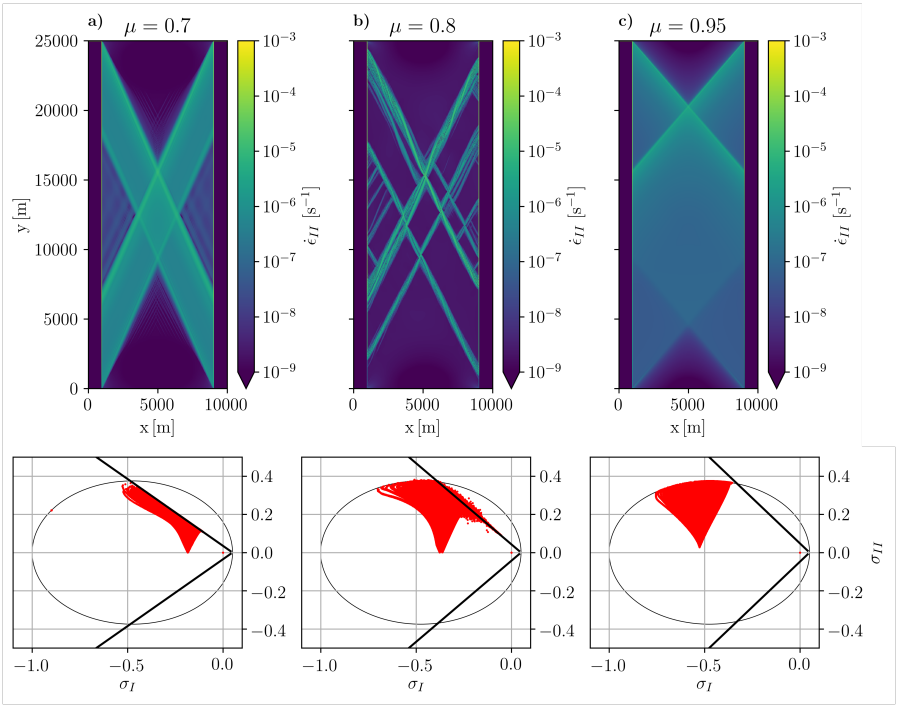

Figure 12. ~~Shear~~ Maximum shear strain ~~$\dot{\epsilon}_{II}$~~ (top) and stress ~~states~~ state in ~~simulation with c=1.4 after 5 seconds~~ stress invariant space (bottom) for different internal angles of ~~simulation : **(top)** $\mu = 0.7$ and $\theta = 23.5°$~~ friction. (a) $\mu = 0.7$ or $\phi = 44°$, ~~**(middle)**~~ (b) $\mu = 0.85$ or $\phi = 58°$ and ~~$\theta \simeq 28$ in average~~(c) $\mu = 0.95$ or $\phi = 72°$ after 5 s of integration. The angles of fracture are $\theta = 23°$, $(28 \pm 2)°$ and ~~**(bottom)** $\mu = 0.95$ and $\theta = 40.9°$~~ $41°$. Fig. 10 illustrates how θ depends on μ for a Coulombic yield curve.

with no confinement pressure ~~,~~ is tangential to the yield curve at the origin (failure in tension) and on the two straight limbs (failure in shear) simultaneously, resulting in ~~instabilities~~a numerical instability. With tensile stress (or confinement pressure) included, the state of stress reaches the yield only on the two limbs of the yield curve ~~.~~ (see Fig. 12a).

~~Figure 12 shows the shear field and stress states for $\mu = 0.7$, $\mu = 0.85$, and~~

For the Coulombic yield curve, there are two distinct regimes of failure. When the σ_2 axis intersects the yield curve on the two straight limbs, which happens for our configuration for angles of friction $\phi < 45°$ (Fig. 12a, left hand side for $\mu = 0.7$ or $\phi = 44°$), the angle of fracture $\theta = \pi/4 - \phi/2$ as per standard theory (Appendix A). When the σ_2 axis intersects the yield curve on the elliptical cap, which happens for $\phi > 45°$ (Fig. 12c, for $\mu = 0.95$ ~~after 5 seconds of simulation. We observe that the fracture pattern is very sensitive to μ. This makes a measuring the fracture angle difficult.We observe four different regimes : Sea ice shear strength is small for small stresses, deformations appear at the border of the ice with high values of deformation. A lot of small LKFs develop but no large fractures appear through the ice floe. The deformation takes place almost exclusively in the flat Mohr-Coulomb part of the yield curve . A distinct fracture patterns is present, similar to the elliptical case. For $\mu = 0.7$, $\theta = 23.5 \pm 2°$ while the Mohr-Coulomb theoretical angle is$\theta_{MC}(\mu) = 22.6°$ from Eq. A. (Top of Figure 12) The~~

~~fracture structure is chaotic. The fracture lines are broad and have an inner structure that seems to be composed of two different angles. The deformation occurs on both parts of the yield curve, Mohr-Coulomb straight limbs and~~ or $\phi = 72°$), we observed a discontinuity in the fracture angle associated with the non-differentiable corner in the yield curve. Note that this corner cannot be removed (by changing the $P^\star$ and e of the elliptical cap~~; presumably, the poor definition of the fracture lines is due to the fact that the stress state touches~~) as the two straight Mohr-Coulomb limbs are defined as a truncation of the ellipse. For $\phi \approx 45°$ in our configuration, the numerical solver has difficulties reaching convergence because of the non-differentiable corner in the yield curve ~~on both part of the yield curve. For $\mu = 0.85$, fractures angles range around $28° \pm 2$.(Middle of Figure 12) The fracture pattern corresponds to~~ between the elliptical cap and the two straight limbs (Fig. 12b, middle panel for $\mu = 0.8$ or $\phi = 53°$). Finally for very small angles ϕ, a large number of fractures, as opposed to single well defined fracture lines, appears because of the weakness of the ~~elliptical yield curve of $e = 1.4$, slightly modified by the 5% tensile strength (not investigated in this paper). Deformation states are on the elliptical part of the modified yield curve. With $\mu = 0.95$, the modeled fracture angle is $\theta = 40.9°$. (Bottom of figure 12)~~ material in shear. This behaviour is not something that is typically observed in uni-axial compressive test of a granular material who generally have higher shear resistance. Note that the value of ϕ that are charactistic for the individual regimes depends on the amount of tensile strength.

4 Discussion

Our idealized ~~experiment~~ experiments using the VP rheologies resolve ~~LKFs~~ fracture lines as described by Hutchings et al. (2005) and akin to observations (Kwok, 2001). The fracturing of the ice floe creates smaller floes in a realistic manner, for example, compared to to Landsat-7 images (Schulson, 2004, Figure 2). At the high resolution of 25 m the original interpretation of the continuity assumption, namely that ~~that~~ each grid cell should represent a distribution of floes (Coon et al., 1974), is no longer valid, but we show that the fracture angle is independent of resolution and scale as expected. Instead, the emerging discontinuities and the polygonal diamond shape of the ~~structures~~ fracture lines that appear as floes spanning many grid cells are a consequence of the mathematical characteristics of the VP model (Pritchard, 1988). Diamond shaped floes are observed in the Arctic ocean (Erlingsson, 1988; Walter and Overland, 1993) and also modeled using a Discrete Element Model (DEM) in an idealized experiment (Wilchinsky et al., 2010). ~~Heorton et al. (2018) compared the Elastic Viscous Plastic (EVP) rheology (Hunke and Dukowicz, 1997) to the Elastic~~ The Elastic Anisotropic Plastic (EAP) rheology ~~, based on the diamond shape property of~~ assumes predominately diamond shaped floes in sea ice (Wilchinsky and Feltham, 2006). ~~They found that~~ A sea ice model with EAP creates sharper fractures than ~~the EVP model and find different regimes of fracture for different convergent and divergent wind forcing. Therefore~~ a model with the Elastic Viscous Plastic (EVP, Hunke and Dukowicz, 1997) rheology (Heorton et al., 2018). The authors concluded that the anisotropic model may improve the fracturing process for sea ice, especially by creating areas of oriented weaknesses, and particularly at coarse resolution where the fracture is not ~~resolve~~ resolved by the grid spacing. In the ~~high-resolution~~ experiments presented here, the VP rheologies ~~appear to model sharp fracture lines~~lead to sharp and anisotropic fracture lines without any additional assumptions.

~~Other experimental choices have been explored to separate the effects of various parameters on the rheology~~ We explored some experimental choices to separate their effects from those of the rheology parameters. The fracture ~~lines~~ angles do not depend on ~~' the experiment's resolution and scale.Thus,~~ the ~~rheology is shown to be scale independent, at least on the scales explored here, in line with observations (Schulson, 2004). Our results show that~~ spatial resolution and domain size as expected in our idealized numerical experiment setup (Sect. 3.2.1, Fig. 5). The maximum viscosities in the VP model are very high and consequently, the VP model can be considered as an ideal plastic material (i.e. a model with an elastic component that has an infinite elastic wave speed). For this reason, fracture in a VP model occurs almost instantaneously. Observed time scales of fracture are on the order of 10 seconds for 60 m floe diameters (Dempsey et al., 2012, Figure 6 top right panel) and from typical elastic wave speeds of 200–2000 $\mathrm{m\,s^{-1}}$, large cracks of order 1000 km can form in minutes to hours (Marsan et al., 2012).

In our setup, the no-slip boundary condition has little effect on the fracture pattern~~within our setup. However, the~~ , but our results suggest that in basin-wide simulations the choice of boundary conditions ~~affect~~ affects the fracture depending on the geometry and stress direction. The no-slip condition ~~appear~~ appears to be unphysical~~and is acting on the stress concentrator on the corner and forcing~~ . It acts to concentrate the stress on the corners of the floe and forces the fracture to occur at this location~~, calling for an~~ . This should motivate a more thorough investigation of the boundary conditions for ~~the shorelines.~~ LKFs that form between one shoreline and another. Similar results were obtained from analytical solutions in idealized geometry for the Morh-Coulomb yield curve with a double sliding deformation law (Sirven and Tremblay, 2014). ~~Confining the ice floe by thinner ice instead of open-water moves the stress states to higher compression and increases the fracture angle. Therefore, we~~

The confining pressure (i.e. thin ice imposed on the side of the domain) changes the distribution of stress within the domain. This results in different deformation patterns (shear and divergence) and different fracture angles because the yield curve is convex and uses a normal flow rule. From this we can conclude that by surrounding our floe with open-water, we get the most acute angles from the rheology in this uni-axial compression setup. This is ~~contradiction~~ not consistent with the behavior of typical granular material ~~that have~~ for which an angle of fracture ~~that~~ is independent of the confining pressure (Hutter and Rajagopal, 1994). ~~A~~ Details of a heterogeneous ice cover ~~shows changes in~~ also affect the fracture pattern. LKFs link the weaknesses in the ice cover, but the pattern still depends on the preferred fracture angles implied by the model rheology. In summary, we are confident that ~~the~~ our choice of parameters allows us to isolate the effects of the rheology and the yield curve on the fracturing process.

In granular material, large shear resistance is linked ~~with~~ to contact normals between floes that oppose the shear motion and ~~leads to dilatation (or divergence). In contrast, our experiment show that adding~~ lead to dilatation (Balendran and Nemat-Nasser, 1993). In our experiments, increasing shear strength in the standard VP model (reducing the ellipse aspect ratio e) does not decrease, but increases the fracture angle~~instead~~. This is ~~contrast with~~ in contrast to the behavior of ~~the granular material that show a decrease in fracture angle for~~ granular material where larger shear strength ~~(~~leads to lower fracture angles — think of a wet sand castle versus a dry ~~sandcastle)~~sand castle. In addition, high shear strength in the VP model with the elliptical yield curve leads to convergence along the fracture plane whereas observations (e.g.~~radarsat deformations~~ RADARSAT derived deformation fields) show a range of positive and negative divergence along LKFs ~~, again contrary to the results obtained with the standard VP model~~ — in accordance with laboratory tests of granular material that show a variable internal angle of friction that depends

on the distribution of the contact normals between individual floes (Hutter and Rajagopal, 1994). Inspection of the stress states in the 2D stress plane suggests that the intersection of the yield curve with the ~~σ_1~~ σ_2 axis has an important role in the fracture process. This intersection point appears to determine the fracture angle~~, but the precise process that determines the fracture angles is unclear. In spite of this, our experiments allow to determine an empirical~~ . In fact, the angle is determined from the intersection of the Mohr's circle of stress with the yield curve to give a theoretical relationship between the fracture ~~angles~~ angle and the ellipse ratio e. ~~Sea ice simulation have been improved~~ With our experiments, we were able to confirm this relationship empirically.

Arctic-wide simulations improve metrics of sea ice concentration, thickness and velocity by decreasing the value of e ~~,~~ ~~thereby~~ of the standard elliptical yield curve, that is, by adding shear and bi-axial tensile and compressive strength ~~(stress states with σ_1 or σ_2 positive, but not both), in Arctic-wide simulations (Miller et al., 2005; Dumont et al., 2009; Bouchat and Tremblay, 2017)~~(Mill The representation of sea ice arches improves with smaller e (Dumont et al., 2009) so do LKF statistics (Bouchat and Tremblay, 2017). Our results, however, show that this ~~would make~~ makes the fracture angles larger, which is in stark contrast to what we expect to be necessary to improve the ~~model~~creation of LKFs in sea ice models.

The fracture angle and the sea ice opening and ridging depending on the deformation states ~~is~~ are consistent with the theory of the yield curve analysis developed in Pritchard (1988) and the Mohr's circle framework that we present in the Appendix. Interestingly, a change of ice maximum compressive strength $P^\star$ with a constant e has no influence on the LKF creation, although $P^\star$ is usually thought of as the principal parameter of sea ice models in climate simulations (e.g. Schmidt et al., 2014). The effects of bi-axial tensile strength $T^\star$ on fracture processes require further investigation, especially given the fact that the assumption of zero-tensile strength is being ~~questions~~ challenged (Coon et al., 2007). The ice strength parameter $C^\star$ (~~The~~ the parameter governing the change of ice strength depending on ice concentration, ~~equation~~Equation 4) was not studied here, although it appears to be an important tuning parameter and it also helps to improve basin-wide simulations (Ungermann et al., 2017). The simulations presented in this study are not realistic and cannot be compared directly to observations of ice floe fracture. For instance, our idealized ice floe is homogeneous while sea ice is known to feature some weaknesses like thermal cracks or melt ponds.

With the ~~coulombic~~ Coulombic yield curve, ~~we can reduce the modeled fracture angle .~~ the simulated fracture angle is smaller. For $\mu = 0.7$ ($\phi = 44°$) theory predicts $\theta_{MC} = 22.8°$ (Appendix B). The observed fracture angle with $\mu = 0.7$ of $\theta = 23.5°$ is close to the $\simeq 20°$ described in Hibler and Schulson (2000)~~, and corresponds to the theoretical framework described in Appendix A~~. Erlingsson (1988) developed ~~another~~ a different Mohr-Coulomb theory linking internal angle of friction and fracture angle. This complex theory ~~take~~ takes into account the fractal (or self-similar) nature of sea ice. It gives different results, but is inadequate for a single ice floe simulated as presented here. ~~The yield curve use here features~~ Based on the results of Pritchard (1988), Wang (2007) used observed fracture patterns to design a *Curved Diamond* yield curve. But this yield curve also contains a non-differentiable point, which will be problematic for numerical reasons. The Coulombic yield curve used here includes a normal flow, ~~while Weiss et al. (2007) shows~~ but in-situ measurements imply that the deformations have an non-normal flow ~~using in-situ measurements~~(Weiss et al., 2007). With the normal flow rule on a Mohr-Coulomb yield curve, the ice only ~~fracture~~ fractures in opening, which is non-physical because sea ice also forms ridges during compressive defor-

mations. ~~The effects of another flow rule may be investigated~~There are alternatives flow rule still to be explored, for example a double-sliding law ~~(Balendran and Nemat-Nasser, 1993; Tremblay and Mysak, 1997)~~(Ip et al., 1991; Balendran and Nemat-Nasser, 1993; Tr

5 Conclusions

Motivated by the observation that the intersection angles in a 2 km Arctic-wide simulation of sea ice are generally larger than in the RGPS dataset (Hutter et al., 2018b), the fracturing of ice under compression was studied with two VP rheologies in a highly idealized geometry and with very small grid spacing of 25 m. The main conclusions are:

~~The fracturing process in a ice floe of 8 by 25 is independent of the experiment resolution and scale, but sensitive to lateral boundary conditions (no-slip or free-slip). The fracture angle is also sensible to the surrounding sea ice cover, in contradiction with the granular nature of sea ice. The model produces a fracture opening with a diamond shape, and several smaller ice floes develop from the initial fracture. Unsurprisingly, the yield curveplays an important role in fracturing sea ice. Increasing the maximum shear strength in the sea ice model increases the fracture angle in contrast to expectations. Even if the fracture process is not fully explained, we~~ In our experimental configuration with uni-axial compression, fracture angles below 30° are not possible in a VP-model with an elliptical yield curve. Observations suggest much lower values. We find an empirical relationship between the fracture angle and the ellipse ratio e of the elliptical yield curve ~~: $\theta \simeq \frac{15}{e^2} + 30$. Therefore, fracture angles below 30are not possible with an elliptical yield curve . In this fully compressive setup,~~ that can be fully explained by the convexity of the yield curve (Appendix B). In contrast to expectations, increasing the maximum shear strength in the sea ice model increases the fracture angle. Along a fracture line, there can be both divergence and convergence depending on the ~~divergence and convergence at the fracture line appear to be dependent in the~~ shear strength of the ice, linked to the ~~normal~~ flow rule. The ~~ice open and create~~ simulated ice opens and creates leads with an ellipse ratio ~~below $e = 1$, and ridge in the inverse case. Using a modified coulombic~~ $e > 1$ (shear strength is smaller than compressive strength), and ridges for $e < 1$ (shear strength is larger than compressive strength).

With a modified Coulombic yield curve, the fracture angle can be decreased to values expected from observations, but the non-differentiable ~~shape~~ corner points of this yield curve ~~introduces numerical issues and an unclear fracture pattern in some cases. Therefore,~~ lead to numerical (convergence) issues and, for some values of the coefficient of internal friction μ, to fracture patterns that are difficult to interpret. At these corner points, two different slopes meet and give two non-unique solutions for fracture angles and deformation directions. We recommend to avoid non-differentiable yield curves (with a normal flow rule) ~~should be avoided~~ in viscous-plastic sea ice models.

More generally, the model produces diamond-shaped fracture patterns. Later the ice floe disintegrates into several smaller floes develop. The fracturing process in the ice floe in our configuration is independent of the experiment resolution and scale, but sensitive to boundary conditions (no-slip or free-slip). The fracture angle in the VP-model is also sensitive to the immediate environment. This is not consistent with the notion of sea ice as a granular material. Unsurprisingly, the yield curve plays an important role in fracturing sea ice in a numerical model as it governs the deformation of the ice as a function of the applied stress.

The idealized experiment of a uni-dimensional compression is useful to explore the effects of the yield curve because all other parameters are controlled. Historically, the discrimination between the different yield ~~curve couldn't have been done~~ curves was not possible because of the scarcity of sea ice drift data. ~~The~~ Model comparisons to recent sea ice deformation ~~dataset from RADARSATalso, through LKFs statistics, indicated~~ datasets, such as from RADARSAT, imply that we would need to increase the shear strength with the ellipse in the standard VP rheology to match observations ~~. This would increase~~ (Bouchat and Tremblay, 2017). We find that this increases the fracture angles, ~~in opposition to the needed improvements~~creating a dilemma. Therefore, the high-resolution idealized experiment presented in this work ~~gives means~~ provides a framework to investigate and discriminate different rheologies ~~–~~ — yield curve and flow rule.

If Arctic-wide sea ice simulations with a resolution of 25 m are not feasible today because of computational cost, we can still imagine ~~such a model~~ small experiments to be useful for process modeling on small scales ~~, for example,~~ when local and high-resolution observations (e.g. wind, ice velocities) are available. For example, such process modeling studies could be used to constrain the rheology with data from the upcoming MOSAiC ~~scientific cruise~~ campaign (Dethloff et al., 2016) that will provide a full year of sea ice observations in pack ice. Such simulations would also need to take into account the effects of heterogeneous ice cover and wind patterns, with potentially convergent and divergent ~~forces from the wind~~ wind forcing. Most climate models use the standard VP rheology (Stroeve et al., 2014) or one of its variants (e.g. EVP). Results presented here~~however points at the need for~~ , however, imply that a more physical yield curve ~~and (~~with a (possibly non-associative) flow rule ~~. A better understanding of the link between the fracture process and the yield curve and the flow rule is necessary for more confidence in the capacity of the rheology to model sea ice dynamic in a consistent way. Once the fracture process within the VP framework is fully understood, the design of a new yield curve, including a different flow rule, that would take into account the granular nature of sea ice and be adapted to high resolution modeling and LKFs creation appears to be necessary.~~

is required. Such a yield curve would have to be continuous in all representations, differentiable without corners, have some cohesion and be consistent with available observations of fracture angles in convergent and divergent flow.

Appendix A: Fracture angle

~~We follow Hibler and Schulson (2000) and Tremblay and Mysak (1997) to~~ Below, we derive a relationship between the fracture angle and the internal angle of friction for ~~the~~ a Mohr-Coulomb ~~curve. The stresses~~ yield criterion for completeness. We consider an arbitrary piece of a 2D medium (Figure A1a) that is subject to stresses in physical stress space σ_{ij} $(i=1,2)$. Computing the change of coordinates as described in Eq. (7), we can consider the principal stresses (σ_1, σ_2) applied on the medium (Figure A1b). From the force balance, the normal stress σ and the shear stress τ on a plane at an angle θ from the principal stress axis ~~(σ_1, σ_2)~~ can be written as (see ~~Figure A1and Popov (1976))~~ Fig. A1b and Popov, 1976)

$$\sigma dA = \sigma_2 \sin(\theta)\sin(\theta)dA + \sigma_1 \cos(\theta)\cos(\theta)dA, \tag{A1}$$

$$\tau dA = \sigma_2 \cos(\theta)\sin(\theta)dA - \sigma_1 \cos(\theta)\sin(\theta)dA, \tag{A2}$$

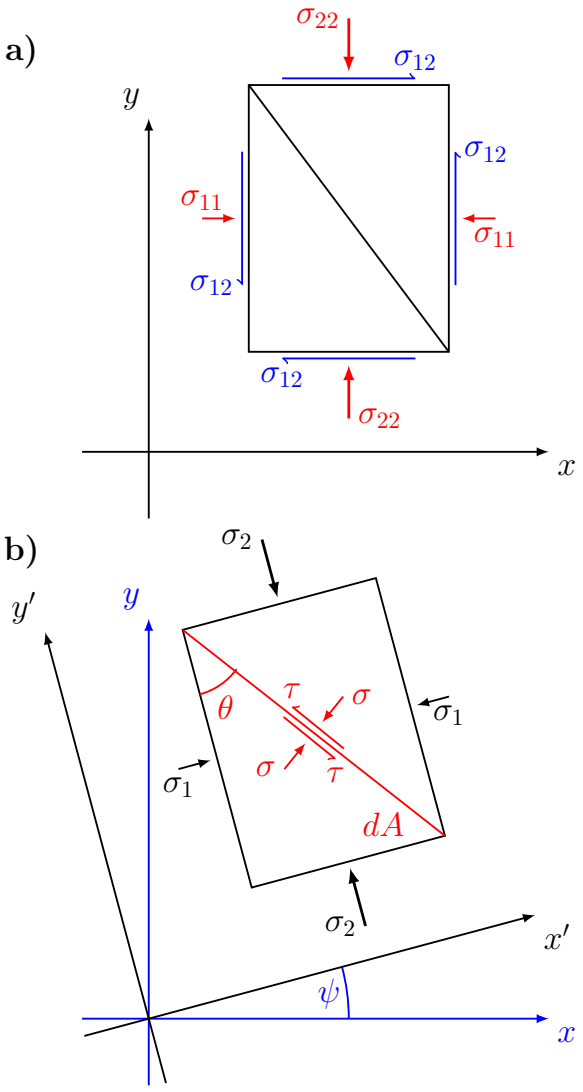

Figure A1. Stress state ~~on an ice element~~ in ~~the reference σ_{ij} **a)** or in principal~~ physical stress space (~~σ_1,σ_2~~a) and ~~along~~ in an arbitrary ~~inclined plane~~ coordinate system oriented at an ~~angles θ **b)**~~angle $theta$ with respect to the principal stress axes (b). The principal ~~axis~~ stresses are the eigenvalues of the stress tensor in an arbitrary coordinate system and the angle ψ ~~comes~~ is derived from the rotation matrix composed of the two eigenvectors. Note that in the study above there is no shear stress ($\sigma 12 = 0$, so principal axes and physical axes are aligned ($\psi = 0$).

where dA is the area of the friction plane ~~. Simplifying using trigonometryrelationships~~on which the stresses are applied (in 2D it is just a line). The second trigonometric term comes from the fact that this surface is tilted compared to the direction of stresses σ_1 and σ_2. Using angle sum and difference identities of trigonometry, we can write the ~~stress~~ stresses σ and τ in terms

of the principal stresses σ_1 and σ_2 as

$$\sigma = \frac{1}{2}(\sigma_1 + \sigma_2) + \frac{1}{2}(\sigma_1 - \sigma_2)\cos(2\theta), \tag{A3}$$

$$\tau = -\frac{1}{2}(\sigma_1 - \sigma_2)\sin(2\theta). \tag{A4}$$

In terms of the stress invariants σ_I and σ_{II} this gives

$$\sigma = \sigma_I + \sigma_{II}\cos(2\theta), \tag{A5}$$

$$\tau = -\sigma_{II}\sin(2\theta). \tag{A6}$$

The Mohr-Coulomb failure criterion can be written in the ~~reference~~ fracture plane stress space (see ~~Figure ??)~~ Fig. A2) as

$$\tau = -\tan(\phi)\,\sigma + c, \tag{A7}$$

where ϕ is the internal angle of friction, and c the cohesion when no ~~stress is applied . Substituting (??~~stresses are applied (Verruijt, 2018).

Substituting (A5) and (~~??~~A6) in (A7) we get

$$-\sigma_{II}\sin(2\theta) = \tan(\phi)\,\sigma_I + \tan(\phi)\,\sigma_{II}\cos(2\theta) + c, \tag{A8}$$

~~that we develop as ,~~ and after multiplying both sides by $\cos(\phi)$

$$\sigma_{II}\left[\sin(2\theta)\cos(\phi) - \cos(2\theta)\sin(\phi)\right] = -\sigma_I\sin(\phi) + c\cos(\phi). \tag{A9}$$

By geometrical construction (see Fig. A2) the MC criterion is satified when (see also Verruijt, 2018, Sect. 20.4),

$$\sigma_{II} = -\sigma_I\sin(\phi) + c\cos(\phi) \tag{A10}$$

so that eq. (A9) becomes

$$\sin(2\theta)\cos(\phi) + \cos(2\theta)\sin(\phi) = \sin(2\theta + \phi) = 1, \tag{A11}$$

from which we get the classical result of material deformation physics:

$$\sigma_{II}\sin(2\theta)\cos(\phi) + \cos(2\theta)\sin(\phi) = \frac{\pi}{2} \Rightarrow \theta = \frac{\pi}{4} - \mu\sigma_I + c\frac{\phi}{2} \tag{A12}$$

~~where we have used the fact that $\mu = \tan(\gamma) = \sin(\phi)$ (see Figure ??) , where μ is the coefficient of internal friction. This then imply that in invariant space~~

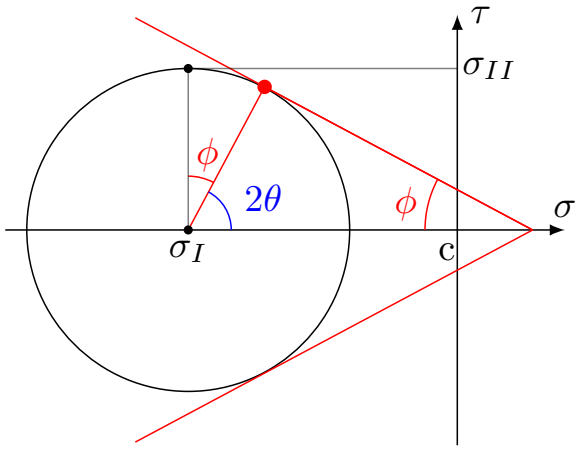

Figure A2. Mohr's circle of stress (black) with Mohr-Coulomb yield criterion (red) of angle of internal friction ϕ (red) and cohesion c in (σ,τ) space. From Eq. (A12, the deformation is created with an angle θ that can be represented in Mohr's circle (blue).

Appendix B: Fracture angle and yield curve

A yield curve can be defined in the local stress (σ_{ij}), principal stress ($\sigma_{1,2}$) or stress invariant ($\sigma_{I,II}$) spaces. The latter gives the center and radius of the Mohr's circle of stress defining all equivalent stress states (σ,τ) for all angles with respect to a reference coordinate system. This allows the translation of the elliptical yield curve from the standard principal or stress invariant space to a local stress coordinate system (σ_{ij}) In this sense, we can plot the yield curve in (σ,τ) space as the envelope of all Mohr's circles for each point on the elliptical yield curve defined in stress invariant coordinates (see Fig. B1 for an illustration with the elliptical yield curve). In the following, we refer to this envelope of all Mohr's circles as the reconstructed yield curve. The tangent to this curve can be expressed as (Figure B2):

$$\sin(\phi) = \tan(\gamma) = \mu = \frac{\partial \sigma_{II}}{\partial \sigma_I}. \tag{B1}$$

We can then express the fracture angle for stress states on the yield curve envelope by placing Eq. (B1) in Eq. (A12) :

$$\theta(\sigma_I) = \frac{\pi}{4} - \frac{1}{2}\arcsin\left(\frac{\partial \sigma_{II}}{\partial \sigma_I}(\sigma_I)\right) = \frac{1}{2}\arccos\left(\frac{\partial \sigma_{II}}{\partial \sigma_I}(\sigma_I)\right). \tag{B2}$$

This is the same relation presented (Pritchard, 1988) and used previously (Wang et al., 2006), but obtained within the (σ,τ) stress space.

B1 Elliptical yield curve

From the previous equations, some implications about the elliptical yield curve immediately follow. As shown in Fig. 4, in a uni-directional compressive setup the slope of a tangent to the yield curve changes with the ellipse ratio. The convexity of the

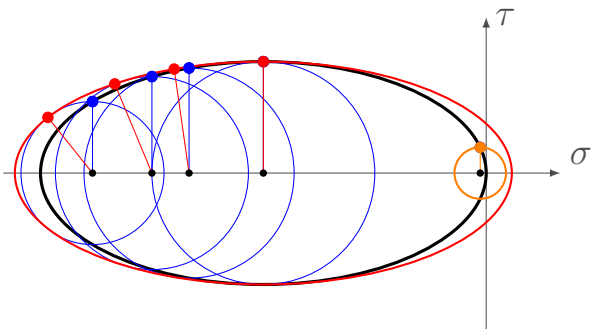

Figure B1. Illustration of the Mohr's circle applied to the elliptical yield curve (black ellipse) in σ,τ space, some examples of Mohr's circles (blue) and the reconstructed yield curve (red) in the fracture plane space. The orange Mohr's circle illustrate the case where no fracture lines exists, for $|\mu| > 1$.

ellipse implies that the ratio $\frac{\tau}{\sigma} = \tan(\phi)$ of shear strength τ to compressive strength σ becomes smaller with smaller e. If we compute the slope of the tangent to the elliptical yield curve at the intersection point between the yield curve and the σ_2 axis, we get

$$\left.\frac{\partial \sigma_{II}}{\partial \sigma_I}\right|_{\sigma_1=0} = \frac{1}{2}\left(\frac{1}{e^2} - 1\right). \tag{B3}$$

Inserted this relationship into Eq. (B2) gives the angle of fracture for uni-axial compressive experiment with an ellipse ratio e:

$$\theta_{th,ell}(e) = \frac{1}{2}\arccos\left[\frac{1}{2}\left(\frac{1}{e^2} - 1\right)\right]. \tag{B4}$$

Note that a yield curve in ($\sigma_{I,II}$) space with a tangent slope above unity does not have a Mohr's circle that can be tangent to the yield curve in (σ,τ) space (Orange circle on in Fig. B1). This implies that no angle of fracture can be derived for these stress states. This is the case for the elliptical yield curve for low and high compressive stresses. It is still unclear what happens in the VP model for stress states on the yield curve that have a tangent with a slope higher than unity (see also Pritchard, 1988). Note also that for some (σ_I,σ_{II})

$$\sin(2\theta)\cos(\phi) + \cos(2\theta)\sin(\phi) = 1$$

states, the ice will actually fail in tension, as the reconstructed yield curve having a few points in the first and fourth quadrant.

~~Therefore we get~~

$$\theta = \frac{\pi}{4} - \frac{\phi}{2} = \frac{\pi}{4} - \frac{\sin^{-1}(\mu)}{2}$$

The shear and bulk viscosities are symmetrical about the center of the ellipse. This implies that they are equal for divergence and convergence. Clearly this is not physical since divergent flow should have less ice-ice interactions and lower viscosities than

convergent flow. While this is non-physical, it does lead to more numerical stability because the extra viscosity or dissipation of energy regularizes the problem. We also note that tensile strength with a slope smaller than one is unphysical, because it would make the ice break with an angle in tension. So adding tensile strength to the elliptical yield curve would not be physical. The slope of the yield curve in the first and fourth quadrant (positive σ_I) should be -1 and 1, respectively.

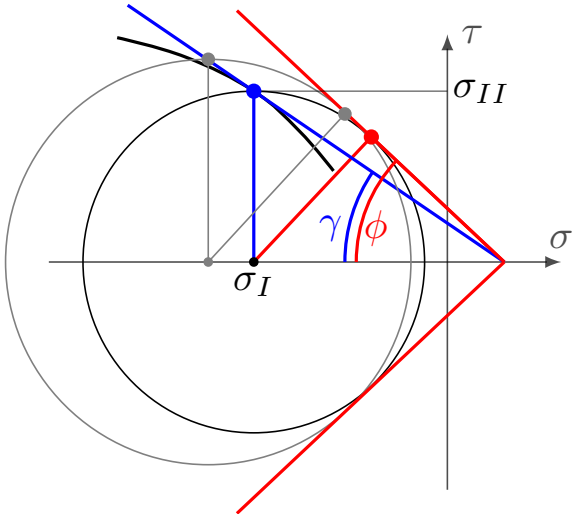

Figure B2. Mohr's circle of stress with an arbitrary yield curve (black line) in the fracture plane reference. $\tan(\gamma) = \mu$ is the tangent to the yield curve, and ϕ the internal angle of friction as described in Appendix A. We note that $\sin(\phi) = \tan(\gamma) = \mu$ (for $|\mu| \leq 1$). For a slightly different Mohr's circle (grey), the blue and and red tangents meet in the same point on the σ axis.

B2 Coulombic yield envelope

Applying Mohr's circle to the Coulombic yield curve explains, why the non-differentiable corners in the yield curve lead to numerical problems (Figure B3). The tangent does not vary smoothly and the reconstructed yield curve in the failure plane (σ, τ) becomes discontinuous (Figure B3, red line). As shown in Sect. 3.3.2, when the stress states fall on only one of the two parts (ellipse or limb) the conjugate faults forms as expected. Using Eq. (B4) with μ as the slope of the Mohr-Coulomb limbs of the Coulombic yield curve, the fracture angle is given by

$$\theta_{th,c}(\mu) = \frac{1}{2}\arccos(\mu), \tag{B5}$$

which is identical to Eq. (A12).

The Truncated Ellipse Method (TEM) yield curve (e.g., Hibler and Schulson, 1997, Appendix) can be seen as a Coulombic yield curve with $\mu = 1$ and a cohesion $c = 0$. The slope $\mu = 1$ implies a breaking angle of zero for all confinement conditions that would make the stress states fall on the limbs. The zero cohesion implies that the ice will deform for small stresses. So this yield curve also appears to us as unphysical.

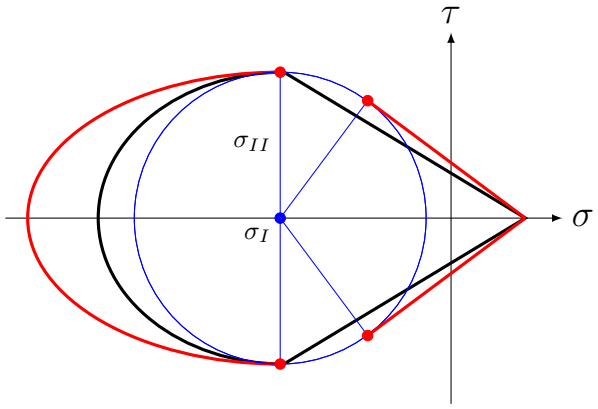

Figure B3. ~~Mohr-Coulomb~~ Mohr's circle ~~of stress in an arbitrary frame of reference at an angle θ with the respect~~ applied to the ~~principal stress. $\tan(\gamma) = \mu$~~coulombic yield curve (in black) in σ,τ space, the ~~slope if~~ Mohr's circle for the cusps between the elliptical cap and the Mohr-Coulomb linear limbs (blue ~~line~~circle), and the yield curve in (σ,τ) space (red). We can see the effect of combining two regimes, for the same Mohr's circle, two different angles coexists (red circles) and are apart from each other.

Author contributions. Damien Ringeisen designed the experiments, ran the simulations, interpreted the results with the help from Martin Losch and Bruno Tremblay. Nils Hutter contributed to the discussion on LKFs in simulations and observations. Damien Ringeisen prepared the manuscript with contributions from all co-authors.

Competing interests. The authors declare that they have no conflict of interest.

Acknowledgements. We would like to thank Jennifer Hutchings and Harry Heorton for their helpful reviews on this paper, as well as Amélie Bouchat and Mathieu Plante for useful discussion during this work. This project was supported by the Deutsche Forschungsgemeinschaft (DFG) through the International Research Training Group "Processes and impacts of climate change in the North Atlantic Ocean and the Canadian Arctic" (IRTG 1904 ArcTrain).

The authors would like to thank the Isaac Newton Institute for Mathematical Sciences for support and hospitality during the program Mathematics of sea ice phenomena when work on this paper was undertaken. This work was supported by: EPSRC grant numbers EP/K032208/1 and EP/R014604/1. This work is a contribution to the Canadian Sea Ice and Snow Evolution (CanSISE) Network funded by the Natural Sciences and Engineering Research Council (NSERC) of Canada, the Marine Environmental Observation Prediction and Response (MEOPAR) Network and the NSERC Discovery Grants Program awarded to Tremblay. "

References

Aksenov, Y. and Hibler, W. D.: Failure Propagation Effects in an Anisotropic Sea Ice Dynamics Model, in: IUTAM Symposium on Scaling Laws in Ice Mechanics and Ice Dynamics, edited by Dempsey, J. P. and Shen, H. H., Solid Mechanics and Its Applications, pp. 363–372, Springer Netherlands, 2001.

Balendran, B. and Nemat-Nasser, S.: Double sliding model for cyclic deformation of granular materials, including dilatancy effects, Journal of the Mechanics and Physics of Solids, 41, 573–612, https://doi.org/10.1016/0022-5096(93)90049-L, http://www.sciencedirect.com/science/article/pii/002250969390049L, 1993.

Bouchat, A. and Tremblay, B.: Energy dissipation in viscous-plastic sea-ice models, Journal of Geophysical Research: Oceans, 119, 976–994, https://doi.org/10.1002/2013JC009436, http://onlinelibrary.wiley.com/doi/10.1002/2013JC009436/abstract, 2014.

Bouchat, A. and Tremblay, B.: Using sea-ice deformation fields to constrain the mechanical strength parameters of geophysical sea ice, Journal of Geophysical Research: Oceans, pp. n/a–n/a, https://doi.org/10.1002/2017JC013020, http://onlinelibrary.wiley.com/doi/10.1002/2017JC013020/abstract, 2017.

Bröhan, D. and Kaleschke, L.: A Nine-Year Climatology of Arctic Sea Ice Lead Orientation and Frequency from AMSR-E, Remote Sensing, 6, 1451–1475, https://doi.org/10.3390/rs6021451, https://www.mdpi.com/2072-4292/6/2/1451, 2014.

Coon, M., Kwok, R., Levy, G., Pruis, M., Schreyer, H., and Sulsky, D.: Arctic Ice Dynamics Joint Experiment (AIDJEX) assumptions revisited and found inadequate, Journal of Geophysical Research: Oceans, 112, C11S90, https://doi.org/10.1029/2005JC003393, http://onlinelibrary.wiley.com/doi/10.1029/2005JC003393/abstract, 2007.

Coon, M. D., Maykut, A., G., Pritchard, R. S., Rothrock, D. A., and Thorndike, A. S.: Modeling The Pack Ice as an Elastic-Plastic Material, AIDJEX BULLETIN, No. 24, 1–106, 1974.

Dansereau, V., Weiss, J., Saramito, P., and Lattes, P.: A Maxwell elasto-brittle rheology for sea ice modelling, The Cryosphere, 10, 1339–1359, https://doi.org/10.5194/tc-10-1339-2016, http://www.the-cryosphere.net/10/1339/2016/, 2016.

Dansereau, V., Démery, V., Berthier, E., Weiss, J., and Ponson, L.: Fault orientation in damage failure under compression, arXiv:1712.08530 [cond-mat, physics:physics], http://arxiv.org/abs/1712.08530, arXiv: 1712.08530, 2017.

Dempsey, J. P., Xie, Y., Adamson, R. M., and Farmer, D. M.: Fracture of a ridged multi-year Arctic sea ice floe, Cold Regions Science and Technology, 76-77, 63–68, https://doi.org/10.1016/j.coldregions.2011.09.012, http://www.sciencedirect.com/science/article/pii/S0165232X11001947, 2012.

Dethloff, K., Rex, M., and Shupe, M.: Multidisciplinary drifting Observatory for the Study of Arctic Climate (MOSAiC), EGU General Assembly Conference Abstracts, 18, https://ui.adsabs.harvard.edu/#abs/2016EGUGA..18.3064D/abstract, 2016.

Dumont, D., Gratton, Y., and Arbetter, T. E.: Modeling the Dynamics of the North Water Polynya Ice Bridge, Journal of Physical Oceanography, 39, 1448–1461, https://doi.org/10.1175/2008JPO3965.1, https://journals.ametsoc.org/doi/abs/10.1175/2008JPO3965.1, 2009.

Erlingsson, B.: Two-dimensional deformation patterns in sea ice, Journal of Glaciology, 34, 301–308, 1988.

Flato, G. M. and Hibler, W. D.: Modeling Pack Ice as a Cavitating Fluid, Journal of Physical Oceanography, 22, 626–651, https://doi.org/10.1175/1520-0485(1992)022<0626:MPIAAC>2.0.CO;2, https://journals.ametsoc.org/doi/abs/10.1175/1520-0485(1992)022%3C0626:MPIAAC%3E2.0.CO%3B2, 1992.

Girard, L., Weiss, J., Molines, J. M., Barnier, B., and Bouillon, S.: Evaluation of high-resolution sea ice models on the basis of statistical and scaling properties of Arctic sea ice drift and deformation, Journal of Geophysical Research: Oceans, 114, C08 015, https://doi.org/10.1029/2008JC005182, http://onlinelibrary.wiley.com/doi/10.1029/2008JC005182/abstract, 2009.

Girard, L., Bouillon, S., Weiss, J., Amitrano, D., Fichefet, T., and Legat, V.: A new modeling framework for sea-ice mechanics based on elasto-brittle rheology, Annals of Glaciology, 52, 123–132, https://doi.org/10.3189/172756411795931499, 2011.

Heorton, H. D. B. S., Feltham, D. L., and Tsamados, M.: Stress and deformation characteristics of sea ice in a high-resolution, anisotropic sea ice model, Phil. Trans. R. Soc. A, 376, 20170 349, https://doi.org/10.1098/rsta.2017.0349, http://rsta.royalsocietypublishing.org/content/376/2129/20170349, 2018.

Herman, A.: Discrete-Element bonded-particle Sea Ice model DESIgn, version 1.3a - model description and implementation, Geoscientific Model Development, 9, https://doi.org/10.5194/gmd-9-1219-2016, https://ui.adsabs.harvard.edu/#abs/2016GMD.....9.1219H/abstract, 2016.

Hibler, W. D.: A viscous sea ice law as a stochastic average of plasticity, Journal of Geophysical Research, 82, 3932–3938, https://doi.org/10.1029/JC082i027p03932, http://onlinelibrary.wiley.com/doi/10.1029/JC082i027p03932/abstract, 1977.

Hibler, W. D.: A Dynamic Thermodynamic Sea Ice Model, Journal of Physical Oceanography, 9, 815–846, https://doi.org/10.1175/1520-0485(1979)009<0815:ADTSIM>2.0.CO;2, http://journals.ametsoc.org/doi/abs/10.1175/1520-0485%281979%29009%3C0815%3AADTSIM%3E2.0.CO%3B2, 1979.

Hibler, W. D. and Schulson, E. M.: On modeling sea-ice fracture and flow in numerical investigations of climate, Annals of Glaciology, 25, 26–32, https://doi.org/10.1017/S0260305500190019, https://www.cambridge.org/core/journals/annals-of-glaciology/article/on-modeling-seaice-fracture-and-flow-in-numerical-investigations-of-climate/DA5C2474CE1E18E0167C748BF6DF8386, 1997.

Hibler, W. D. and Schulson, E. M.: On modeling the anisotropic failure and flow of flawed sea ice, Journal of Geophysical Research: Oceans, 105, 17 105–17 120, https://doi.org/10.1029/2000JC900045, http://onlinelibrary.wiley.com/doi/10.1029/2000JC900045/abstract, 2000.

Hibler, W. D., Hutchings, J. K., and Ip, C. F.: sea-ice arching and multiple flow States of Arctic pack ice, Annals of Glaciology, 44, 339–344, https://doi.org/10.3189/172756406781811448, https://www.cambridge.org/core/journals/annals-of-glaciology/article/seaice-arching-and-multiple-flow-states-of-arctic-pack-ice/6E8D3407E6860F9F29E0CC6EF5F83BA2, 2006.

Hundsdorfer, W., Koren, B., van Loon, M., and Verwer, J.: A Positive Finite-Difference Advection Scheme, Journal of Computational Physics, 117, 35–46, 1995.

Hunke, E. C.: Viscous–Plastic Sea Ice Dynamics with the EVP Model: Linearization Issues, Journal of Computational Physics, 170, 18–38, https://doi.org/10.1006/jcph.2001.6710, http://www.sciencedirect.com/science/article/pii/S0021999101967105, 2001.

Hunke, E. C. and Dukowicz, J. K.: An Elastic–Viscous–Plastic Model for Sea Ice Dynamics, Journal of Physical Oceanography, 27, 1849–1867, https://doi.org/10.1175/1520-0485(1997)027<1849:AEVPMF>2.0.CO;2, http://journals.ametsoc.org/doi/abs/10.1175/1520-0485(1997)027%3C1849:AEVPMF%3E2.0.CO;2, 1997.

Hutchings, J. K., Jasak, H., and Laxon, S. W.: A strength implicit correction scheme for the viscous-plastic sea ice model, Ocean Modelling, 7, 111–133, https://doi.org/10.1016/S1463-5003(03)00040-4, http://www.sciencedirect.com/science/article/pii/S1463500303000404, 2004.

Hutchings, J. K., Heil, P., and Hibler, W. D.: Modeling Linear Kinematic Features in Sea Ice, Monthly Weather Review, 133, 3481–3497, https://doi.org/10.1175/MWR3045.1, http://journals.ametsoc.org/doi/abs/10.1175/MWR3045.1, 2005.

Hutter, K. and Rajagopal, K. R.: On flows of granular materials, Continuum Mechanics and Thermodynamics, 6, 81–139, https://doi.org/10.1007/BF01140894, https://doi.org/10.1007/BF01140894, 1994.

Hutter, N., Martin, L., and Dimitris, M.: Scaling Properties of Arctic Sea Ice Deformation in a High-Resolution Viscous-Plastic Sea Ice Model and in Satellite Observations, Journal of Geophysical Research: Oceans, 123, 672–687, https://doi.org/10.1002/2017JC013119, https://agupubs.onlinelibrary.wiley.com/doi/abs/10.1002/2017JC013119, 2018a.

Hutter, N., Zampieri, L., and Losch, M.: Leads and ridges in Arctic sea ice from RGPS data and a new tracking algorithm, The Cryosphere Discussions, pp. 1–27, https://doi.org/https://doi.org/10.5194/tc-2018-207, https://www.the-cryosphere-discuss.net/tc-2018-207/, 2018b.

Ip, C. F., Hibler, W. D., and Flato, G. M.: On the effect of rheology on seasonal sea-ice simulations, Annals of Glaciology, 15, 17–25, 1991.

Kwok, R.: Deformation of the Arctic Ocean Sea Ice Cover between November 1996 and April 1997: A Qualitative Survey, in: IUTAM Symposium on Scaling Laws in Ice Mechanics and Ice Dynamics, edited by Dempsey, J. P. and Shen, H. H., no. 94 in Solid Mechanics and Its Applications, pp. 315–322, Springer Netherlands, https://doi.org/10.1007/978-94-015-9735-7_26, http://link.springer.com/chapter/10.1007/978-94-015-9735-7_26, 2001.

Lemieux, J.-F. and Tremblay, B.: Numerical convergence of viscous-plastic sea ice models, Journal of Geophysical Research: Oceans, 114, https://doi.org/10.1029/2008JC005017, https://agupubs.onlinelibrary.wiley.com/doi/abs/10.1029/2008JC005017, 2009.

Lemieux, J.-F., Tremblay, B., Sedláček, J., Tupper, P., Thomas, S., Huard, D., and Auclair, J.-P.: Improving the numerical convergence of viscous-plastic sea ice models with the Jacobian-free Newton–Krylov method, Journal of Computational Physics, 229, 2840–2852, https://doi.org/10.1016/j.jcp.2009.12.011, http://www.sciencedirect.com/science/article/pii/S0021999109006822, 2010.

Lindsay, R. W. and Rothrock, D. A.: Arctic sea ice leads from advanced very high resolution radiometer images, Journal of Geophysical Research: Oceans, 100, 4533–4544, https://doi.org/10.1029/94JC02393, https://agupubs.onlinelibrary.wiley.com/doi/abs/10.1029/94JC02393, 1995.

Linow, S. and Dierking, W.: Object-Based Detection of Linear Kinematic Features in Sea Ice, Remote Sensing, 9, https://doi.org/10.3390/rs9050493, http://www.mdpi.com/2072-4292/9/5/493, 2017.

Losch, M., Menemenlis, D., Campin, J.-M., Heimbach, P., and Hill, C.: On the formulation of sea-ice models. Part 1: Effects of different solver implementations and parameterizations, Ocean Modelling, 33, 129–144, https://doi.org/10.1016/j.ocemod.2009.12.008, https://www.sciencedirect.com/science/article/pii/S1463500309002418, 2010.

Marko, J. R. and Thomson, R. E.: Rectilinear leads and internal motions in the ice pack of the western Arctic Ocean, Journal of Geophysical Research, 82, 979–987, https://doi.org/10.1029/JC082i006p00979, https://agupubs.onlinelibrary.wiley.com/doi/10.1029/JC082i006p00979, 1977.

Marsan, D., Weiss, J., Larose, E., and Métaxian, J.-P.: Sea-ice thickness measurement based on the dispersion of ice swell, The Journal of the Acoustical Society of America, 131, 80–91, https://doi.org/10.1121/1.3662051, https://asa.scitation.org/doi/full/10.1121/1.3662051, 2012.

Marshall, J., Adcroft, A., Hill, C., Perelman, L., and Heisey, C.: A finite-volume, incompressible Navier Stokes model for studies of the ocean on parallel computers, Journal of Geophysical Research: Oceans, 102, 5753–5766, https://doi.org/10.1029/96JC02775, http://onlinelibrary.wiley.com/doi/10.1029/96JC02775/abstract, 1997.

Miller, P. A., Laxon, S. W., and Feltham, D. L.: Improving the spatial distribution of modeled Arctic sea ice thickness, Geophysical Research Letters, 32, https://doi.org/10.1029/2005GL023622, https://agupubs.onlinelibrary.wiley.com/doi/abs/10.1029/2005GL023622, 2005.

Overland, J. E., McNutt, S. L., Salo, S., Groves, J., and Li, S.: Arctic sea ice as a granular plastic, Journal of geophysical research, 103, 21 845–21 868, https://www.researchgate.net/profile/James_Overland/publication/240487097_Arctic_sea_ice_as_a_granular_plastic/links/55cb6a2c08aeb975674c796b.pdf, 1998.

Popov, E. P.: Mechanics of Materials, Prentice Hall, Englewood Cliffs, N.J, 2 edition edn., 1976.

Pritchard, R. S.: An Elastic-Plastic Constitutive Law for Sea Ice, Journal of Applied Mechanics, 42, 379–384, https://doi.org/10.1115/1.3423585, http://appliedmechanics.asmedigitalcollection.asme.org/article.aspx?articleid=1402443, 1975.

Pritchard, R. S.: Mathematical characteristics of sea ice dynamics models, Journal of Geophysical Research: Oceans, 93, 15 609–15 618, https://doi.org/10.1029/JC093iC12p15609, http://onlinelibrary.wiley.com/doi/10.1029/JC093iC12p15609/abstract, 1988.

Rampal, P., Bouillon, S., Ólason, E., and Morlighem, M.: neXtSIM: a new Lagrangian sea ice model, The Cryosphere, 10, 1055–1073, https://doi.org/10.5194/tc-10-1055-2016, http://www.the-cryosphere.net/10/1055/2016/, 2016.

Rothrock, D. A.: The steady drift of an incompressible Arctic ice cover, Journal of Geophysical Research, 80, 387–397, https://doi.org/10.1029/JC080i003p00387, http://onlinelibrary.wiley.com/doi/10.1029/JC080i003p00387/abstract, 1975.

Rothrock, D. A. and Thorndike, A. S.: Measuring the sea ice floe size distribution, Journal of Geophysical Research: Oceans, 89, 6477–6486, https://doi.org/10.1029/JC089iC04p06477, http://onlinelibrary.wiley.com/doi/10.1029/JC089iC04p06477/abstract, 1984.

Schmidt, G. A., Kelley, M., Nazarenko, L., Ruedy, R., Russell, G. L., Aleinov, I., Bauer, M., Bauer, S. E., Bhat, M. K., Bleck, R., Canuto, V., Chen, Y.-H., Cheng, Y., Clune, T. L., Genio, A. D., Fainchtein, R. d., Faluvegi, G., Hansen, J. E., Healy, R. J., Kiang, N. Y., Koch, D., Lacis, A. A., LeGrande, A. N., Lerner, J., Lo, K. K., Matthews, E. E., Menon, S., Miller, R. L., Oinas, V., Oloso, A. O., Perlwitz, J. P., Puma, M. J., Putman, W. M., Rind, D., Romanou, A., Sato, M., Shindell, D. T., Sun, S., Syed, R. A., Tausnev, N., Tsigaridis, K., Unger, N., Voulgarakis, A., Yao, M.-S., and Zhang, J.: Configuration and assessment of the GISS ModelE2 contributions to the CMIP5 archive, Journal of Advances in Modeling Earth Systems, 6, 141–184, https://doi.org/10.1002/2013MS000265, https://agupubs.onlinelibrary.wiley.com/doi/abs/10.1002/2013MS000265, 2014.

Schreyer, H. L., Sulsky, D. L., Munday, L. B., Coon, M. D., and Kwok, R.: Elastic-decohesive constitutive model for sea ice, Journal of Geophysical Research: Oceans, 111, C11S26, https://doi.org/10.1029/2005JC003334, http://onlinelibrary.wiley.com/doi/10.1029/2005JC003334/abstract, 2006.

Schulson, E. M.: Compressive shear faults within arctic sea ice: Fracture on scales large and small, Journal of Geophysical Research: Oceans, 109, C07 016, https://doi.org/10.1029/2003JC002108, http://onlinelibrary.wiley.com/doi/10.1029/2003JC002108/abstract, 2004.

Sirven, J. and Tremblay, B.: Analytical Study of an Isotropic Viscoplastic Sea Ice Model in Idealized Configurations, Journal of Physical Oceanography, 45, 331–354, https://doi.org/10.1175/JPO-D-13-0109.1, https://journals.ametsoc.org/doi/abs/10.1175/JPO-D-13-0109.1, 2014.

Spreen, G., Kwok, R., Menemenlis, D., and Nguyen, A. T.: Sea-ice deformation in a coupled ocean–sea-ice model and in satellite remote sensing data, The Cryosphere, 11, 1553–1573, https://doi.org/10.5194/tc-11-1553-2017, https://www.the-cryosphere.net/11/1553/2017/, 2017.

Stroeve, J., Barrett, A., Serreze, M., and Schweiger, A.: Using records from submarine, aircraft and satellites to evaluate climate model simulations of Arctic sea ice thickness, The Cryosphere, 8, 1839–1854, https://doi.org/10.5194/tc-8-1839-2014, http://www.the-cryosphere.net/8/1839/2014/, 2014.

Sulsky, D., Schreyer, H., Peterson, K., Kwok, R., and Coon, M.: Using the material-point method to model sea ice dynamics, Journal of Geophysical Research: Oceans, 112, C02S90, https://doi.org/10.1029/2005JC003329, http://onlinelibrary.wiley.com/doi/10.1029/2005JC003329/abstract, 2007.

Tremblay, L.-B. and Mysak, L. A.: Modeling Sea Ice as a Granular Material, Including the Dilatancy Effect, Journal of Physical Oceanography, 27, 2342–2360, https://doi.org/10.1175/1520-0485(1997)027<2342:MSIAAG>2.0.CO;2, http://journals.ametsoc.org/doi/abs/10.1175/1520-0485(1997)027%3C2342:MSIAAG%3E2.0.CO;2, 1997.

Tsamados, M., Feltham, D. L., and Wilchinsky, A. V.: Impact of a new anisotropic rheology on simulations of Arctic sea ice, Journal of Geophysical Research: Oceans, 118, 91–107, https://doi.org/10.1029/2012JC007990, http://onlinelibrary.wiley.com/doi/10.1029/2012JC007990/abstract, 2013.

Ungermann, M., Tremblay, L. B., Martin, T., and Losch, M.: Impact of the Ice Strength Formulation on the Performance of a Sea Ice Thickness Distribution Model in the Arctic, Journal of Geophysical Research: Oceans, pp. n/a–n/a, https://doi.org/10.1002/2016JC012128, http://onlinelibrary.wiley.com/doi/10.1002/2016JC012128/abstract, 2017.

Verruijt, A.: An Introduction to Soil Mechanics, Theory and Applications of Transport in Porous Media, Springer International Publishing, //www.springer.com/gp/book/9783319611846, 2018.

Walter, B. A. and Overland, J. E.: The response of lead patterns in the Beaufort Sea to storm-scale wind forcing, Annals of Glaciology, 17, 219–226, https://doi.org/10.3189/S0260305500012878, https://www.cambridge.org/core/journals/annals-of-glaciology/article/div-classtitlethe-response-of-lead-patterns-in-the-beaufort-sea-to-storm-scale-wind-forcingdiv/43BF1A611FEAF0F5EA4DFFAA9236F11F, 1993.

Wang, K.: Observing the yield curve of compacted pack ice, Journal of Geophysical Research: Oceans, 112, C05 015, https://doi.org/10.1029/2006JC003610, http://onlinelibrary.wiley.com/doi/10.1029/2006JC003610/abstract, 2007.

Wang, K., Leppäranta, M., and Kõuts, T.: A study of sea ice dynamic events in a small bay, Cold Regions Science and Technology, 45, 83–94, https://doi.org/10.1016/j.coldregions.2006.02.002, http://www.sciencedirect.com/science/article/pii/S0165232X0600022X, 2006.

Wang, Q., Danilov, S., Jung, T., Kaleschke, L., and Wernecke, A.: Sea ice leads in the Arctic Ocean: Model assessment, interannual variability and trends, Geophysical Research Letters, 43, 7019–7027, https://doi.org/10.1002/2016GL068696, https://agupubs.onlinelibrary.wiley.com/doi/abs/10.1002/2016GL068696, 2016.

Weiss, J., Schulson, E. M., and Stern, H. L.: Sea ice rheology from in-situ, satellite and laboratory observations: Fracture and friction, Earth and Planetary Science Letters, 255, 1–8, https://doi.org/10.1016/j.epsl.2006.11.033, http://www.sciencedirect.com/science/article/pii/S0012821X06008430, 2007.

Wilchinsky, A. V. and Feltham, D. L.: Anisotropic model for granulated sea ice dynamics, Journal of the Mechanics and Physics of Solids, 54, 1147–1185, https://doi.org/10.1016/j.jmps.2005.12.006, http://www.sciencedirect.com/science/article/pii/S0022509606000032, 2006.

Wilchinsky, A. V., Feltham, D. L., and Hopkins, M. A.: Effect of shear rupture on aggregate scale formation in sea ice, Journal of Geophysical Research: Oceans, 115, C10 002, https://doi.org/10.1029/2009JC006043, http://onlinelibrary.wiley.com/doi/10.1029/2009JC006043/abstract, 2010.

Zhang, J. and Hibler, W. D.: On an efficient numerical method for modeling sea ice dynamics, Journal of Geophysical Research: Oceans, 102, 8691–8702, https://doi.org/10.1029/96JC03744, http://onlinelibrary.wiley.com/doi/10.1029/96JC03744/abstract, 1997.

Zhang, J. and Rothrock, D. A.: Effect of sea ice rheology in numerical investigations of climate, Journal of Geophysical Research: Oceans, 110, C08 014, https://doi.org/10.1029/2004JC002599, http://onlinelibrary.wiley.com/doi/10.1029/2004JC002599/abstract, 2005.